MICROPHYSIOLOGICAL MODELS OF THE HUMAN PLACENTA

THE DESIGN AND CHARACTERIZATION OF MICROPHYSIOLOGICAL
PLATFORMS TO MODEL THE HUMAN PLACENTA

By MICHAEL K. WONG, M.Sc., B.Sc.

A Thesis Submitted to the School of Graduate Studies in Partial Fulfilment of the
Requirements for the Degree Doctor of Philosophy

DOCTOR OF PHILOSOPHY (2020)

Graduate Program in Medical Sciences

McMaster University, Hamilton, Ontario, Canada

TITLE: The design and characterization of microphysiological platforms to model

the human placenta

AUTHOR: Michael K. Wong, M.Sc., B.Sc.

SUPERVISOR: Dr. Sandeep Raha

NUMBER OF PAGES: xxiii, 207

LAY ABSTRACT

The human placenta is an important organ that helps regulate the health of both the mother and fetus during pregnancy. Researchers have traditionally studied the placenta through the use of animals or isolated cells, but these have been criticized for not being similar enough to the human placenta. Our objective was to build models that better resembled the structure and environment experienced by the human placenta within the body, such that we could better study its function. During the course of my doctoral work, I built and analyzed three models of the human placenta using human cells that were grown in three dimensions, in multiple layers, and/or in a specific environment. Our first model demonstrated that placental cell behaviour and function can be controlled by altering the thickness of the surface we grew them on. Our second model grew placental cells in three-dimensions and mimicked the invasion process into the mother's uterus during early pregnancy. Our third model grew placental cells with blood vessel cells to form the barrier that regulates the passage of all substances between the mother and fetus during pregnancy. We also tested the impact of low oxygen on the placental barrier's formation and function. Overall, we discovered that placental cells could indeed function more similarly to how we expect them to in the body when we design platforms that better resemble their structure and environment. Our model development work provides new information about placental biology and may serve as valuable tools in research and drug development.

ABSTRACT

The human placenta facilitates many key functions during pregnancy, including uterine invasion, vascular remodeling, hormone secretion, immune regulation, and maternal-fetal exchange. Placental research, however, has been limited in part by the unrepresentative nature of traditional models. The objective of this doctoral thesis was to build and characterize novel, *in vitro* models that reintegrated important anatomical and environmental elements of the human placenta, thus enabling more physiologically-accurate assessments of placental function. In our first model, we manipulated the thickness of the extracellular matrix surface to promote the self-assembly of trophoblast cells into three-dimensional (3D) aggregates that exhibited increased genetic and functional markers of syncytial fusion. In our second model, we established a high-throughput platform to generate 3D trophoblast spheroids that underwent dynamic invasion and migration, expressed transcriptomic profiles redolent of the extravillous trophoblast phenotype, and responded to various drugs relevant to pregnancy. In our third model, we developed a trophoblast-endothelial co-culture model of the placental barrier that underwent syncytial fusion, exhibited size-specific barrier permeability, and functioned under physiologically-relevant oxygen tensions. In conclusion, our models may each serve as valuable tools for researchers, contribute to investigations of different aspects of placental biology, and aid in the screening of drugs and toxins for pregnancy.

ACKNOWLEDGEMENTS

It would be naïve to think that the greats throughout history achieved their successes through their own sheer intellect or ability. Nothing is ever independently achieved or deserved. The pursuit of science may demand much from the scientist, but it in many ways ends up demanding even more from the individuals who care for the scientist. I hope to acknowledge some of those who made substantial sacrifices for me – without whom, I simply would not have been capable.

To my supervisor, Dr. Sandeep Raha – thank you for taking me on as a doctoral student. Thank you for the freedom you provided me to design and run my own projects, attend conferences, and pursue extracurriculars. These things have all had a huge impact on my education and development. Furthermore, I am grateful for your readiness to listen to all of my ideas and opinions, and commitment to communicating even when it is difficult. Thank you for your caring and understanding nature that supported me to have a family during my PhD. You have taught me that in many situations, it is more important to care for the person. Thank you for the sacrifices you have made for me, and I wish you the best as you also grow in the ways that you lead your lab and foster your research.

To my committee, Dr. Tom Hawke and Dr. Ravi Selvaganapathy – thank you for taking the time to provide me with advice and guidance on my research. Your knowledge shared during our meetings have made a difference in where I am as a scientist today.

To my undergraduate thesis students, Madeline Green, Mohamed Adam, Sarah Shawky, Mishquatul Wahed, and Edward Li, thank you for your contributions to our research together. Your efforts in the lab have helped shape and progress this thesis in so many ways. I know that I have been tough on you at times (*e.g.,* manually pipetting 384-well plate), but I have truly appreciated all the hours you put into our projects together.

To my friends and venture partners, Dr. William Gwynne and Athan Dial – Thank you for joining me in the building of Industry Link and ARCHITECHealth together. The things we have been able to try and (occasionally) accomplish have defined my time as a doctoral student. Entrepreneurship is not taught in a classroom; it is experienced through decisive action and hard work as you create something new. I am very thankful that I was able to experience it with you both. I could not have asked for better mates during my time at McMaster.

To my family-in-law, James and Wendy Lam, and Valerie, Nolan, and Seth Bentley, thank you for your continued care and love. I have appreciated the interest you have shown in my research and how you have supported us through meals, babysitting, and more.

To my family, Dad, Mum, and Nicole, thank you for your unwavering love and support throughout my life. Family can be one of the most important foundations that someone can have in their life, and I am grateful that you provided that for me. Thank you for your willingness to give me everything, so that I could grow up with the freedom to pursue anything.

To my dearest wife, Tiffany – Thank you for choosing to walk through life with me. From your decision to come with me to Hamilton together so that I could attend McMaster to our next chapter after that, thank you for the countless sacrifices you have made. You taught me that love is not about pursuing happiness, fulfilment, stability, equality, nor ambition – though these things can come with it – but rather about selflessness. Love seeks to do nothing with selfish ambition or conceit, but to count others more significant than yourselves. Love looks not only to their own interests, but to the interests of others. I would be a fool to think that any accomplishment achieved during the course of my doctorate were solely earned or deserved. You sacrificed your interests so that I could pursue mine. This has made all the difference.

To our beloved son, Riley – May the research that is performed today lead to science and medicine that benefits you tomorrow. You are teaching me what it means to truly sacrifice for someone else's gain.

TABLE OF CONTENTS

LIST OF FIGURES AND TABLES

Chapter 1

Chapter 2

Chapter 3

Chapter 4

Chapter 5

LIST OF ALL ABBREVIATIONS AND SYMBOLS

2D – two-dimensional or two-dimension

3D – three-dimensional or three-dimension

ANOVA – analysis of variance

ATP – adenosine triphosphate

BSA – bovine serum albumin

CON – control

cDNA – complementary deoxyribonucleic acid

DAPI – 4′,6-diamidino-2-phenylindole

DNA – deoxyribonucleic acid

ECM – extracellular matrix

EGF – epidermal growth factor

ELISA – enzyme-linked immunosorbent assay

EMT – epithelial-mesenchymal transition

ERVWE-1 – endogenous retrovirus group W member 1

EVT – extravillous trophoblasts

FDR – false discovery rate

FSK – forskolin

FUS – fusion or fused

GCM1 – glial cells missing transcription factor 1

GFP – green fluorescent protein

GO – gene ontology

GSEA – gene set enrichment analysis

hCG – human chorionic gonadotropin

H&E – Hematoxylin and eosin

HIF – hypoxia-inducible factor

HLA-G – histocompatibility antigen, class I, G

HUVEC – human umbilical vein endothelial cell

IL – interleukin

ITG – integrin

mmHg – millimeters mercury

MMP – matrix metalloproteinase

mRNA – messenger ribonucleic acid

RT-qPCR – real time-quantitative polymerase chain reaction

PDMS – polydimethylsiloxane

PLGF – placental growth factor

RFP – red fluorescent protein

RIPA – radioimmunoprecipitation assay

RNA – ribonucleic acid

SEM – standard error of mean

THC – $\triangle 9$ – tetrahydrocannabinol

TIMP – tissue inhibitor of metalloproteinase

ULA – ultra-low attachment

VEGF – vascular endothelial growth factor

DECLARATION OF ACADEMIC ACHIEVEMENT

Michael Wong contributed to the writing, experimental design, conducting of experiments, literature research, data analysis, interpretation of results, and figure generation for all chapters of this thesis.

Sandeep Raha contributed to experimental design and interpretation of results for all chapters of this thesis.

Ponnambalam R. Selvaganapathy contributed to experimental design and interpretation of results for Chapters 2 and 4 of this thesis.

Madeline Green conducted experiments for Chapter 2.

Aditya Aryasomayajula conducted experiments and data analysis for Chapter 2.

Tom Ewart contributed to experimental design for Chapter 2.

Sarah Shawky conducted experiments for Chapters 2 and 3.

Mishquatul Wahed conducted experiments for Chapter 3.

Anna Dvorkin-Gheva conducted data and bioinformatic analyses for Chapter 3.

Edward Li conducted experiments for Chapter 4.

Mohamed Adam conducted experiments for Chapter 4.

CHAPTER 1: INTRODUCTION

An infinitely complex biological phenomenon paired with an interconnected impact on nearly every system within the body, the establishment of pregnancy is arguably one of the most defining experiences in human physiology. Pregnancy is robust and adaptive, persisting as a means for life, survival, and fitness in nearly all animal species in one way or another. Yet, pregnancy is also delicate, dependent on numerous factors for success, and may be vulnerably plagued with disease and complication. While pregnancy is medically characterized by the National Institutes of Health as "the period in which a *fetus* develops inside a woman's uterus", it is also the period in which another entity develops in parallel known as the *placenta.* This uniquely-temporal organ sits as the conductor orchestrating the symphony of human development, maintaining the health of not only the fetus, but the mother as well. In this doctoral thesis, I hope to convince you of the biological marvel of this organ, its many implications for science and health, and the necessity to build stronger model systems to study it.

The Human Placenta

Overview of early placentation

The human placenta is anatomically-defined as the discoid-shaped, fetal-derived organ comprised of a fusion of fetal and maternal tissues [1]. In addition to its involvement in establishing pregnancy, this multifaceted organ bears the pivotal

role of maintaining the growth and survival of the fetus during the nine months through uterine invasion and vascular remodeling, substance exchange, immune and barrier protection, and endocrine regulation [2].

The placenta originates alongside the fetus, sharing the same genetic blueprint, from an early developmental structure known as the blastocyst [3]. Approximately one-week post-fertilization, the blastocyst implants into the epithelial layer of the maternal uterine endothelium, where the polar trophectoderm layer then differentiates into the cytotrophoblast and primitive syncytiotrophoblast cell layers of the early placenta. The mononuclear, stem-like cytotrophoblast cells rapidly proliferate, differentiate, and fuse to expand the multinucleated, primitive syncytiotrophoblast layer. The primitive syncytiotrophoblast is responsible for hormone secretion, enzyme-mediated digestion and invasion into the maternal uterine endometrium [2,4]. The invading syncytiotrophoblasts penetrate and rupture maternal capillaries, which causes maternal blood to pool into fluid-filled spaces within the syncytiotrophoblast layer known as syncytial lacunae. At two weeks post-fertilization, chorionic villi emerge forth into the blood-filled syncytial lacunae, consisting of a solid core of cytotrophoblast cells surrounded by a syncytiotrophoblast layer. At three weeks post-fertilization, mesenchymal cells from the underlying extraembryonic mesoderm penetrate into the cytotrophoblast core of the chorionic villi and differentiate into embryonic blood vessels to enable more efficient exchange between fetal and maternal systems. At four weeks post-fertilization, the umbilical cord is derived to connect placental and fetal circulations

[5]. At five weeks post-fertilization, the cytotrophoblast core of the chorionic villi expand and breach the syncytiotrophoblast layer to reach the decidua basalis of the maternal uterus. As this occurs, the syncytial lacunae give rise to a large cavity between the chorionic and basal plates of the placenta known as the maternal intervillous space [1]. At approximately 10-12 weeks post-fertilization, the maternal intervillous space fills with oxygenated blood sourced from the remodelled, uterine spiral arteries – becoming the primary supply of nutrition and oxygen for both the placenta and fetus for the remainder of pregnancy [11]. The placenta continues to grow and develop at a proportionate rate as the fetus in order to provide adequate support, with clinical evidence suggesting strong, correlative relationships between placental surface area, volume, weight, and various morphologies with fetal growth and health [6,7]. However, the specific developmental events in the second and third trimester remain elusive due to scarcity of available literature (likely owing to limitations in modern imaging and sampling techniques.) At term, the placenta possesses a weight of approximately 500 g, diameter of 15-20 cm, thickness of 2-3 cm, and surface area of 15 m^2 [8].

Overall, the proper development of the placenta is crucial in maintaining maternal and fetal health during pregnancy. Poor establishment of early placentation has been strongly associated with pregnancy-related diseases like preeclampsia, one of the leading causes of maternal and fetal morbidity and mortality currently plaguing 5-7% of all pregnancies globally [9].

The chorionic villi

One of the major functional structures within the placenta is known as the chorionic villi. Resembling tree-like or finger-like projections, thirty to forty chorionic villi extend from the chorionic plate into the maternal intervillous space of the human placenta. The chorionic villi may be further divided into two key units known as the anchoring and terminal villi (**Figure 1**). These units play important roles in establishing the direct contact between the placenta and maternal blood, thus defining the haemochorial nature of the human placenta. This unique anatomical structure is particularly defining of the human placenta, and has been historically difficult to study using animal models, which we will further discuss the section below entitled "*In vivo animal models*".

The anchoring villi extend from the tips of the chorionic villi to attach to the decidua basalis of the maternal uterus and secure the placenta and fetus in place. Solid, trophoblast cell columns give rise to the extravillous trophoblast cells (EVTs), which are responsible for deep uterine invasion into the endometrium and a third of the myometrium and colonization and remodeling of the maternal spiral arteries. The invasion and migration of interstitial EVT cells are driven by a variety of factors, including chemoattraction to oxygen and nutrients present in the maternal blood and interactions with uterine immune factors (*e.g.,* natural killer cells and macrophages) [10-12]. In early pregnancy, the EVT cells form "trophoblast plugs" within the spiral arteries to minimize blood flow into the placenta [13]. This intentionally retains the placenta in a low oxygen environment (~2-3%), which

promotes specific elements of development (*e.g.,* proliferation of cytotrophoblasts [14]) and vascularization/angiogenesis [15]. As described above, the plugs degrade by the end of the first trimester and the remodeled spiral arteries as high-capacitance, low-resistance vessels immerse the chorionic villi within the intervillous space with oxygenated, maternal blood [13,15].

The terminal villi of the chorionic villi branch outwards into the maternal blood to engage in nutrient and waste exchange, hormone secretion, and barrier protection [16]. Related to its key functions, these units are also known as the "placental barrier". The placental barrier consists of an outer layer of syncytiotrophoblasts that is directly exposed to the maternal blood, an underlying population of cytotrophoblast cells, various mesenchymal, fibroblastic, macrophages, and extracellular matrix proteins that make up the stroma, and fetal vascular endothelial cells that make up the fetal blood vessels. Underlying cytotrophoblasts continually fuse upwards to maintain the syncytiotrophoblast layer, but the placental barrier eventually thins out to mainly consist of the syncytiotrophoblast and fetal endothelial layers to enhance maternal-fetal exchange. Fetal vasculature within these villi also continue to expand and mature, primarily through branching angiogenesis in the second trimester, and non-branching angiogenesis in the third trimester again to maximize maternal-fetal exchange [5].

In summary, the highly orchestrated development and functioning of the anchoring and terminal chorionic villi play an essential role in establishing the maternal and fetal circulations within the placenta.

Placental Trophoblast Cell Types

Despite the highly heterogeneous composition of the placenta, it is clear from implantation to delivery that the trophoblast cell remains one of the central cell types responsible for placental function. While the full details of its origins and differentiation events are still being uncovered, we have some understanding of how the human trophoblast lineage emerges and differentiates (please refer to Gamage, et al. [17] for a systematic review). In brief, present research suggests that the inner cell mass gives rise to the ectodermic, mesodermic, and endodermic fetal tissues, whereas the outer trophectoderm layer of the blastocyst derives the pluripotent trophoblast stem cells that form the placenta (**Figure 2A**). The cytotrophoblast lineage then diverges down one of two pathways, resulting in either the villous cytotrophoblast and syncytiotrophoblast cells or the EVTs [4]. However, the majority of these traditional classifications were made through measuring only a few RNA or protein markers expressed by the distinct cell type. Emergent technologies like single-cell RNA-sequencing now enable full characterizations of genetic signatures, serving to identify more nuanced trophoblast cell subtypes (**Figure 2B**) [18].

Villous cytotrophoblast cells

Villous cytotrophoblasts are epithelial, mononucleated cells found between the syncytiotrophoblast layer and the basement membrane of the chorionic villi [4]. Cytotrophoblast cells generally begin as a complete layer between the basement membrane and syncytiotrophoblasts, but gradually decrease in prominence to about 15% of the total trophoblast population by the end of pregnancy [4,19]. Recent single-cell RNA-sequencing experiments revealed that three functional subtypes of cytotrophoblasts may exist by 8 weeks of gestation: (1) proliferative, (2) non-proliferative, Syncytin-2-positive, and (3) non-proliferative, Syncytin-2-negative **(Figure 2B)** [18]. The first subtype likely serves as the stem cell population to replenish cytotrophoblast pools, and the second subtype acts as the committed progenitor cytotrophoblast that fuses into the syncytiotrophoblast layer. The role of the third, non-proliferative, Syncytin-2-negative subtype is not fully known, but could perhaps act as progenitors to the EVT lineage [18]. Additional work is required to characterize these novel cytotrophoblast subtypes.

Villous syncytiotrophoblast cells

The multinucleated syncytiotrophoblasts make up the outermost layer of the placental barrier. It remains debated whether a single, continuous syncytial layer covers the entire surface of the chorionic villi, or if there are several, connected large segments [4]. They do not proliferate, thus depend on the syncytial fusion of the underlying cytotrophoblast layer for maintenance and growth (**Figure 3**) [20].

Cellular fusion is the genetically- and environmentally-regulated joining of two or more adjacent cells into a single entity, resulting in the merging of plasma membranes and cytoplasmic contents [21]. There are three main steps involved in cellular fusion: competence (or ability to fuse through possessing the necessary fusogenic proteins, *e.g.,* syncytins), commitment (or physical positioning in a manner to undergo fusion, through direct contact with a neighbouring, fusogenic cell), and undergoing the actual fusion event [22]. This process is unique to only a few cell types in the human body, including myoblasts [23], osteoclasts [24], and placental cytotrophoblasts [25]. Syncytial fusion or syncytialization, which is the cellular fusion of cytotrophoblasts into syncytiotrophoblasts, may be observed in two main phases during placentation [21]. The initial phase occurs during implantation of the embryo into the maternal endometrium, where the trophectoderm layer of the blastocyst must undergo syncytial fusion to form the primitive syncytia/syncytiotrophoblasts to promote implantation. The second phase occurs throughout pregnancy, where the underlying cytotrophoblasts continuously fuse into the syncytiotrophoblast layer in order to maintain the placental barrier [21].

Given their direct contact with maternal blood in the intervillous space, the syncytiotrophoblasts play a crucial role in regulating the transport of substances between the mother and fetus. As pregnancy progresses, the syncytiotrophoblast layer has also been demonstrated to facilitate exchange at higher rates, through increase in microvilli formation to enhance surface area, and at greater specificity, through apical and basal expression of nutrient and drug transporters (*e.g.,* glucose

transporters, ATP-binding cassette transporters, solute carrier protein transporters, and more) [26]. Syncytiotrophoblasts are also a highly endocrinological cell type, responsible for a variety of secretions that maintain and regulate pregnancy (*e.g.,* hormones, syncytial knots, extracellular vesicles) [27]. Expression of high levels of chorionic gonadotropin, cytokeratin-7, progesterone, and/or estradiol have classically been used to identify syncytiotrophoblast cells (**Figure 2A**).

Extravillous trophoblast (EVT) cells

The EVT lineage emerges as proliferative pressures among the cytotrophoblasts separate a specific population from the basement membrane to form the cell columns of the anchoring villi (**Figure 4**) [28]. EVTs are uniquely capable of anchoring the placenta to the uterine wall, deep uterine invasion, and remodeling the uterine vasculature [20,29]. These functions are enabled in part by increased expression of matrix metalloproteinases and a phenotypic switch known as epithelial-to-mesenchymal transition (EMT) [30,31]. Similar to when tumours undergo malignancy, EMT is governed by a number of upstream signalling cascades (*e.g.,* Fibroblast growth factor, Wnt, transforming growth factor-β) and transcription factors that lead to the down-regulation of epithelial markers (*e.g.,* E-Cadherin, occludins, and zona occludens-1) and up-regulation of mesenchymal markers (*e.g.,* integrins, vimentins, fibronectin, N-cadherins, and more). As the name describes, the result is a transition from a terminal epithelial cell type towards a mobile, dynamic mesenchymal cell type [30]. Expression of high levels of HLA-G have classically been used to identify EVTs (**Figure 2A**) [32].

However, different subpopulations of EVTs are responsible for various roles. Interstitial EVTs are the initial population that emerge from the cell columns to undergo deep invasion through the maternal endometrium and inner third of the myometrium [33]. A complex network of interactions with the maternal immune system, growth factors, and oxygen gradient have been demonstrated to regulate EVTs invasion and localization to uterine vasculature [34-38]. Interstitial EVTs also assist in the anchorage of the placenta to the uterine wall through secretion of extracellular matrices, like matrix-type fibrinoid [39,40]. Once they reach the myometrium, some imaging studies have demonstrated the terminal differentiation of interstitial EVTs into non-invasive, multinucleated, trophoblast giant cells [15,41]. However, this trophoblast cell type has not been extensively studied in the human compared to the rodent [42].

Once within the maternal uterine tissues, they further branch off into several subpopulations [28]. Endovascular EVTs (endoarterial, endovenous, endolymphatic, endoglandular) localize and remodel the various maternal uterine vasculatures. The most studied are the endoarterial EVTs, which infiltrate and displace the arterial vascular and smooth muscle cells to remodel the spiral arteries into large, high-flowing vessels. During the first trimester, they also infiltrate the arterial lumen and form trophoblast plugs to prevent premature blood flow and oxygenation of the placenta [43]. EVTs were recently demonstrated to also remodel maternal veins (endovenous EVTs) and lymphatic system (endolymphatic EVTs) [44]. Endovenous EVTs help establish blood flow from the intervillous space back into maternal

circulation and perhaps facilitate passage of fetal or placental secretions (*e.g.,* free-floating DNA, cells, or exosomes). The current hypothesis for endolymphatic EVTs is that they may help coordinate immune tolerance for the pregnancy, though much more work is required to verify these speculations [28]. Endoglandular EVTs invade uterine glands and merge them into the intervillous space at the beginning of pregnancy to provide nutrition for the fetus in a histiotrophic manner during the first trimester [45].

However, it is important to note that these EVT subpopulations were classified mainly based on localization of the cells within the placenta and uterus. It remains unclear to date whether they possess predetermined trajectories prior to invasion, or if they arbitrarily migrate and assume the subtype after they arrive at a specific location [28]. Single-cell RNA-sequencing performed on 8-week and 24-week placental samples revealed EVT subtypes with distinct transcriptomic signatures while still within the trophoblast cell column [18]. Amongst the 8-week EVT subtypes, subtype 1 was RRM2-positive (DNA replication) and found at the proximal end of the cell column [18]. Subtype 2 was RRM2-negative, SERPINE1-positive and subtype 3 was RRM2-negative, SERPINE1-negative – both found at the distal end of the cell column [18]. From this, we may postulate that either (or both) EVT subtypes 2 and 3 may exhibit the functional phenotypic categorizations of interstitial and endovascular EVTs that others have previously identified (**Figure 2B)**. The two, 24-week EVT subtypes exhibited more complex transcriptomic signatures, where subtype 1 exhibited an invasive, migratory-like gene profile and

subtype 2 exhibited a secretory and stimuli-responsive gene profile [18]. The functional implications of these are not yet known.

Future work must build upon these elegant, emergent approaches by further defining the functional differences between subtypes, collecting samples from larger anatomical regions (*e.g.,* all types of uterine vasculature), and harvesting from more time-points. Such efforts will expand our understanding of the heterogeneous, but orchestrated, functions of placental cells throughout pregnancy.

Placental Microenvironment

In addition to many cells that weave together to form the organ, there are also a multitude of factors surrounding the cells that regulate their function and behaviour through physical or chemical interactions. This collective of non-cellular factors is known as the cellular microenvironment [46]. The microenvironment has been shown to play fundamental roles in dictating basic functions like cell cycle, differentiation, and motility in tumours, immune cells, and stem cells – yet, we possess a poor understanding of its impact on trophoblasts cells [47,48]. In the following section, we will provide a brief review of two major microenvironmental factors: the extracellular matrix and oxygen.

Extracellular matrix (ECM)

The ECM is a network of macromolecules that exist outside of the cell and provides structural and biochemical support. Specific to placentation, the role of the ECM is evident as early on as blastocyst attachment and implantation [49]. Early

immunofluorescence experiments revealed an abundance of fibronectin, laminin, collagens, entactins, and proteoglycans on the surface of the uterine decidua of the mother during the first trimester [50]. Recent proteomic analyses of decellularized, placental ECM have further uncovered protein families and peptide fractions of laminins (0.222-0.44), collagens (0.082-0.14), fibronectin (0.068-0.11), heparin sulfate proteoglycans (0.09), among others [51,52]. These ECM molecules likely assist in various aspects of implantation and placentation, though the significance of their proportionate combination *in vivo* has yet to be identified.

In return, trophoblast cells also possess a variety of mechanisms to modulate and interact with the ECM. For example, the integrins are one of the major interacting partners with the decidual ECM molecules [53], and matrix metalloproteinases may be secreted to degrade and remodel collagens within the ECM [54]. While cell-ECM interactions are speculated to play crucial roles throughout placentation, there remain a limited number of studies investigating their specific influences on trophoblast biology [55]. This is an area truly requiring more research, and we hoped to contribute to that in Chapter 2 of this thesis.

Tissue stiffness is one factor heavily influenced by the ECM known to regulate many aspects of cellular differentiation, behaviour, and even organogenesis. Atomic force microscopy revealed that various reproductive tissues differ in their stiffness at the maternal-fetal interface. For example, the decidua basalis was around 10^3 Pascals and the decidua parietalis, non-pregnant endometrium, and placenta were all around 10^2 Pascals [55]. Mice embryos cultured

on 10^3 Pa polydimethylsiloxane surfaces *in vitro* experienced a significantly increased success rate of development to 2-cell, blastocyst, and hatching blastocyst stages, compared to embryos cultured on 10^6 Pa polystyrene surfaces [56]. In addition to the embryo, we and others hypothesize that the mechanical and biophysical cues that placental trophoblast cells experience can influence their behaviour and function [55]. Collectively, there are a multitude of tunable factors in the placental ECM alongside tissue stiffness, and future work must uncover their roles in dictating development and function.

Oxygen tension

Another major, dynamic microenvironmental factor involved in placentation is the oxygen tension. During the first trimester of pregnancy, oxygen levels in the human placenta averaged 20 mmHg (2-3%), as measured through a probe that transited the vaginal and uterine cavities, directly inserting into placental tissue *in vivo* [57]. This low oxygen environment is crucial for promoting cytotrophoblast proliferation during the first trimester, and premature onset of blood flow and hyperoxygenation was associated with higher risk of miscarriage [58,59]. At around 10-12 weeks, around the end of the first trimester, oxygen levels rise to approximately 50-60 mmHg (6-8%), coinciding with the disintegration of trophoblast plugs and commencement of maternal blood flow into the placenta via the remodelled spiral arteries [16,60]. Direct *in vivo* sampling of blood oxygen levels in the intervillous space have not been attempted beyond the second trimester, likely due to risk of endangering the developing fetus. However, several indirect

measurements provide estimations: From 25-40 weeks, oxygen levels of around 30 mmHg (4%) were calculated, using near-infrared spectroscopy measurements of oxygenated hemoglobin concentration in placental tissue [61]. At 37-40 weeks, oxygen levels of around 30 mmHg (4%) were also calculated, using oxygen measurements of the uterine vein blood (45 mmHg) taken during Caesarean sections divided by a known ratio of 1.5 between the gas levels in uterine vein and intervillous space [62]. Thus, despite this chronically low oxygen environment present in the placenta relative to atmosphere air (21%), there has never been any evidence of detrimental hypoxic damage (*e.g.,* necrosis, compromised energy expenditure), stressing the need to consider states of normoxia and hypoxia in cell- and tissue-specific manners [63,64].

One of the major pathways by which cells sense their oxygen microenvironment is through hypoxia-inducible factors (HIF) and prolyl hydroxylase domain (PHD) enzymes [65]. In brief, oxygen activates PHD, generating a binding site for the von Hippel-Lindau (pVHL) tumor suppressor protein, which is part of a ubiquitin ligase complex. Under oxygenated environments, HIF1/2α is ubiquitinated and targeted for degradation [65]. The scientists who uncovered and characterized this phenomenon, Drs. Kaelin Jr., Ratcliffe, and Semenza, were recently awarded the 2019 Nobel Prize in Physiology or Medicine. Seminal work by Caniggia, et al. [14] and others have demonstrated the critical role of HIF1α in governing the differentiation patterns and behaviours of trophoblasts – highlighting a need to incorporate correct oxygen levels into trophoblast models.

Counter to the common assumption that placental hypoxia causes or is linked with preeclampsia, placental expert Huppertz, et al. [16] argues that no one has ever actually shown measurements of decreased placental oxygen in patients with this pathology. While it is true that low oxygen levels can experimentally inhibit EVT differentiation and function [14], the link between impaired EVT remodeling of spiral arteries and preeclampsia *in vivo* is weak. A newer model of preeclampsia suggests its origins lie in failed villous development and poor syncytiotrophoblast function during early placentation, whereas impaired EVT-remodeling of spiral arteries is more likely associated with intrauterine growth restriction [9]. Even then, there are several reports of hyperoxia associated with preterm birth and intrauterine growth restriction. Measurements of uterine vein blood oxygen levels in Caesarean sections of preterm, intrauterine growth restricted infants revealed calculated intervillous oxygen levels of 42 mmHg (5.5%) at 24-36 weeks, approximately 1.3 times elevated compared to healthy controls (30 mmHg; 4%) [66]. Tissue oxygenation measurements using near-infrared spectroscopy further found calculated placental oxygen levels of 48 mmHg (6.3%) in intrauterine growth-restricted infants compared to 30 mmHg (4%) oxygen levels in healthy controls [61]. Clearly, the etiology of placental diseases and the role of the oxygen microenvironment remains controversial, necessitating the development of novel techniques and models to provide greater accuracy and insight.

Traditional Placental Model Systems

A stronger understanding of the mechanisms underlying placental development and function may unlock many new treatment avenues for prominent pregnancy/placenta-related diseases, and provide better safety profiling of maternal exposure to various drugs or toxins. However, our ability to tackle these issues is highly dependent upon the capabilities of experimental models to accurately recapitulate this complex organ. The ideal model for a human placenta should be discerned based upon the specific scientific question being asked and decided upon based on how well the model can directly address the question. In the following section, we will provide a review of the traditional model systems, and their advantages and limitations.

In vivo animal models

There is a long history of animal experimentation in placental research [67]. Animal modeling is advantageous as researchers are able to investigate developmental progression, complex organ-to-organ interactions, behavioural change, and more in a whole-body system. These variables would be far more challenging, and even impossible in some cases, to study in isolated models.

Larger animals like the non-human primates and sheep were popular in prior decades due to similarities in size, gestational period, and/or cotyledon anatomy, but decreasing accessibility to large-animal facilities in recent years has severely limited their usability [68]. The rodent model is one of the most practical *in vivo* animal models to date due to ease of handling, resemblances in hemochorial and

discoid structure, and trophoblast-directed spiral artery remodeling in the uterus [68-70]. There are also many, validated laboratory tools available to analyze rodent biology, such as antibodies and genetic sequence databases. Among the rodent species, the rat has ben more popular for physiological and anatomical studies given a relatively greater depth of invasion, but the mouse currently remains better optimized for genetic manipulation [71,72].

Despite these advantages, some of the major differences compared to humans include fewer spiral arteries, shallow implantation, a far shorter gestation period of 21 days (which can also be advantageous for rapid data generation), and multiparous gestations [69]. These inhibit the translatability of specific processes, like embryonic implantation and decidualization. Moreover, many animals are not naturally vulnerable to the same placentally-related diseases as humans and require interventions to initiate the disease, such as placenta accreta or carcinoma [73]. Altogether, the notable limitation in animal models is the species-specific differences in placental anatomy and physiology, challenging our ability to translate and apply the findings to humans (**Figure 5**).

Ex vivo human models

The most ideal placenta models must be human-based. However, humans remain difficult to use as *in vivo* systems for pregnancy research given ethical considerations and the risk of invasive experimentation on the fetus. This is subject to change as advanced, non-invasive imaging techniques improve in quality, accessibility, and cost-effectiveness [74-76]. In the meantime, whole human placental

testing is mostly restricted to after the pregnancy has concluded, whether through vaginal delivery, caesarean section, or premature termination. Full placentae may then be obtained and sampled to undergo molecular analyses, or utilized in *ex vivo* perfusion-based systems [67].

For *ex vivo* perfusion experiments, fresh, intact placentae are selected and placed in a temperature-controlled chamber. The artery-vein pairs and intervillous spaces are then catheterized to establish circulation (schematic of circulation and images of perfusion set-up may be seen in **Figure 6**). *Ex vivo* placental perfusion systems have proven their utility for whole-organ studies of maternal-fetal transport [77,78]. However, they are unable to be extensively applied for investigation due to their short lifespan of several hours post-delivery. This further prevents the study of developing processes or dynamic cellular behaviours, such as the migration of EVTs from the anchoring villus and invasion into the endometrium.

In vitro models: Primary villous explants

Alternatively, placental sections or cells may be isolated from the fresh human placenta for longer-term *in vitro* culture as explants or primary cells [67]. Major advantages of using *in vitro* cultures include the ability to isolate specific cell types for study, longer lifespan compared to *ex vivo*, relative ease of manipulation, and greater experimental permissibility to elucidate cellular mechanisms, pathways, and functions.

Explants may be dissected from placentae at any term, and cultured on a tissue culture-treated plastic plate, hydrogel surface (*e.g.,* Matrigel, collagen),

transwell insert, or freely-floating support system [79]. Historically, placental explants have been useful for studying cellular uptake and secretions, transport, cell-cell/cell-matrix interactions, differentiation, and pathologies [67,79-81]. A major advantage is that the native, multicellular structure and milieu may be retained within an *in vitro* setting. However, a major limitation is the inability to discern individual cellular effects and contributions given the heterogenous mixture of cell types present in the explant.

In vitro models: Primary placental cell cultures

For investigations of specific cell types in isolation, primary trophoblast cells (and other placental cell types) may be digested, isolated, and purified from placentae at any term and cultured for a multitude of different applications [82-86]. Primary cultures are particularly useful for elucidating and manipulating cellular mechanisms and molecular pathways. However, the traditional plastic, 2D "petri dish" platform upon which cells are grown has been criticized for producing results that are difficult to translate back to whole organ and body systems [87]. Furthermore, primary cells and explants both have relatively limited proliferative potential (thus cannot be expanded) and are highly dependent on the availability of clinical sources (*e.g.,* availability of placentae from labour and delivery units.)

In vitro models: Trophoblastic cell lines

As a result, scientists were motivated to create surrogate cell lines that could survive and remain robust through longer experimentation. There are three major methods by which cell lines may be immortalized: (1) Isolation of a cancerous cell

line from a tumour in an organ/region of interest (*e.g.,* BeWo or JEG-3 trophoblastic

cells isolated from choriocarcinoma [88-90]), (2) Transfection with a gene that

deregulates cell cycle to favour immortalization (*e.g.,* HTR8/SVneo first trimester

extravillous cell line [91]), and (3) Hybridizing a normal cell with a cancerous one

(ACH1P created from fusion of primary trophoblast cells with AC1-1

choriocarcinoma [92].) Cancerous and immortalized cell lines have demonstrated

immense value throughout scientific history, possessing the same advantages as

primary cells in enabling extensive manipulations of cell biology and deep

elucidations of the mechanisms that underlie various physiology and disease [93]. For

comprehensive reviews of the available placental cell lines, please refer to Orendi,

et al. [94] and Huckle [95].

One of the most extensively-published and characterized is the BeWo

trophoblastic cell line, which was originally derived from human choriocarcinoma

[89,90]. BeWo cells have retained impressive functions native to human villous

cytotrophoblasts such as syncytial fusion [96], placental hormone secretion (*e.g.,*

human chorionic gonadotropin, placental lactogen, estradiol, progesterone [94,97]),

microvilli formation [98,99], and polarity of transport [98-100]. There are several

biochemical factors known to induce syncytial fusion in placental trophoblast cells.

Growth factors, including epidermal growth factor (EGF), vascular endothelial

growth factor (VEGF), placental growth factor (PlGF), insulin-like growth factor

(IGF), and others, have been demonstrated to act at the placental barrier, potentially

facilitating syncytial fusion. Indeed, EGF and VEGF were shown to promote

syncytial fusion *in vitro* in primary cytotrophoblasts [101], and monolayer formation in BeWo cells [102]. Additionally, cell-permeable derivatives of cyclic adenosine monophosphate (cAMP), cAMP analogues (8-Br-cAMP, dibutyryl-cAMP), and forskolin have also been demonstrated to induce syncytial fusion in BeWo cells, where forskolin was frequently reported as an effective agent for short-term syncytial fusion [103-105]. Forskolin induces fusion by activating adenylate cyclase to elevate intracellular cAMP levels, and is advantageous in that it provides a highly-controlled manner to induce fusion compared to the spontaneous fusion that occurs in primary cytotrophoblasts. Numerous studies have further profiled the specific transcriptomic, epigenomic, and proteomic landscapes associated with forskolin-mediated fusion in BeWo cells [97,105-109].

However, cell lines have also received heavy criticisms in that they possess carcinogenic factors, may have deviated in genotype and phenotype due to their long history of use [94], and may contain heterogenous cell populations if not maintained well [93]. Thus, results from cell line research has been increasingly dismissed as irrelevant to human physiology [67,110]. This common lack of translatability from many preclinical models to whole human systems poses as a serious hindrance not only for academic research, but also for drug development and industrial applications [111]. This ultimately carries implications for the innovation and advancement of pregnancy healthcare, revealing the dire need to develop novel, human cell-based platforms for placental investigation.

Alternative microphysiological models

The National Institute of Child Health and Human Development launched the "Human Placenta Project" in 2014, a global initiative urging the necessity of multidisciplinary, collaborative human placental research [112]. Motivated in part by the limitations that plague today's placental model systems, one of the major aims of the Human Placenta Project was to facilitate new collaborations between different disciplines to lead to the creation of alternative biological models and platforms [95]. The simplicity of traditional *in vitro* culture had served its purpose for the last century, but placental research must now embrace modern technologies and partnerships to progress in biomedical sophistication, physiological accuracy, and clinical translatability.

Three-dimensional (3D) culture: Spheroids and organoids

Spheroid and organoid formation (also referred to in literature as 3D culture or mini/micro-tissues) involves the culturing of cells in 3D aggregates [113]. In contrast to two-dimensional (2D) cultures, 3D cultures have been shown to better reflect the phenotypes redolent of their respective organs [87,113-116]. In particular, spheroid and organoid cultures enable the restoration of features such as tissue-specific cell density, microarchitecture, and cell-cell and cell-ECM interactions that are often absent in 2D. As a result, 3D cultures have also been demonstrated to enable more *in vivo*-like function, drug and toxin resistance, and invasive behaviour in both organ and tumour research [113,117-119]. A major difference between the two terms is that organoid culture often refers to the use of undifferentiated, stem or

progenitor cells as the starting cell type that is then differentiated into a specific, functional cell types through the culture platform, whereas spheroid culture is more generalizable to any type of sphere-like, 3D culturing.

While organoid and spheroid cultures remain in infancy in the placental field, some notable studies were recently published. Haider, et al. [120] cultured primary, first-trimester cytotrophoblasts as stem-like organoids using Matrigel and a unique organoid media. They demonstrated comparable gene expression profiles as primary cytotrophoblasts and the capacity to differentiate across trophoblast lineages through alterations in the media formulation. Interestingly, they also characterized the role of Wnt in directing differentiation into EVTs [120]. Turco, et al. [121] followed up with a publication several months later, similarly culturing primary cytotrophoblasts as organoids using Matrigel and a unique organoid media. They use extensive transcriptomic, methylomic, and secretomic analyses to compare their organoids with first trimester placental villi. They also demonstrate the ability of their organoids to differentiate into syncytiotrophoblasts and invasive, HLA-G-expressing EVTs, and impressively maintain in culture for up to a year [121]. Nandi, et al. [122] formed trophoblast spheroids using HTR8/SVneo and primary placental cells that could be propagated multiple times and differentiated down various lineages (*e.g.,* syncytiotrophoblast). They further apply their model to study decorin and its role in trophoblast self-renewal and differentiation [122]. Lastly, we contributed our own work to this field by developing an invasive, EVT spheroid

model that could be applied for drug and toxin screening (further discussed in Chapter 3 [123]). Several other spheroid publications may be found here [124-128].

Organ-on-a-chip platforms

"Organ-on-a-chip" is another novel paradigm that aims to recreate fundamental units of human organs within *in vitro* platforms. The original promise of organ-on-a-chip was centered around its intentional design of cellular architecture using microfluidic engineering and other advanced fabrication techniques, leading to the creation of systems that are more anatomically-accurate and dynamic [129]. In its simplest form, organ-on-a-chip devices consist of hollow, microfluidic channels etched within polymeric units (*i.e.,* polydimethylsiloxane; PDMS) that sandwich a semi-porous membrane. Cells may then be seeded onto contralateral sides of the membranes to form confluent layers, and media may be perfused through the microfluidic channels using a syringe pump or gravity flow system to supply nutrients for the cells (**Figure 7**). Excitement around the utility of organ-on-a-chip platforms has soared since the pioneering Lung-on-a-Chip publication in *Science* by Huh, et al. [130]. In the last decade, the number of organ-on-a-chip publications on PubMed has grown from single digits in 2010, to around 40 per year in 2015, to over 150 per year in 2019 (**Figure 8**).

At the current stage, the majority of organ-on-a-chip devices are personally designed by the researcher using a computer-aided design (CAD) software and fabricated in-house. However, professional manufacturing companies, such as Emulate, Mimetas, CNBio Innovations, TARA Biosystems, and Z-Microsystems,

are beginning to emerge into the market. The microarchitectural design, channel shape and size, flow rate, and cell types will vary depending on the organ system being modelled. Organ-on-chip devices are currently most readily applied to mimic highly perfused barrier units within the body (*e.g.,* blood-air interface of alveoli in lung, gut barrier) [130,131]. They carry the promise to entirely replace conventional cell cultures in organ investigation and pre-clinical drug discovery, and may better complement animal and human testing [132].

Several placenta-on-a-chip device prototypes have been published in recent years to model the placental barrier, demonstrating a rapidly growing interest in the reproduction field [98,99,133-137]. The majority of devices follow the classic, two-channel design (**Figure 9A-E**) and demonstrate capabilities in microvilli formation [134], bacterial infection and inflammatory response [137], and maternal-fetal transport of glucose [99,133], glyburide [98], heparin [98], caffeine [136], and nanoparticles [135]. One of the major disadvantages of the aforementioned placenta-on-a-chip prototypes is the inability to emulate the maternal intervillous space. Microfluidic technology is proficient at reinstating capillary-like flow dynamics into cell culture, which is advantageous for the fetal capillaries within the terminal villi, but the maternal intervillous space that the syncytiotrophoblast layer is exposed to is a slow-flowing pool mixing oxygenated and deoxygenated blood [2] (**Figure 9B, C**). The closest representation may be found in the model by Miura, et al. [134], where a wide, circular channel is used instead of the narrow, linear channel used in all other designs. While there is no evidence to date to validate nor invalidate the use of a microfluidic

channel to model the maternal space, it certainly does not represent it well anatomically [2].

3D bioprinting

3D bioprinting is a technique commonly applied in tissue engineering, but has recently emerged in experimental model construction. Bioprinting is the precise positioning and deposition of live cells embedded within a biomaterial scaffold (*e.g.,* hydrogel, extracellular matrix cocktail) to fabricate 3D-layered constructs [138]. One of the major promises of this technique is the ability to custom-design complex, functional tissues that resemble the architecture within the organ [138]. This is most commonly performed by designing the desired construct on a computer-aided design software and fabricating using an extrusion-based printer (*e.g.,* inkjet), though more advanced systems are being developed regularly (*e.g.,* laser-assisted) [139]. Generally, a cell type of interest will be mixed into a scaffolding biomaterial in liquid form to create the "bioink" [140]. Biomaterial scaffolds are used as the delivery medium and assist in handling of the cells to be bioprinted [140]. The bioink is then loaded into the 3D bioprinter and extruded in a precise pattern based on the design created via computer-aided design. The precision, resolution, size, and depth of the printed construct depends heavily on the printer's capabilities. The printed construct will then be cured through a means specific to the scaffolding material (*e.g.,* temperature, ultraviolet light, or exposure to a curing agent) [139,141-143].

To date, there has only been one main research group building 3D-bioprinted placental models [51,144-146]. Using gelatin methacrylate as their base

hydrogel scaffolding material, they demonstrated the bioprinting of BeWo cells [51,145,146] and HTR8 cells [51] to study various aspects of placental barrier function and EVT invasion. One potential limitation is the requirement of ultraviolet light to cure gelatin methacrylate into a solid construct, which may risk introducing DNA damage in the cells. To overcome this risk, a variety of other available biomaterials may be considered as the scaffold [140]. Additionally, 3D bioprinting may be prohibitive to many research labs given the cost of biomaterials and the 3D printer, and a general lack of training with computer-aided design software amongst biologists and clinicians. As these barriers-to-entry decrease, we will begin to see greater advancements in this promising approach.

Hypothesis

Ultimately, this all raised the central question: What if we could enable better investigations of placental biology and function through focusing on the design and development of more anatomically- and physiologically-relevant *in vitro* platforms?

We hypothesized that the development of *in vitro* models that better incorporated the structural anatomy and microenvironment of the placenta will provide more physiologically-relevant, investigations of human placental function.

Objectives

The **long-term objective** was to build and characterize novel microphysiological platforms to model the human placenta, and assess their utility in investigating various placental functions compared to traditional models.

The **short-term objectives** were:

1. To investigate trophoblast self-assembly and syncytial fusion through the manipulation of extracellular matrix thickness.

2. To investigate extravillous trophoblast invasion and drug and toxin response through the development of a 3D invading spheroid system.

3. To investigate placental barrier transport through the development of a trophoblast-endothelial co-culture platform, and the impact of physiologically-low oxygen tension on placental barrier formation and function.

References

1   Burton, G. J. & Fowden, A. L. The placenta: a multifaceted, transient organ. *Philosophical transactions of the Royal Society of London. Series B, Biological sciences* **370**, 20140066, doi:10.1098/rstb.2014.0066 (2015).

2   Huppertz, B., Ghosh, D. & Sengupta, J. An integrative view on the physiology of human early placental villi. *Prog Biophys Mol Biol* **114**, 33-48, doi:10.1016/j.pbiomolbio.2013.11.007 (2014).

3   James, J. L., Carter, A. M. & Chamley, L. W. Human placentation from nidation to 5 weeks of gestation. Part I: What do we know about formative placental development following implantation? *Placenta* **33**, 327-334, doi:10.1016/j.placenta.2012.01.020 (2012).

4   Huppertz, B. The anatomy of the normal placenta. *J Clin Pathol* **61**, 1296-1302, doi:10.1136/jcp.2008.055277 (2008).

5   Boss, A. L., Chamley, L. W. & James, J. L. Placental formation in early pregnancy: how is the centre of the placenta made? *Hum Reprod Update* **24**, 750-760, doi:10.1093/humupd/dmy030 (2018).

6   Capellini, I., Venditti, C. & Barton, R. A. Placentation and maternal investment in mammals. *Am Nat* **177**, 86-98, doi:10.1086/657435 (2011).

7   Salavati, N. *et al.* The Possible Role of Placental Morphometry in the Detection of Fetal Growth Restriction. *Front Physiol* **9**, 1884, doi:10.3389/fphys.2018.01884 (2018).

8   Griffiths, S. K. & Campbell, J. P. Placental structure, function and drug transfer. *Continuing Education in Anaesthesia Critical Care & Pain* **15**, 84-89, doi:10.1093/bjaceaccp/mku013 (2015).

9   Huppertz, B. Placental origins of preeclampsia: challenging the current hypothesis. *Hypertension* **51**, 970-975, doi:10.1161/HYPERTENSIONAHA.107.107607 (2008).

10   Wallace, A. E., Host, A. J., Whitley, G. S. & Cartwright, J. E. Decidual natural killer cell interactions with trophoblasts are impaired in pregnancies at increased risk of preeclampsia. *The American journal of pathology* **183**, 1853-1861, doi:10.1016/j.ajpath.2013.08.023 (2013).

11   Wallace, A. E., Fraser, R. & Cartwright, J. E. Extravillous trophoblast and decidual natural killer cells: a remodelling partnership. *Hum Reprod Update* **18**, 458-471, doi:10.1093/humupd/dms015 (2012).

12   Smith, S. D., Dunk, C. E., Aplin, J. D., Harris, L. K. & Jones, R. L. Evidence for immune cell involvement in decidual spiral arteriole remodeling in early human pregnancy. *The American journal of pathology* **174**, 1959-1971, doi:10.2353/ajpath.2009.080995 (2009).

13   Roberts, V. H. J. *et al.* Early first trimester uteroplacental flow and the progressive disintegration of spiral artery plugs: new insights from contrast-enhanced ultrasound and tissue histopathology. *Hum Reprod* **32**, 2382-2393, doi:10.1093/humrep/dex301 (2017).

14   Caniggia, I., Winter, J., Lye, S. J. & Post, M. Oxygen and placental development during the first trimester: implications for the pathophysiology of pre-eclampsia. *Placenta* **21 Suppl A**, S25-30, doi:10.1053/plac.1999.0522 (2000).

15   Knofler, M. *et al.* Human placenta and trophoblast development: key molecular mechanisms and model systems. *Cellular and molecular life sciences : CMLS* **76**, 3479-3496, doi:10.1007/s00018-019-03104-6 (2019).

16   Huppertz, B., Weiss, G. & Moser, G. Trophoblast invasion and oxygenation of the placenta: measurements versus presumptions. *J Reprod Immunol* **101-102**, 74-79, doi:10.1016/j.jri.2013.04.003 (2014).

17   Gamage, T. K., Chamley, L. W. & James, J. L. Stem cell insights into human trophoblast lineage differentiation. *Hum Reprod Update* **23**, 77-103, doi:10.1093/humupd/dmw026 (2016).

18   Liu, Y. *et al.* Single-cell RNA-seq reveals the diversity of trophoblast subtypes and patterns of differentiation in the human placenta. *Cell Res* **28**, 819-832, doi:10.1038/s41422-018-0066-y (2018).

19   Mayhew, T. M. *et al.* Proliferation, differentiation and apoptosis in villous trophoblast at 13-41 weeks of gestation (including observations on annulate lamellae and nuclear pore complexes). *Placenta* **20**, 407-422, doi:10.1053/plac.1999.0399 (1999).

20   Tarrade, A. *et al.* Characterization of human villous and extravillous trophoblasts isolated from first trimester placenta. *Lab Invest* **81**, 1199-1211 (2001).

21   Gerbaud, P. & Pidoux, G. Review: An overview of molecular events occurring in human trophoblast fusion. *Placenta* **36 Suppl 1**, S35-42, doi:10.1016/j.placenta.2014.12.015 (2015).

22   Aguilar, P. S. *et al.* Genetic basis of cell-cell fusion mechanisms. *Trends Genet* **29**, 427-437, doi:10.1016/j.tig.2013.01.011 (2013).

23   van den Eijnde, S. M. *et al.* Transient expression of phosphatidylserine at cell-cell contact areas is required for myotube formation. *Journal of Cell Science* **114**, 3631-3642 (2001).

24   Vignery, A. Osteoclasts and giant cells: macrophage-macrophage fusion mechanism. *Int J Exp Pathol* **81**, 291-304 (2000).

25   Kliman, H. J., Nestler, J. E., Sermasi, E., Sanger, J. M. & Strauss, J. F., 3rd. Purification, characterization, and in vitro differentiation of cytotrophoblasts from human term placentae. *Endocrinology* **118**, 1567-1582, doi:10.1210/endo-118-4-1567 (1986).

26   Liu, L. & Liu, X. Contributions of Drug Transporters to Blood-Placental Barrier. *Advances in experimental medicine and biology* **1141**, 505-548, doi:10.1007/978-981-13-7647-4_11 (2019).

27   Han, C. *et al.* Syncytiotrophoblast-Derived Extracellular Vesicles in Pathophysiology of Preeclampsia. *Front Physiol* **10**, 1236, doi:10.3389/fphys.2019.01236 (2019).

28   Moser, G., Windsperger, K., Pollheimer, J., de Sousa Lopes, S. C. & Huppertz, B. Human trophoblast invasion: new and unexpected routes and functions. *Histochem Cell Biol* **150**, 361-370, doi:10.1007/s00418-018-1699-0 (2018).

29   James, J. L., Stone, P. R. & Chamley, L. W. Cytotrophoblast differentiation in the first trimester of pregnancy: evidence for separate progenitors of extravillous trophoblasts and syncytiotrophoblast. *Reproduction* **130**, 95-103, doi:10.1530/rep.1.00723 (2005).

30   Davies, J. E. *et al.* Epithelial-mesenchymal transition during extravillous trophoblast differentiation. *Cell Adh Migr* **10**, 310-321, doi:10.1080/19336918.2016.1170258 (2016).

31   Huppertz, B., Kertschanska, S., Demir, A. Y., Frank, H. G. & Kaufmann, P. Immunohistochemistry of matrix metalloproteinases (MMP), their substrates, and their inhibitors (TIMP) during trophoblast invasion in the human placenta. *Cell Tissue Res* **291**, 133-148, doi:10.1007/s004410050987 (1998).

32   Moser, G. *et al.* The art of identification of extravillous trophoblast. *Placenta* **32**, 197-199, doi:10.1016/j.placenta.2010.11.008 (2011).

33   Kaufmann, P., Black, S. & Huppertz, B. Endovascular trophoblast invasion: implications for the pathogenesis of intrauterine growth retardation and preeclampsia. *Biology of reproduction* **69**, 1-7, doi:10.1095/biolreprod.102.014977 (2003).

34   Weiss, G., Huppertz, B., Siwetz, M., Lang, I. & Moser, G. Arterial endothelial cytokines guide extravillous trophoblast invasion towards spiral arteries; an in-vitro study with the trophoblast cell line ACH-3P and female non-uterine endothelial cells. *Placenta* **38**, 49-56, doi:10.1016/j.placenta.2015.12.010 (2016).

35   Champion, H., Innes, B. A., Robson, S. C., Lash, G. E. & Bulmer, J. N. Effects of interleukin-6 on extravillous trophoblast invasion in early human pregnancy. *Mol Hum Reprod* **18**, 391-400, doi:10.1093/molehr/gas010 (2012).

36   Knofler, M. Critical growth factors and signalling pathways controlling human trophoblast invasion. *Int J Dev Biol* **54**, 269-280, doi:10.1387/ijdb.082769mk (2010).

37   Pringle, K. G., Kind, K. L., Sferruzzi-Perri, A. N., Thompson, J. G. & Roberts, C. T. Beyond oxygen: complex regulation and activity of hypoxia inducible factors in pregnancy. *Hum Reprod Update* **16**, 415-431, doi:10.1093/humupd/dmp046 (2010).

38   Librach, C. L. *et al.* Interleukin-1 beta regulates human cytotrophoblast metalloproteinase activity and invasion in vitro. *The Journal of biological chemistry* **269**, 17125-17131 (1994).

39   Huppertz, B. *et al.* Extracellular matrix components of the placental extravillous trophoblast: immunocytochemistry and ultrastructural distribution. *Histochem Cell Biol* **106**, 291-301 (1996).

40   Kaufmann, P., Huppertz, B. & Frank, H. G. The fibrinoids of the human placenta: origin, composition and functional relevance. *Annals of anatomy = Anatomischer Anzeiger : official organ of the Anatomische Gesellschaft* **178**, 485-501, doi:10.1016/s0940-9602(96)80102-6 (1996).

41   al-Lamki, R. S., Skepper, J. N. & Burton, G. J. Are human placental bed giant cells merely aggregates of small mononuclear trophoblast cells? An ultrastructural and immunocytochemical study. *Hum Reprod* **14**, 496-504, doi:10.1093/humrep/14.2.496 (1999).

42   Hu, D. & Cross, J. C. Development and function of trophoblast giant cells in the rodent placenta. *Int J Dev Biol* **54**, 341-354, doi:10.1387/ijdb.082768dh (2010).

43   Weiss, G., Sundl, M., Glasner, A., Huppertz, B. & Moser, G. The trophoblast plug during early pregnancy: a deeper insight. *Histochem Cell Biol* **146**, 749-756, doi:10.1007/s00418-016-1474-z (2016).

44   He, N. *et al.* Human Extravillous Trophoblasts Penetrate Decidual Veins and Lymphatics before Remodeling Spiral Arteries during Early Pregnancy. *PloS one* **12**, e0169849, doi:10.1371/journal.pone.0169849 (2017).

45   Moser, G., Weiss, G., Gauster, M., Sundl, M. & Huppertz, B. Evidence from the very beginning: endoglandular trophoblasts penetrate and replace uterine glands in situ and in vitro. *Hum Reprod* **30**, 2747-2757, doi:10.1093/humrep/dev266 (2015).

46   Barthes, J. *et al.* Cell microenvironment engineering and monitoring for tissue engineering and regenerative medicine: the recent advances. *Biomed Res Int* **2014**, 921905, doi:10.1155/2014/921905 (2014).

47   Gong, Q. *et al.* Importance of cellular microenvironment and circulatory dynamics in B cell immunotherapy. *J Immunol* **174**, 817-826, doi:10.4049/jimmunol.174.2.817 (2005).

48   Sun, Y., Chen, C. S. & Fu, J. Forcing stem cells to behave: a biophysical perspective of the cellular microenvironment. *Annu Rev Biophys* **41**, 519-542, doi:10.1146/annurev-biophys-042910-155306 (2012).

49   Armant, D. R. Blastocysts don't go it alone. Extrinsic signals fine-tune the intrinsic developmental program of trophoblast cells. *Dev Biol* **280**, 260-280, doi:10.1016/j.ydbio.2005.02.009 (2005).

50   Kisalus, L. L., Herr, J. C. & Little, C. D. Immunolocalization of extracellular matrix proteins and collagen synthesis in first-trimester human decidua. *The Anatomical Record* **218**, 402-415 (1987).

51   Kuo, C. Y. *et al.* Placental basement membrane proteins are required for effective cytotrophoblast invasion in a three-dimensional bioprinted placenta model. *J Biomed Mater Res A* **106**, 1476-1487, doi:10.1002/jbm.a.36350 (2018).

52   Arumugasaamy, N., Gudelsky, A., Hurley-Novatny, A., Kim, P. C. W. & Fisher, J. P. Model Placental Barrier Phenotypic Response to Fluoxetine and Sertraline: A Comparative Study. *Adv Healthc Mater* **8**, e1900476, doi:10.1002/adhm.201900476 (2019).

53   Wang, J. & Armant, D. R. Integrin-mediated adhesion and signaling during blastocyst implantation. *Cells Tissues Organs* **172**, 190-201, doi:10.1159/000066970 (2002).

54   Cohen, M., Meisser, A. & Bischof, P. Metalloproteinases and human placental invasiveness. *Placenta* **27**, 783-793, doi:10.1016/j.placenta.2005.08.006 (2006).

55   Abbas, Y. *et al.* Tissue stiffness at the human maternal-fetal interface. *Hum Reprod* **34**, 1999-2008, doi:10.1093/humrep/dez139 (2019).

56   Kolahi, K. S. *et al.* Effect of substrate stiffness on early mouse embryo development. *PloS one* **7**, e41717, doi:10.1371/journal.pone.0041717 (2012).

57   Rodesch, F., Simon, P., Donner, C. & Jauniaux, E. Oxygen measurements in endometrial and trophoblastic tissues during early pregnancy. *Obstet Gynecol* **80**, 283-285 (1992).

58   Genbacev, O., Zhou, Y., Ludlow, J. W. & Fisher, S. J. Regulation of human placental development by oxygen tension. *Science* **277**, 1669-1672, doi:10.1126/science.277.5332.1669 (1997).

59   Zhou, S., Xie, Y., Puscheck, E. E. & Rappolee, D. A. Oxygen levels that optimize TSC culture are identified by maximizing growth rates and minimizing stress. *Placenta* **32**, 475-481, doi:10.1016/j.placenta.2011.03.013 (2011).

60   Jauniaux, E. *et al.* Onset of Maternal Arterial Blood Flow and Placental Oxidative Stress. *The American journal of pathology* **157**, 2111-2122, doi:10.1016/s0002-9440(10)64849-3 (2000).

61   Kakogawa, J., Sumimoto, K., Kawamura, T., Minoura, S. & Kanayama, N. Noninvasive monitoring of placental oxygenation by near-infrared spectroscopy. *Am J Perinatol* **27**, 463-468, doi:10.1055/s-0030-1247600 (2010).

62   Schaaps, J. P. *et al.* Shunting the intervillous space: new concepts in human uteroplacental vascularization. *American journal of obstetrics and gynecology* **192**, 323-332, doi:10.1016/j.ajog.2004.06.066 (2005).

63   Burton, G. J., Jauniaux, E. & Murray, A. J. Oxygen and placental development; parallels and differences with tumour biology. *Placenta* **56**, 14-18, doi:10.1016/j.placenta.2017.01.130 (2017).

64   Cindrova-Davies, T. *et al.* Energy status and HIF signalling in chorionic villi show no evidence of hypoxic stress during human early placental development. *Mol Hum Reprod* **21**, 296-308, doi:10.1093/molehr/gau105 (2015).

65   Kaelin, W. G., Jr. & Ratcliffe, P. J. Oxygen sensing by metazoans: the central role of the HIF hydroxylase pathway. *Mol Cell* **30**, 393-402, doi:10.1016/j.molcel.2008.04.009 (2008).

66   Sibley, C. P. *et al.* Pathogenesis of intrauterine growth restriction (IUGR)-conclusions derived from a European Union Biomed 2 Concerted Action project 'Importance of Oxygen Supply in Intrauterine Growth Restricted

Pregnancies'-a workshop report. *Placenta* **23 Suppl A**, S75-79, doi:10.1053/plac.2002.0796 (2002).

67   Gohner, C. *et al.* The placenta in toxicology. Part IV: Battery of toxicological test systems based on human placenta. *Toxicol Pathol* **42**, 345-351, doi:10.1177/0192623313482206 (2014).

68   Grigsby, P. L. Animal Models to Study Placental Development and Function throughout Normal and Dysfunctional Human Pregnancy. *Semin Reprod Med* **34**, 11-16, doi:10.1055/s-0035-1570031 (2016).

69   Soares, M. J., Chakraborty, D., Karim Rumi, M. A., Konno, T. & Renaud, S. J. Rat placentation: an experimental model for investigating the hemochorial maternal-fetal interface. *Placenta* **33**, 233-243, doi:10.1016/j.placenta.2011.11.026 (2012).

70   Caluwaerts, S., Vercruysse, L., Luyten, C. & Pijnenborg, R. Endovascular trophoblast invasion and associated structural changes in uterine spiral arteries of the pregnant rat. *Placenta* **26**, 574-584, doi:10.1016/j.placenta.2004.09.007 (2005).

71   Fonseca, B. M., Correia-da-Silva, G. & Teixeira, N. A. The rat as an animal model for fetoplacental development: a reappraisal of the post-implantation period. *Reproductive Biology* **12**, 97-118, doi:10.1016/s1642-431x(12)60080-1 (2012).

72   Malassine, A., Frendo, J. L. & Evain-Brion, D. A comparison of placental development and endocrine functions between the human and mouse model. *Hum Reprod Update* **9**, 531-539, doi:DOI 10.1093/humupd/dmg043 (2003).

73   Chen, Y. *et al.* The depletion of MARVELD1 leads to murine placenta accreta via integrin beta4-dependent trophoblast cell invasion. *J Cell Physiol* **233**, 2257-2269, doi:10.1002/jcp.26098 (2018).

74   Slator, P. *et al.* Placenta Imaging Workshop 2018 report: Multiscale and multimodal approaches. *Placenta* **79**, 78-82, doi:10.1016/j.placenta.2018.10.010 (2019).

75   Wu, C. & Bayer, C. L. Imaging placental function: current technology, clinical needs, and emerging modalities. *Phys Med Biol* **63**, 14TR01, doi:10.1088/1361-6560/aaccd9 (2018).

76   Andescavage, N. N., du Plessis, A. & Limperopoulos, C. Advanced MR imaging of the placenta: Exploring the in utero placenta-brain connection. *Seminars in perinatology* **39**, 113-123, doi:10.1053/j.semperi.2015.01.004 (2015).

77   Mandelbrot, L. *et al.* Placental transfer and tissue accumulation of dolutegravir in the ex vivo human cotyledon perfusion model. *PloS one* **14**, e0220323, doi:10.1371/journal.pone.0220323 (2019).

78   Dallmann, A., Liu, X. I., Burckart, G. J. & van den Anker, J. Drug Transporters Expressed in the Human Placenta and Models for Studying Maternal-Fetal Drug Transfer. *J Clin Pharmacol* **59 Suppl 1**, S70-S81, doi:10.1002/jcph.1491 (2019).

79   Miller, R. K. *et al.* Human placental explants in culture: approaches and assessments. *Placenta* **26**, 439-448, doi:10.1016/j.placenta.2004.10.002 (2005).

80   Wat, J. M., Hawrylyshyn, K., Baczyk, D., Greig, I. R. & Kingdom, J. C. Effects of glycol-split low molecular weight heparin on placental, endothelial, and anti-inflammatory pathways relevant to preeclampsia. *Biology of reproduction* **99**, 1082-1090, doi:10.1093/biolre/ioy127 (2018).

81   Liu, H. *et al.* Estimation of the burden of human placental micro- and nano-vesicles extruded into the maternal blood from 8 to 12 weeks of gestation. *Placenta* **72-73**, 41-47, doi:10.1016/j.placenta.2018.10.009 (2018).

82   Huang, X. *et al.* Establishment of a confluent monolayer model with human primary trophoblast cells: novel insights into placental glucose transport. *Mol Hum Reprod* **22**, 442-456, doi:10.1093/molehr/gaw018 (2016).

83   Sagrillo-Fagundes, L. *et al.* Human Primary Trophoblast Cell Culture Model to Study the Protective Effects of Melatonin Against Hypoxia/reoxygenation-induced Disruption. *J Vis Exp*, doi:10.3791/54228 (2016).

84   Morrish, D. W. *et al.* In vitro cultured human term cytotrophoblast: a model for normal primary epithelial cells demonstrating a spontaneous differentiation programme that requires EGF for extensive development of syncytium. *Placenta* **18**, 577-585 (1997).

85   Kaitu'u-Lino, T. J. *et al.* Characterization of protocols for primary trophoblast purification, optimized for functional investigation of sFlt-1 and soluble endoglin. *Pregnancy Hypertens* **4**, 287-295, doi:10.1016/j.preghy.2014.09.003 (2014).

86   Highet, A. R. *et al.* First trimester trophoblasts forming endothelial-like tubes in vitro emulate a 'blood vessel development' gene expression profile. *Gene Expr Patterns*, doi:10.1016/j.gep.2016.05.001 (2016).

87   Shamir, E. R. & Ewald, A. J. Three-dimensional organotypic culture: experimental models of mammalian biology and disease. *Nature reviews. Molecular cell biology* **15**, 647-664, doi:10.1038/nrm3873 (2014).

88   Rothbauer, M. *et al.* A comparative study of five physiological key parameters between four different human trophoblast-derived cell lines. *Scientific reports* **7**, 5892, doi:10.1038/s41598-017-06364-z (2017).

89   Pattillo, R. A. & Gey, G. O. The establishment of a cell line of human hormone-synthesizing trophoblastic cells in vitro. *Cancer research* **28**, 1231-1236 (1968).

90   Hertz, R. Choriocarcinoma of Women Maintained in Serial Passage in Hamster and Rat. *Proceedings of the Society for Experimental Biology and Medicine* **102**, 77-81, doi:10.3181/00379727-102-25149 (1959).

91   Graham, C. H. *et al.* Establishment and characterization of first trimester human trophoblast cells with extended lifespan. *Experimental cell research* **206**, 204-211 (1993).

92   Frank, H. G. *et al.* Cytogenetic and DNA-fingerprint characterization of choriocarcinoma cell lines and a trophoblast/choriocarcinoma cell hybrid. *Cancer Genet Cytogenet* **116**, 16-22, doi:10.1016/s0165-4608(99)00107-7 (2000).

93   Maqsood, M. I., Matin, M. M., Bahrami, A. R. & Ghasroldasht, M. M. Immortality of cell lines: challenges and advantages of establishment. *Cell Biol Int* **37**, 1038-1045, doi:10.1002/cbin.10137 (2013).

94   Orendi, K. *et al.* Placental and trophoblastic in vitro models to study preventive and therapeutic agents for preeclampsia. *Placenta* **32 Suppl**, S49-54, doi:10.1016/j.placenta.2010.11.023 (2011).

95   Huckle, W. R. Cell- and Tissue-Based Models for Study of Placental Development. *Progress in molecular biology and translational science* **145**, 29-37, doi:10.1016/bs.pmbts.2016.12.002 (2017).

96   Kudo, Y. *et al.* Quantifying the syncytialisation of human placental trophoblast BeWo cells grown in vitro. *Biochimica et Biophysica Acta (BBA) - Molecular Cell Research* **1640**, 25-31, doi:10.1016/s0167-4889(03)00004-1 (2003).

97   Orendi, K., Gauster, M., Moser, G., Meiri, H. & Huppertz, B. The choriocarcinoma cell line BeWo: syncytial fusion and expression of syncytium-specific proteins. *Reproduction* **140**, 759-766, doi:10.1530/REP-10-0221 (2010).

98   Blundell, C. *et al.* Placental Drug Transport-on-a-Chip: A Microengineered In Vitro Model of Transporter-Mediated Drug Efflux in the Human Placental Barrier. *Adv Healthc Mater* **7**, doi:10.1002/adhm.201700786 (2018).

99   Blundell, C. *et al.* A microphysiological model of the human placental barrier. *Lab Chip*, doi:10.1039/c6lc00259e (2016).

100   Li, H., van Ravenzwaay, B., Rietjens, I. M. & Louisse, J. Assessment of an in vitro transport model using BeWo b30 cells to predict placental transfer of compounds. *Arch Toxicol* **87**, 1661-1669, doi:10.1007/s00204-013-1074-9 (2013).

101   Crocker, I. P. *et al.* Vascular endothelial growth factor but not placental growth factor promotes trophoblast syncytialization in vitro. *Journal of the Society for Gynecologic Investigation* **8**, 341-346 (2001).

102   Crowe, A. & Keelan, J. A. Development of a model for functional studies of ABCG2 (breast cancer resistance protein) efflux employing a standard BeWo clone (B24). *Assay Drug Dev Technol* **10**, 476-484, doi:10.1089/adt.2011.441 (2012).

103   Seamon, K. B., Padgett, W. & Daly, J. W. Forskolin: unique diterpene activator of adenylate cyclase in membranes and in intact cells. *Proceedings of the National Academy of Sciences of the United States of America* **78**, 3363-3367 (1981).

104   Wice, B., Menton, D., Geuze, H. & Schwartz, A. L. Modulators of cyclic AMP metabolism induce syncytiotrophoblast formation in vitro. *Experimental cell research* **186**, 306-316 (1990).

105   Al-Nasiry, S., Spitz, B., Hanssens, M., Luyten, C. & Pijnenborg, R. Differential effects of inducers of syncytialization and apoptosis on BeWo and JEG-3 choriocarcinoma cells. *Hum Reprod* **21**, 193-201, doi:10.1093/humrep/dei272 (2006).

106   Msheik, H. *et al.* Transcriptomic Profiling of Trophoblast Fusion Using BeWo and JEG-3 Cell Lines. *Molecular human reproduction*, gaz061, doi:10.1093/molehr/gaz061 (2019).

107   Zheng, R. *et al.* Deep RNA sequencing analysis of syncytialization-related genes during BeWo cell fusion. *Reproduction*, doi:10.1530/REP-16-0343 (2016).

108   Shankar, K. *et al.* Transcriptomic and epigenomic landscapes during cell fusion in BeWo trophoblast cells. *Placenta* **36**, 1342-1351, doi:10.1016/j.placenta.2015.10.010 (2015).

109   Nampoothiri, L. P., Neelima, P. S. & Rao, A. J. Proteomic profiling of forskolin-induced differentiated BeWo cells: an in-vitro model of cytotrophoblast differentiation. *Reprod Biomed Online* **14**, 477-487 (2007).

110   Tuuli, M. G., Longtine, M. S. & Nelson, D. M. Review: Oxygen and trophoblast biology--a source of controversy. *Placenta* **32 Suppl 2**, S109-118, doi:10.1016/j.placenta.2010.12.013 (2011).

111   Jaroch, K., Jaroch, A. & Bojko, B. Cell cultures in drug discovery and development: The need of reliable in vitro-in vivo extrapolation for pharmacodynamics and pharmacokinetics assessment. *J Pharm Biomed Anal* **147**, 297-312, doi:10.1016/j.jpba.2017.07.023 (2018).

112   Sadovsky, Y., Clifton, V. L. & Burton, G. J. Invigorating placental research through the "Human Placenta Project". *Placenta* **35**, 527, doi:10.1016/j.placenta.2014.06.367 (2014).

113   Fennema, E., Rivron, N., Rouwkema, J., van Blitterswijk, C. & de Boer, J. Spheroid culture as a tool for creating 3D complex tissues. *Trends Biotechnol* **31**, 108-115, doi:10.1016/j.tibtech.2012.12.003 (2013).

114   Schweiger, P. J. & Jensen, K. B. Modeling human disease using organotypic cultures. *Current opinion in cell biology* **43**, 22-29, doi:10.1016/j.ceb.2016.07.003 (2016).

115   Skardal, A., Shupe, T. & Atala, A. Organoid-on-a-chip and body-on-a-chip systems for drug screening and disease modeling. *Drug Discov Today*, doi:10.1016/j.drudis.2016.07.003 (2016).

116   Clevers, H. Modeling Development and Disease with Organoids. *Cell* **165**, 1586-1597, doi:10.1016/j.cell.2016.05.082 (2016).

117   Wang, Y. & Wang, J. Mixed hydrogel bead-based tumor spheroid formation and anticancer drug testing. *Analyst* **139**, 2449-2458, doi:10.1039/c4an00015c (2014).

118   Tseng, H. *et al.* A spheroid toxicity assay using magnetic 3D bioprinting and real-time mobile device-based imaging. *Scientific reports* **5**, 13987, doi:10.1038/srep13987 (2015).

119   Vinci, M. *et al.* Advances in establishment and analysis of three-dimensional tumor spheroid-based functional assays for target validation and drug evaluation. *BMC Biol* **10**, 29, doi:10.1186/1741-7007-10-29 (2012).

120   Haider, S. *et al.* Self-Renewing Trophoblast Organoids Recapitulate the Developmental Program of the Early Human Placenta. *Stem Cell Reports* **11**, 537-551, doi:10.1016/j.stemcr.2018.07.004 (2018).

121   Turco, M. Y. *et al.* Trophoblast organoids as a model for maternal-fetal interactions during human placentation. *Nature* **564**, 263-267, doi:10.1038/s41586-018-0753-3 (2018).

122   Nandi, P., Lim, H., Torres-Garcia, E. J. & Lala, P. K. Human trophoblast stem cell self-renewal and differentiation: Role of decorin. *Scientific reports* **8**, 8977, doi:10.1038/s41598-018-27119-4 (2018).

123   Wong, M. K., Wahed, M., Shawky, S. A., Dvorkin-Gheva, A. & Raha, S. Transcriptomic and functional analyses of 3D placental extravillous trophoblast spheroids. *Scientific reports* **9**, 12607, doi:10.1038/s41598-019-48816-8 (2019).

124   Ebegboni, V. J., Balahmar, R. M., Dickenson, J. M. & Sivasubramaniam, S. D. The effects of flavonoids on human first trimester trophoblast spheroidal stem cell self-renewal, invasion and JNK/p38 MAPK activation: Understanding the cytoprotective effects of these phytonutrients against oxidative stress. *Biochemical pharmacology* **164**, 289-298, doi:10.1016/j.bcp.2019.04.023 (2019).

125   You, Y. *et al.* Novel 3D in vitro models to evaluate trophoblast migration and invasion. *Am J Reprod Immunol* **81**, e13076, doi:10.1111/aji.13076 (2019).

126   Seno, K. *et al.* Aggregation of Human Trophoblast Cells into Three-Dimensional Culture System Enhances Anti-Inflammatory Characteristics through Cytoskeleton Regulation. *Int J Mol Sci* **19**, doi:10.3390/ijms19082322 (2018).

127   Rai, A. & Cross, J. C. Three-dimensional cultures of trophoblast stem cells autonomously develop vascular-like spaces lined by trophoblast giant cells. *Dev Biol* **398**, 110-119, doi:10.1016/j.ydbio.2014.11.023 (2015).

128   Wang, H. *et al.* A novel model of human implantation: 3D endometrium-like culture system to study attachment of human trophoblast (Jar) cell spheroids. *Mol Hum Reprod* **18**, 33-43, doi:10.1093/molehr/gar064 (2012).

129   Esch, E. W., Bahinski, A. & Huh, D. Organs-on-chips at the frontiers of drug discovery. *Nature reviews. Drug discovery* **14**, 248-260, doi:10.1038/nrd4539 (2015).

130   Huh, D. *et al.* Reconstituting organ-level lung functions on a chip. *Science* **328**, 1662-1668, doi:10.1126/science.1188302 (2010).

131   Kim, H. J., Huh, D., Hamilton, G. & Ingber, D. E. Human gut-on-a-chip inhabited by microbial flora that experiences intestinal peristalsis-like motions and flow. *Lab Chip* **12**, 2165-2174, doi:10.1039/c2lc40074j (2012).

132   Huh, D. *et al.* Microfabrication of human organs-on-chips. *Nat Protoc* **8**, 2135-2157, doi:10.1038/nprot.2013.137 (2013).

133   Lee, J. S. *et al.* Placenta-on-a-chip: a novel platform to study the biology of the human placenta. *The Journal of Maternal-Fetal & Neonatal Medicine*, 1-9, doi:10.3109/14767058.2015.1038518 (2015).

134   Miura, S., Sato, K., Kato-Negishi, M., Teshima, T. & Takeuchi, S. Fluid shear triggers microvilli formation via mechanosensitive activation of TRPV6. *Nat Commun* **6**, 8871, doi:10.1038/ncomms9871 (2015).

135   Yin, F. *et al.* A 3D human placenta-on-a-chip model to probe nanoparticle exposure at the placental barrier. *Toxicology in vitro : an international journal published in association with BIBRA* **54**, 105-113, doi:10.1016/j.tiv.2018.08.014 (2019).

136   Pemathilaka, R. L., Caplin, J. D., Aykar, S. S., Montazami, R. & Hashemi, N. N. Placenta-on-a-Chip: In Vitro Study of Caffeine Transport across Placental Barrier Using Liquid Chromatography Mass Spectrometry. *Global Challenges* **3**, doi:10.1002/gch2.201800112 (2019).

137   Zhu, Y. *et al.* Placental Barrier-on-a-Chip: Modeling Placental Inflammatory Responses to Bacterial Infection. *ACS Biomaterials Science & Engineering* **4**, 3356-3363, doi:10.1021/acsbiomaterials.8b00653 (2018).

138   Attalla, R., Ling, C. & Selvaganapathy, P. Fabrication and characterization of gels with integrated channels using 3D printing with microfluidic nozzle for tissue engineering applications. *Biomedical microdevices* **18**, 17, doi:10.1007/s10544-016-0042-6 (2016).

139   Mittal, R. *et al.* Organ-on-chip models: Implications in drug discovery and clinical applications. *J Cell Physiol* **234**, 8352-8380, doi:10.1002/jcp.27729 (2019).

140   Hospodiuk, M., Dey, M., Sosnoski, D. & Ozbolat, I. T. The bioink: A comprehensive review on bioprintable materials. *Biotechnol Adv* **35**, 217-239, doi:10.1016/j.biotechadv.2016.12.006 (2017).

141   Hong, N., Yang, G. H., Lee, J. & Kim, G. 3D bioprinting and its in vivo applications. *J Biomed Mater Res B Appl Biomater*, doi:10.1002/jbm.b.33826 (2017).

142   Datta, P., Ayan, B. & Ozbolat, I. T. Bioprinting for vascular and vascularized tissue biofabrication. *Acta Biomater* **51**, 1-20, doi:10.1016/j.actbio.2017.01.035 (2017).

143   Yue, K. *et al.* Synthesis, properties, and biomedical applications of gelatin methacryloyl (GelMA) hydrogels. *Biomaterials* **73**, 254-271, doi:10.1016/j.biomaterials.2015.08.045 (2015).

144   Kuo, C. Y. *et al.* Trophoblast-endothelium signaling involves angiogenesis and apoptosis in a dynamic bioprinted placenta model. *Biotechnol Bioeng* **116**, 181-192, doi:10.1002/bit.26850 (2019).

145   Arumugasaamy, N. *et al.* Biomimetic Placenta-Fetus Model Demonstrating Maternal-Fetal Transmission and Fetal Neural Toxicity of Zika Virus. *Ann Biomed Eng* **46**, 1963-1974, doi:10.1007/s10439-018-2090-y (2018).

146   Kuo, C.-Y. *et al.* Development of a 3D Printed, Bioengineered Placenta Model to Evaluate the Role of Trophoblast Migration in Preeclampsia. *ACS Biomaterials Science & Engineering* **2**, 1817-1826, doi:10.1021/acsbiomaterials.6b00031 (2016).

147   Leiser, R. & Kaufmann, P. Placental structure: in a comparative aspect. *Experimental and clinical endocrinology* **102**, 122-134, doi:10.1055/s-0029-1211275 (1994).

148   Malek, A., Sager, R., Lang, A. B. & Schneider, H. Protein transport across the in vitro perfused human placenta. *Am J Reprod Immunol* **38**, 263-271, doi:10.1111/j.1600-0897.1997.tb00513.x (1997).

149   Conings, S., Amant, F., Annaert, P. & Van Calsteren, K. Integration and validation of the ex vivo human placenta perfusion model. *J Pharmacol Toxicol Methods* **88**, 25-31, doi:10.1016/j.vascn.2017.05.002 (2017).

150   Pemathilaka, R. L., Reynolds, D. E. & Hashemi, N. N. Drug transport across the human placenta: review of placenta-on-a-chip and previous approaches. *Interface Focus* **9**, 20190031, doi:10.1098/rsfs.2019.0031 (2019).

Figures and Figure Legends
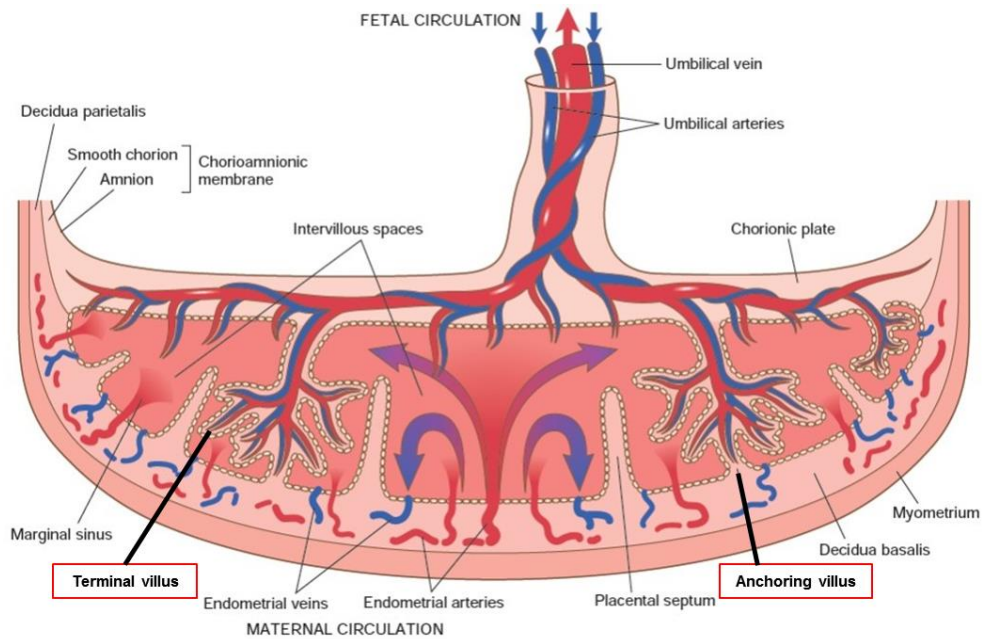
Figure 1. Simplified diagram of a term human placenta highlighting the anchoring and terminal villi. Image adapted from: http://medicinase.com/wp-content/uploads/2015/05/Placental-Anatomy-1024x621.jpg.
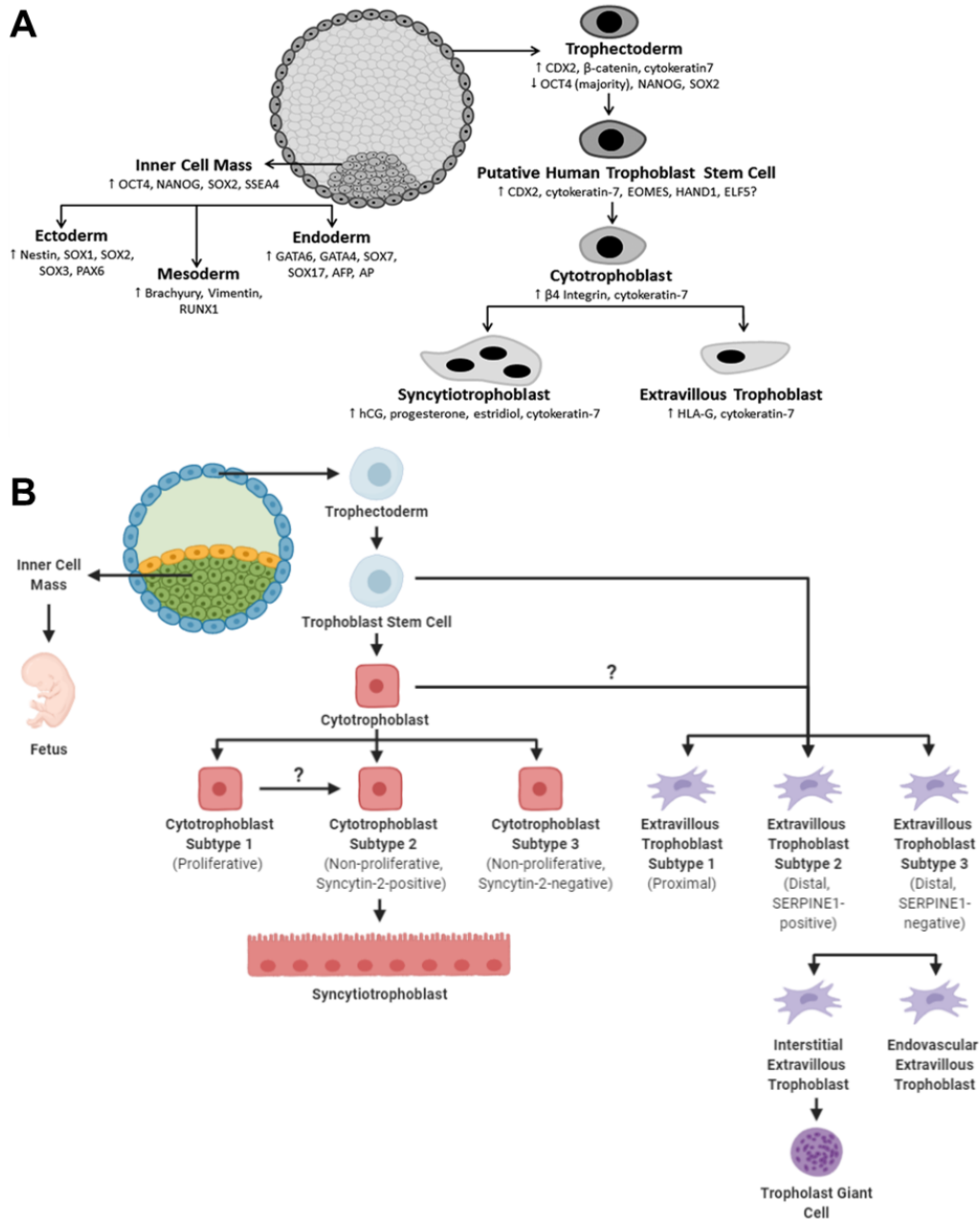
Figure 2. Schematic outlining (**A**) the traditional, hypothesized human trophoblast lineage and associated genetic markers, adapted from Gamage, et al. [17], and (**B**) the modern, hypothesized trophoblast lineage based on novel single-cell RNA-sequencing. Question marks indicate speculated differentiation pathways.
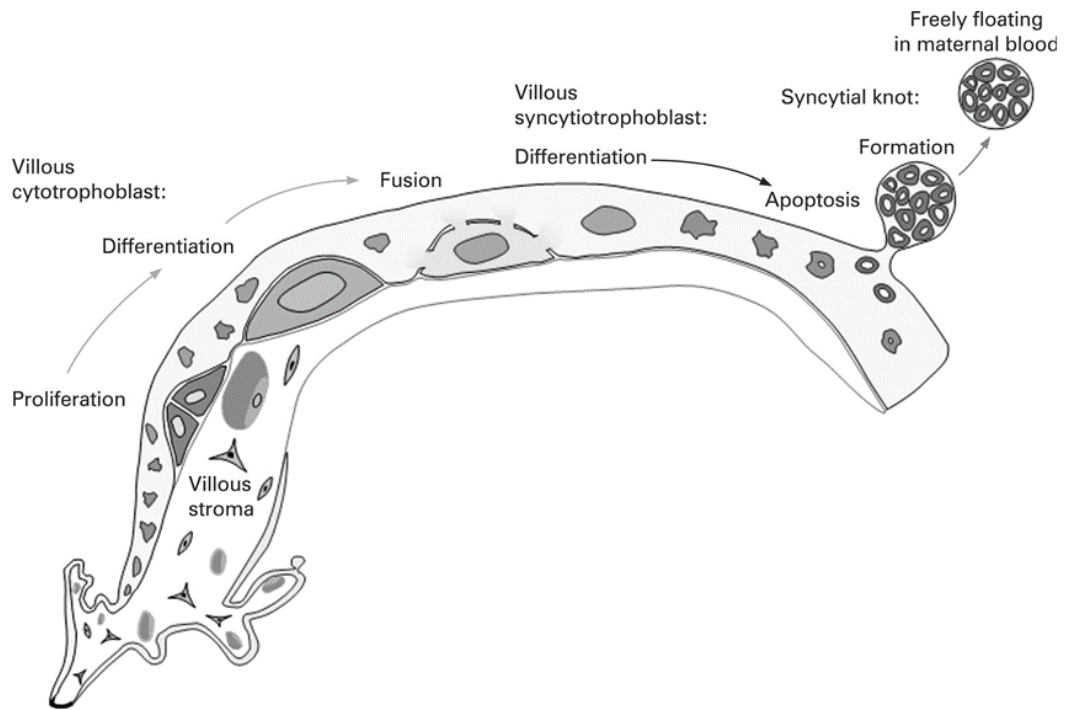
Figure 3. Schematic of the villous cytotrophoblast and syncytiotrophoblast life cycle. Figure adapted from Huppertz [4].
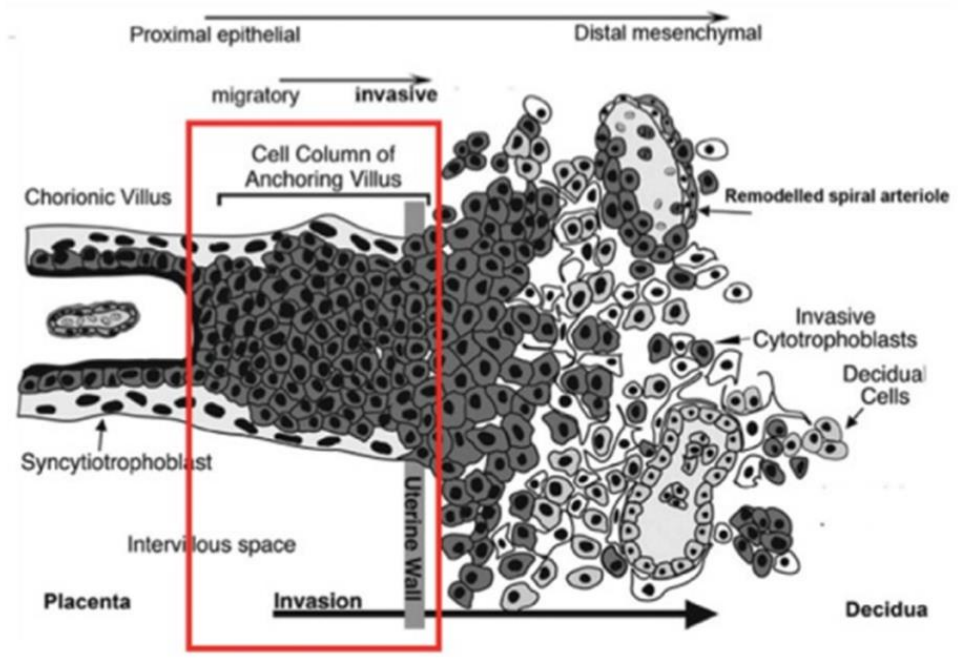
Figure 4. Schematic of EVT invasion and migration from cell column of anchoring villi into maternal uterine decidua. Red box highlighting cell column from which EVT cells emerge. Figure adapted from Davies, et al. [30].
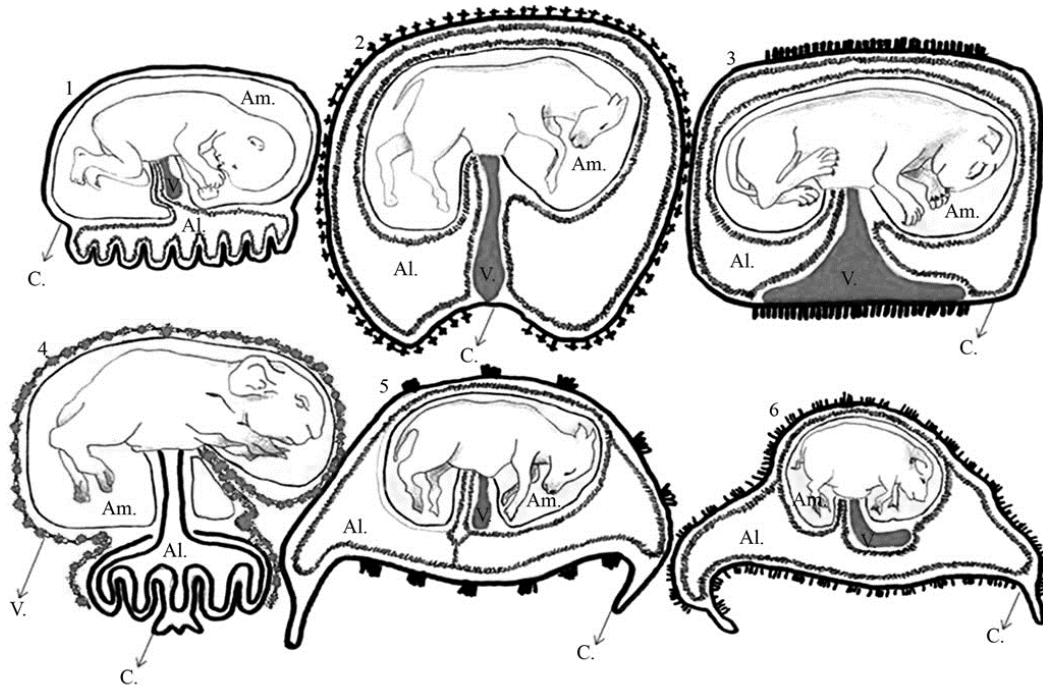
Figure 5. Comparison of placentae from different animal species. (1) Human placenta; (2) Equine; (3) Feline; (4) Rodent; (5) Ruminant; (6) Swine. Am, amnion, Al, allantois, V, yolk sac, and C, chorion. Figure from Leiser and Kaufmann [147].
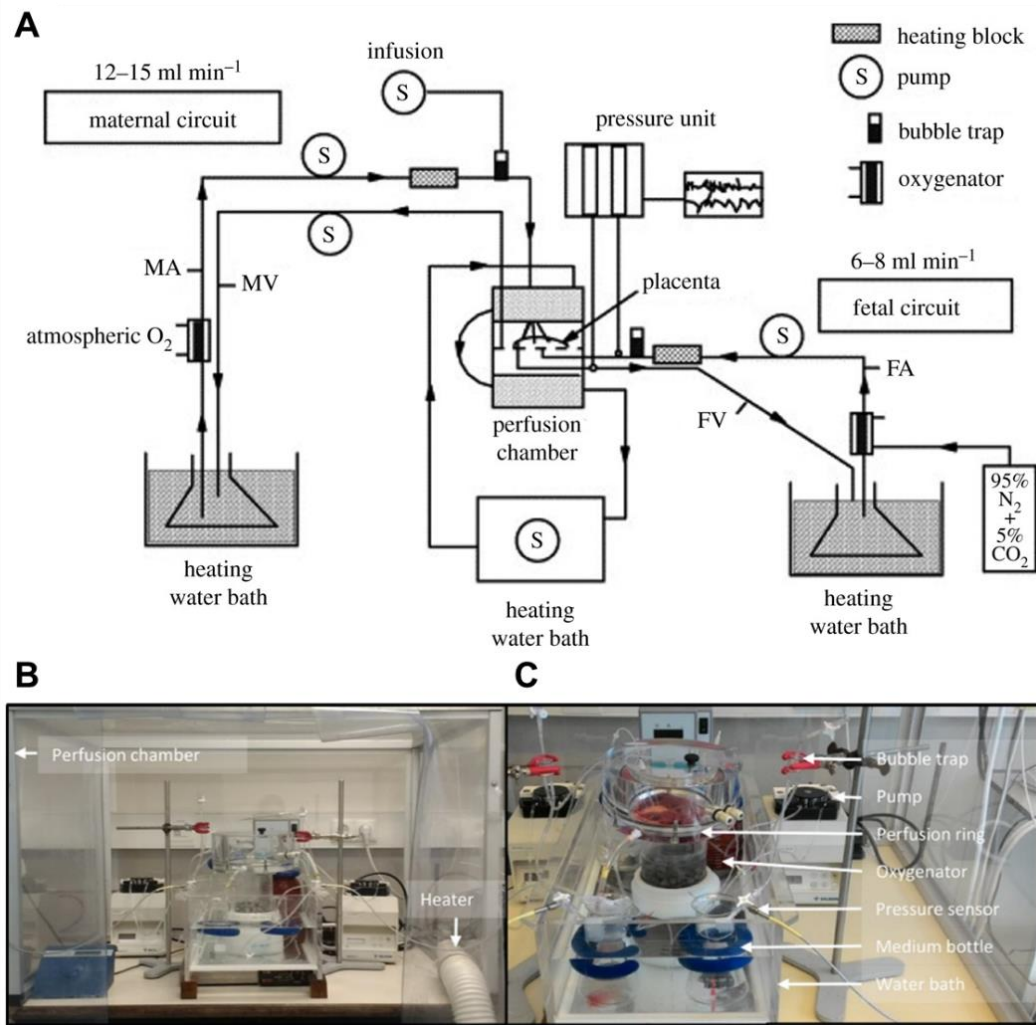
Figure 6. Ex vivo placental perfusion system. (**A**) Schematic of a human *ex vivo* placenta perfusion system. (**B, C**) Photos of a live perfusion system. Figure adapted from [148-150].
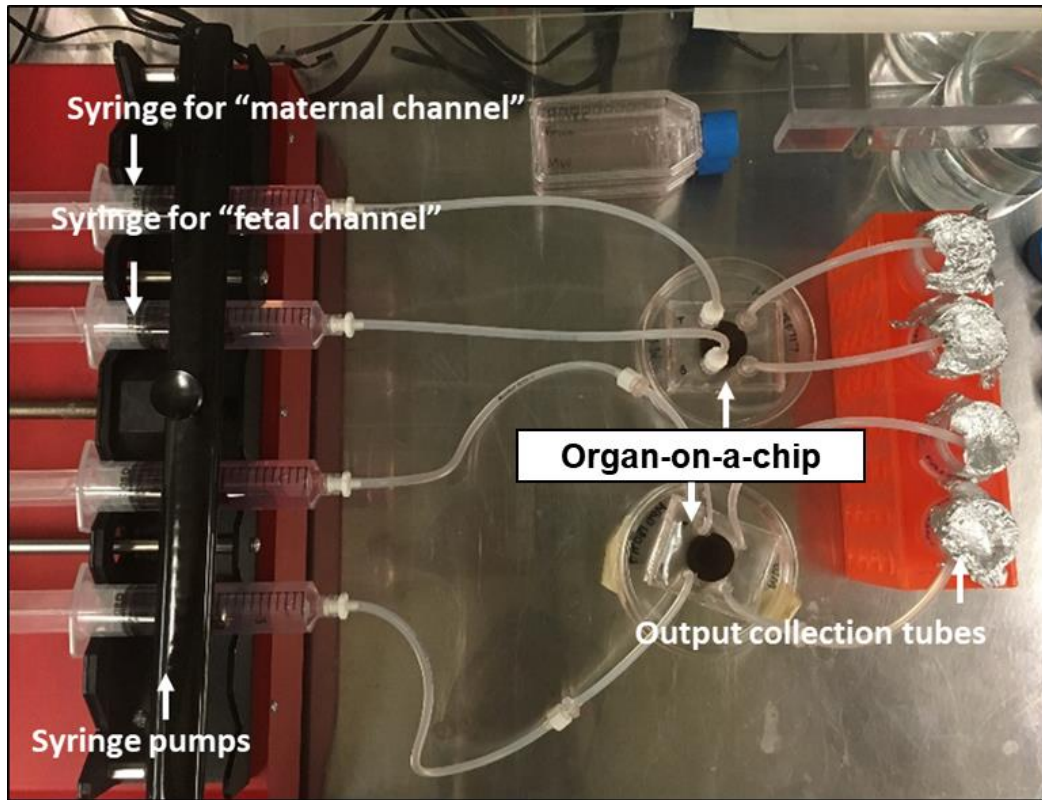
Figure 7. Image of sample organ-on-a-chip set-up with two devices connected to a syringe pump.
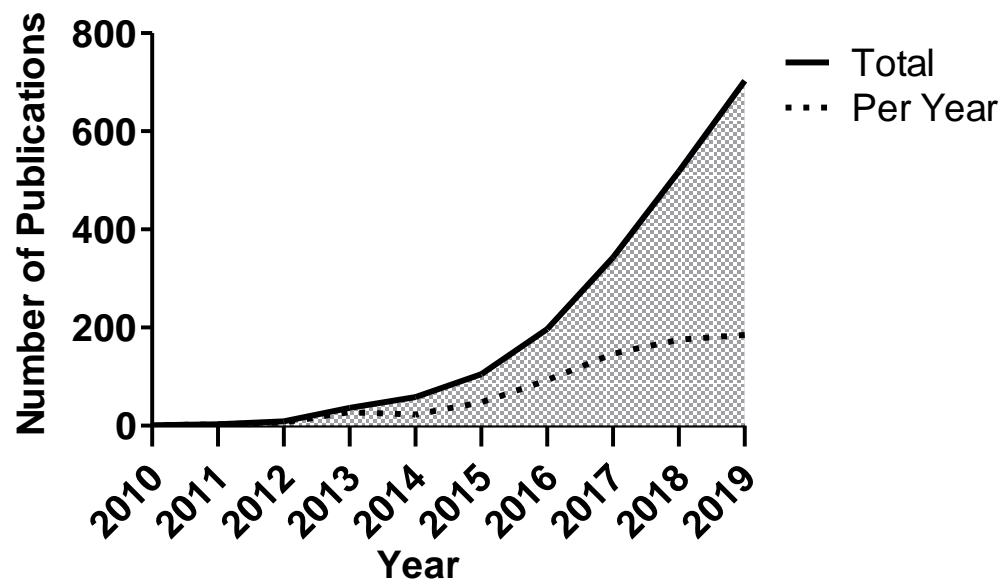
Figure 8. Number of organ-on-a-chip publications per year and in total. Search terms ("organ-on-a-chip" OR "organ-on-chip" OR "organs-on-chips") used on PubMed.
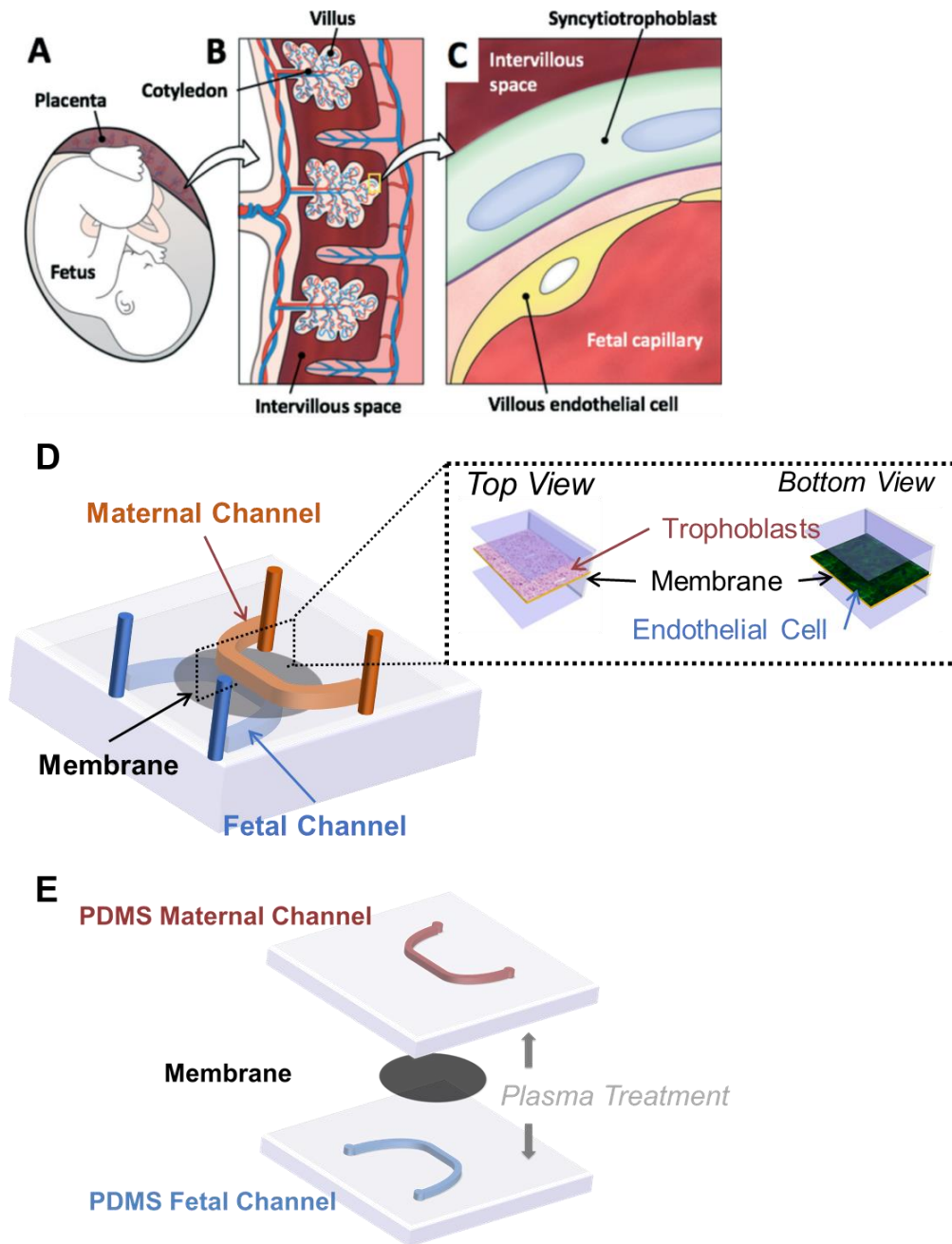
Figure 9. Schematic of human placenta and placenta-on-a-chip microfluidic device. (**A**) Diagram of human fetus and placenta during pregnancy. (**B**) Cross-sectional diagram of chorionic villi within placenta. (**C**) Cross-sectional diagram of major cell layers that constitute the placental barrier. A-C adapted from Blundell, et al. [99]. (**D**) Computer-Aided Design images of a simulated placenta-on-a-chip device made with straight maternal and fetal channels sandwiching a membrane that supports cell growth. Blue and red colours only for purpose of illustrating channels. (**E**) Deconstructed placenta-on-a-chip device.

CHAPTER 2: EXTRACELLULAR MATRIX SURFACE REGULATES SELF-ASSEMBLY OF THREE-DIMENSIONAL PLACENTAL TROPHOBLAST SPHEROIDS

Chapter Preface

This chapter is a reprint of the original article: Wong, M. K., Shawky, S. A., Aryasomayajula, A., Green, M. A., Ewart, T., Selvaganapathy, P. R., & Raha, S. (2018). Extracellular matrix surface regulates self-assembly of three-dimensional placental trophoblast spheroids. PLoS One, 13(6), e0199632. This article is published under the CC-BY license, which allows download, reuse, reprint, modify, distribute, and/or copy (**Appendix 1**).

The importance of the tissue culture surface in determining cellular phenotype and function remains poorly understood, though recognition of its biochemical and biophysical contributions is growing in the scientific community. In this first model, we describe the ability of the thickness and stiffness of the extracellular matrix surface to drive the self-assembly of trophoblast cells into three-dimensional spheroids that exhibit greater levels of syncytial fusion and associated markers. This is particularly impactful as there have been very few papers published to date investigating the mechanical impact of the surface on trophoblast cell behaviour and function. Our work provides a robust model for future studies to continue diving deeper into this important anatomical and environmental variable in manipulating placental function.

Abstract

The incorporation of the extracellular matrix (ECM) is essential for generating *in vitro* models that truly represent the microarchitecture found in human tissues. However, the cell-cell and cell-ECM interactions *in vitro* remains poorly understood in placental trophoblast biology. We investigated the effects of varying the surface properties (surface thickness and stiffness) of two ECMs, collagen I and Matrigel, on placental trophoblast cell morphology, viability, proliferation, and expression of markers involved in differentiation/syncytial fusion. Most notably, thicker Matrigel surfaces were found to induce the self-assembly of trophoblast cells into 3D spheroids that exhibited thickness-dependent changes in viability, proliferation, syncytial fusion, and gene expression profiles compared to two-dimensional cultures. Changes in F-actin organization, cell spread morphologies, and integrin and matrix metalloproteinase gene expression profiles, further reveal that the response to surface thickness may be mediated in part through cellular stiffness-sensing mechanisms. Our derivation of self-assembling trophoblast spheroid cultures through regulation of ECM surface alone contributes to a deeper understanding of cell-ECM interactions, and may be important for the advancement of *in vitro* platforms for research or diagnostics.

Introduction

The human placenta is pivotal in the growth and survival of the fetus during pregnancy due to its involvement in maternal-fetal exchange, immune and barrier protection, and endocrine regulation [1,2]. To achieve an understanding of the complex processes underpinning this rapidly developing tissue requires a diverse range of experimental approaches including both *in vivo* and *in vitro* models. There has recently been great interest in emulating placental barrier function utilizing *in vitro* models comprised of monolayers of trophoblast cells or more complex assemblies of multiple cell types referred to as microphysiological systems [3-5]. However, many of these *in vitro* platforms are developed in the absence of the non-cellular scaffold present *in vivo* known as the extracellular matrix (ECM) [6,7]. The ECM is not routinely incorporated in most culture systems, where cells are simply cultured on two-dimensional (2D) polystyrene or glass surfaces. The physical properties of these 2D surfaces are known to be quite distinct from that which exists *in vivo* [8]. Considering that the ECM provides numerous biochemical and biomechanical cues that are important for regulating cell behavior [9], the incorporation of ECM for *in vitro* modeling and testing may be of central importance to accurately understanding placental barrier function.

While the importance of considering the three-dimensional (3D) ECM for *in vitro* cell culture models is becoming evident [10], our understanding of the regulatory role of cell-matrix interactions on cell function is still incomplete. Specific to placental development, trophoblast cells grown on various ECMs have

demonstrated phenotypic changes, such as altered gene and protein expressions, that are indicative of a more differentiated population [11-15]. Yet, the functional consequences of these biointerface-driven changes in phenotype have yet to be fully elucidated. In particular, there is a disparity in our understanding of parameters such as surface thickness and stiffness in the context of trophoblast biology. As ECM properties may provide key cues to direct cell fate and behaviour [16,17], inconsistencies in tuning the growth surface may have implications on the translatability of resultant findings. Hence, there is a need to understand how the ECM parameters employed during *in vitro* culture impact trophoblast growth and function. While the literature does not provide highly defined measures of human placental ECM thickness and stiffness, we do know that changes in these parameters are associated with placental pathologies such as intrauterine growth restriction [18]. Therefore, when developing *in vitro* microphysiological systems, failure to clearly define the ECM may result in abnormal representation of cellular function.

In the current study, we investigated the impact of the ECM on placental trophoblast cells *in vitro*. We hypothesized that altering ECM surface thickness and stiffness would affect cellular organization, function, and expression profiles. A deeper understanding of the biointerface-driven effects of ECM thickness on trophoblast cell phenotype will be fundamental in the development of more *in vivo*-like models for pregnancy research, drug/toxin testing, and prognosis of placental pathologies.

Materials and Methods

ECM hydrogel surface fabrication

Collagen I (Corning; 2 mg/mL) and Matrigel (Corning; 5 mg/mL) were used as ECM hydrogels for this study as they are two of the most commonly-utilized ECM growth surfaces for cells [19,20]. Matrigel is a reconstituted basement membrane extract from the Engelbreth-Holm-Swarm mouse sarcoma, which consists of approximately 60% laminin, 30% collagen IV, 8% entactin, and other proteins and growth factors (Corning). Growth factor-reduced Matrigel was used in this study to minimize the effect of growth factors and to increase comparability to collagen I, which is also growth factor-free [21]. Two surface thicknesses (50 and 250 µm) were selected on basis of the most commonly used ranges previously seen in literature for trophoblast culture [11-15]. In order to calculate the volume of hydrogel required to produce a specific surface thickness, the following equation was used: *Volume = (surface area of cell growth) x (calculated thickness)*. A controlled volume of liquid hydrogel material was deposited onto glass or polystyrene surfaces via micropipetting and spread evenly over the surface. Matrigel was gelled via incubation at 37 °C for 1 hour. Collagen I was gelled via the addition of 10X phosphate-buffered saline (PBS) and 1N sodium hydroxide, and incubated at 37 °C for 1 hour, according to the manufacturer's protocol.

Analysis of ECM surface properties and mechanical testing of substrate stiffness

Analysis and mechanical testing of ECM surfaces were carried out using the MicroSquisher instrument (CellScale). Images were captured using the MicroSquisher camera and the data was recorded using the SquisherJoy software (CellScale). Actual thicknesses of the surfaces were measured by cross-sectional imaging of the hydrogel and glass coverslip and using a measurement tool within the SquisherJoy software. A total of five measurements were taken per sample along the edge to the centre of the ECM surface.

A 2 mm x 2 mm steel plate glued to a cylindrical cantilever of 203.2 µm diameter was used to perform the mechanical testing for the experiment. All samples were tested in phosphate-buffered saline bath at room temperature. The cantilever was lowered until it made gentle contact with the top of the ECM sample. Samples were compressed to 10 % engineering strain at a strain rate of 1.61 µm/second and held at a constant deformation for 10 s followed by a release strain rate of 1.61 µm/second. Force was measured during the compression, deformation and release cycle. All the gels showed an elastic region between 3-5% of the strain values which were used for analysis. Substrate stiffness was determined by assessing the force required to compress the sample to a constant displacement.

Cell culture

BeWo cells (ATCC) are one of the most extensively-used cell lines in placental trophoblast research to model villous trophoblasts, syncytial fusion, and many aspects of placental function and disease [22,23]. BeWo cells were cultured at

37 $^{\circ}$C in 95% room air/5% CO_2 in F-12 media (Corning) supplemented with 10% fetal bovine serum, 1% L-glutamine, and 1% penicillin-streptomycin. The media was changed every two days. Cells between the passages of 10-15 were used for all experiments, and seeded at an initial density of 1×10^4 cells/cm^2 on glass coverslips or 6-well polystyrene plates that were either uncoated (2D control) or coated with varying thicknesses of collagen I or Matrigel.

Live cell imaging of cellular organization

Cells were imaged under a phase-contrast filter and images captured using an AE2000 inverted microscope (Motic) and Moticam X2 camera (Motic). Images of cellular organization were captured at 4x objective magnification.

Immunofluorescence

Cells were fixed for 10 minutes in 2% paraformaldehyde with 0.1% glutaraldehyde and permeabilized for 5 minutes with 0.1% Triton X-100 in PBS. Samples were then blocked for 2 hours using 0.01% Tween-20, 10% goat serum and 1% bovine serum albumin (BSA) in PBS. Afterwards, samples were incubated with either Anti-E-Cadherin primary antibody (Abcam; ab40772; rabbit monoclonal; 1:500) overnight at 4 degrees and then incubated with Goat Anti-Rabbit IgG H&L Alexa Fluor® 488 secondary antibody (Abcam; ab150077; goat polyclonal; 2μg/mL) for 1 hour, or with CytoPainter Phalloidin-iFluor 555 reagent (Abcam; ab176756; 1:1000) for 1 hour. All blocking and incubations were performed at room temperature, unless otherwise stated. Samples were counterstained with 4′,6-diamidino-2-phenylindole dihydrochloride (DAPI; Santa

Cruz; 1.5 µg/mL) and mounted onto glass slides using Fluoromount™ Aqueous Mounting Medium (Sigma-Aldrich). Slides were visualized using an Eclipse Ti-E Inverted Fluorescence Microscope (Nikon). Z-stack images were taken in 0.5 µm steps to capture all layers. Images were analyzed using Fiji (National Institutes of Health) and NIS Elements software (Nikon). To assess syncytial fusion, E-Cadherin was visualized to identify cell borders (as E-Cadherin is localized to the plasma membrane [24]) and DAPI to identify cell nuclei. When merged, E-Cadherin and DAPI enabled the visualization of syncytial fusion [25]. Cell fusion may be quantified with the following equation [26]: *Total Fusion Percentage (%) = (Number of nuclei in syncytia/Total number of nuclei) x 100 %*. Cell spread area was determined by quantifying the binary area of Phalloidin staining, normalized to the mean intensity of DAPI as an indicator of cell number [27].

Cell viability and proliferation

BeWo cells were incubated with Calcein AM (Thermo Scientific; C1430; 1:200) and Ethidium homodimer-1 (Thermo Scientific; E1169; 1:200) and imaged using an Eclipse Ti-E Inverted Fluorescence Microscope (Nikon). Green fluorescence indicated live cells and red fluorescence indicated dead cells. Images were analyzed using Fiji (National Institutes of Health) and NIS Elements software (Nikon), and the percentage ratio of live to dead cells were calculated by dividing the mean intensity of live cells (as determined by fluorescence of Calcein AM stain) by the mean intensity of the dead cells (as determined by fluorescence of Ethidium homodimer-1 stain).

Cell proliferation was determined using a CellTiter 96® AQueous Non-Radioactive Cell Proliferation Assay kit (MTS Assay; Promega). The absorbance was measured at 490 nm on a Multiskan® Spectrum spectrophotometer (Thermo Scientific). Given that the absorbance is directly proportional to the number of live cells, relative rate of cell proliferation was determined by calculating the fold change in absorbance compared to the 2D control. Matrigel samples with no cells seeded were used to correct for any potential background absorbance.

RNA Extraction and Real-Time Quantitative Polymerase Chain Reaction (qPCR)

Cells were isolated from hydrogels using Cell Recovery Solution (Corning). Total RNA was extracted from cells using TRIzol Reagent (Invitrogen) and Direct-zol RNA MiniPrep Kit (Zymo Research), following the manufacturer's protocol. A total of 1 μg of RNA was reverse-transcribed to cDNA using High-Capacity cDNA Reverse Transcription Kit (Applied Biosystems). Primer sets directed against gene targets of interest were designed through National Center for Biotechnology Information's Primer-BLAST primer designing tool and synthesized at McMaster's Mobix Labs (**Table 1**). Quantitative analysis of mRNA expression was performed via qPCR using fluorescent nucleic acid dye PerfeCTa SYBR Fastmix (Quanta) and CFX384 Touch Real-Time PCR Detection System (BioRad). The cycling conditions were 95 °C for 10 min, followed by 40 cycles of 95 °C for 10 secs and 60 °C for 10 secs and 72 °C for 15 secs. Relative fold changes were calculated using the comparative cycle times (Ct) method, normalizing all values to an endogenous control gene (18S). The endogenous control gene was selected based on

experimentally-determined Ct stability across all treatment groups. Given that all primer sets had equal priming efficiency, the ΔCt values for each primer set were calibrated to the average of all control Ct values, and the relative abundance of each primer set compared with calibrator was determined by the formula $2^{\Delta\Delta Ct}$, in which ΔΔCt was the normalized value. Matrigel samples with no cells seeded were also analyzed to ensure that any potential traces of RNA found in hydrogels alone did not confound measurements.

Enzyme-Linked Immunosorbent Assay (ELISA)

Cell media was collected and protein levels of secreted hCGβ were analyzed via ELISA. In brief, 96-well high binding polystyrene microtiter plates (Costar) were coated with a detector anti-hCGβ antibody (Meridian; mAF05-19; monoclonal mouse; 2.94 µg/mL) for 2 hours, and then blocked with 1% BSA in tris-buffered saline overnight at 4 °C. Media samples were then incubated in the wells for 2 hours. Plates were incubated with a reporter anti-hCG antibody (Hytest; 27E8; monoclonal mouse; 0.3 µg/mL) conjugated to horseradish peroxidase for 1 hour. Plates were then incubated with TMB substrate (Sigma; T8665) for 30 minutes. Absorbances was measured at 550 nm and 450 nm on a Multiskan® Spectrum spectrophotometer (Thermo Scientific), and 450 nm values were subtracted from 550 nm values to correct for optimal imperfections in microplate. Protein levels were normalized to the absorbance calculated from the MTS proliferation assay, as the absorbance is directly proportional to the number of live cells (method adapted from [15]).

Statistical Analysis

All statistical analyses were performed using Prism 5 software (GraphPad). Results were expressed as means of normalized values ± standard error of the mean (SEM). Experiments were repeated at least three times (n≥3), unless otherwise specified. The significance of differences (p<0.05) between normalized mean values were then evaluated using unpaired t-test or one-way analysis of variance (ANOVA) followed by Tukey's post-test, as appropriate for the experiment.

Results

ECM surface type and thickness differentially regulates cellular organization and morphology

BeWo cells were seeded onto 2D polystyrene surfaces, or thin or thick surfaces of collagen I or Matrigel, and live cellular organization was examined using phase-contrast microscopy. Differences in cellular organization were seen within 24 hrs of seeding (day 1; **Fig 1A-E**), with long, strand-like morphologies particularly evident on thin Matrigel surfaces (**Fig 1D**), and small aggregates seen on thick surfaces (**Fig 1E**). By day 7, BeWo cells cultured on thin collagen I and Matrigel appeared more densely populated than the 2D control, but retained sheet-like, confluent growth and were no longer distinct in terms of cellular organization (**Fig 1F, G, I**). However, BeWo cells cultured on thick collagen I formed undefined aggregates at day 7 (**Fig 1H**), whereas cells cultured on thick Matrigel self-assembled into distinct, spheroid-shaped aggregates at day 7 (**Fig 1J**). By day 21,

BeWo cells cultured on thin surfaces no longer appeared different in organization compared to the 2D control (**Fig 1K, L, N**). In contrast, the cultures grown on thick collagen I samples did not exhibit differences compared to the 2D control (**Fig 1K, M**). Notably, thick Matrigel-induced trophoblast spheroids maintained in shape and integrity, but grew in size from day 7 to day 21 (**Fig 1J, O**). Collectively, thick surfaces were required for aggregate formation, and thick Matrigel was specifically required for spheroid self-assembly and maintenance.

Matrigel led to thickness-dependent increases in cell viability and proliferation

Self-assembling, 3D cell spheroids and microtissues are of great interest as they have been shown to better recapitulate the phenotypes redolent of their respective organs compared to two-dimensional (2D) cultures, such as tissue-specific cell density, microarchitecture, cell-cell interactions [10,28-31]. Given the potential value, we further characterized the thick Matrigel-induced trophoblast spheroids at day 7. Cell viability, as determined through the ratio of live to dead cells, significantly increased in a thickness-dependent manner ($p < 0.05$ for 2D to thin; $p < 0.001$ for 2D to thick; $p < 0.01$ for thin to thick; **Fig 2A, B**), with the greatest viability in cells grown on the thick Matrigel surface (91.3 ± 0.2 %). Interestingly, the mean of the cell proliferation rate appeared to increase in a thickness-dependent manner, with significant differences evident in the thick Matrigel surface when compared to the other two groups (181.0 ± 29.3 %, $p < 0.001$ for 2D to thick; $p < 0.05$ for thin to thick; **Fig 2C**).

The effect of ECM surface thickness on syncytial fusion

Due to the robust effects on cellular organization, spheroid self-assembly, viability, and proliferation, we investigated the impact of surface thickness on syncytial fusion, which is an essential feature of syncytiotrophoblast differentiation. Interestingly, BeWo cells grown on thick Matrigel appeared to be very highly fused with minimal E-Cadherin staining at the center of spheroids compared to cells grown on 2D or thin Matrigel (**Fig 3A-C**). However, due to the high density of DAPI-positive nuclear clustering in thin and thick Matrigel surfaces, it was not possible to accurately distinguish nuclei from one another, preventing the accurate quantification of the percentage of syncytial fusion. Thus, we assessed the degree of syncytial fusion through gene expression profiling to verify this qualitative fusion increase seen in thick Matrigel-induced spheroids.

Thick Matrigel-induced spheroids exhibited a significant two-fold increase in mRNA levels of glial cells missing homolog 1 (*GCM1*), a transcription factor for many syncytialization-related genes [32], compared to cells grown on 2D surfaces ($p < 0.05$; **Fig 4A**). Placental lactogen (*PL*) mRNA levels were significantly increased in a thickness-dependent manner ($p < 0.01$ for 2D to thin; $p < 0.001$ for 2D to thick; **Fig 4B**). Endogenous retrovirus group W member 1 (*ERVWE1*) mRNA levels only increased in the thin Matrigel group ($p < 0.05$ for 2D to thin; **Fig 4C**), but endogenous retrovirus group FRD member 1 (*ERVFRD1*) mRNA levels contrastingly decreased ($p < 0.01$ for 2D to thick; $p < 0.05$ for thin to thick; **Fig 4D**). Human chorionic gonadotropin α (*CGA*) mRNA levels were unchanged (**Fig 4E**),

but human chorionic gonadotropin β (*CGB*) mRNA levels were significantly increased in a thickness-dependent manner (p<0.05 for 2D to thin; p<0.001 for 2D to thick; p<0.01 for thin to thick; **Fig 4F**). Collectively, surface thickness/stiffness alone was able to induce increases in several key markers of syncytial fusion (*GCM1, PL, ERVWE1, CGB*).

In accordance, surface thickness/stiffness alone also induced significant increases secreted protein levels of human chorionic gonadotropin β (*hCGβ)* in the cell media (p<0.05; **Fig 5**).

Cellular stiffness response to changes in ECM surface thickness

As substrate stiffness inversely correlated with changes in surface thickness, as seen in our findings (**S1 Fig**) and that of others [16], we were interested in further elucidating potential stiffness-sensing mechanisms involved in spheroid formation with the thick Matrigel ECM. The cells' ability to spread over a surface is a known stiffness-response marker [16], and may be assessed via F-actin (phalloidin) immunofluorescent staining. At day 3, cell spread areas were significantly decreased as surface thickness increased (p<0.001; **Fig 6A, B**), and a similar trend was present at day 7 (p<0.001; **Fig 6A, C**).

Thick ECM surface up-regulated genes related to stiffness sensing and invasion

Lastly, we investigated the impact of Matrigel thickness on expression of genes related to stiffness sensing and invasion/migration. At day 7, *ITGA1* and *ITGA5* mRNA levels significantly increased in cells grown on thin and thick Matrigel surfaces compared to the 2D control (p<0.001 and p<0.05, respectively;

Fig 7A, B). *MMP2* and *TIMP1* mRNA levels also significantly increased in cells grown on thin and thick Matrigel surfaces compared to the 2D control (p<0.001 and p<0.05, respectively; **Fig 7E, G**). mRNA levels of *ITGAV, ITGB3, MMP9, and TIMP2* did not significantly change across various surface thicknesses (**Fig 7C, D, F, H**).

Discussion

The current study demonstrates that the nature of the ECM alone impacts not only the self-assembly behaviour of trophoblast cells, but also the expression profiles of genes related to differentiation and cell-ECM interaction, and functionally alter syncytial fusion and hormone secretion. The ability to manipulate surface thickness, as a parameter to alter substrate stiffness, allows for the evaluation of how cellular function and phenotype are regulated by changing ECM stiffness without altering the composition of the ECM hydrogel. The importance of exploring such relationships is underscored in reports that have demonstrated that self-assembling spheroids are of great value as they are known to possess cellular interactions and densities that are more similar to the *in vivo* state than 2D cultures [10,29,30]. While the generation of placental trophoblast spheroids has been attempted by a few prior studies [33-36], the cellular phenotype and techniques required for their derivation had yet to be well-characterized. Some studies utilized non-adherent or rotating wall vessel bioreactors to generate spheroids, but these models lack the cell-ECM interactions that are essential *in vivo* [33-36]. Our study reveals the

importance of understanding the cell-ECM interactions to influence cell-cell interactions, as seen through spheroid formation. Importantly, the novelty in our work demonstrates that the physical properties of the ECM contributes to not only to cellular reorganization, but also alters key cellular functions such as the trophoblasts' secretion of hCGβ, which is crucial in regulating hormone production, trophoblast fusion and invasion, and many other aspects of maternal and fetal health *in vivo* [37,38]. This connection between ECM and cellular function may prove to be a vital factor in dictating adverse pregnancy outcomes. Therefore, *in vitro* models of placental function using trophoblasts should consider clearly defining the ECM used within these constructs.

In the current manuscript, we demonstrate that the type of ECM plays a key role in regulating the self-assembly and maintenance of 3D trophoblast spheroids in BeWo cells. The differential abilities of collagen I and Matrigel in maintaining spheroid integrity is consistent with the work of Nguyen-Ngoc, et al. [39] showing that human breast cancer cells exhibited greater disassociation from pre-formed tumour spheroids when grown on or embedded in collagen I compared to Matrigel alone [19,39]. Collectively, this suggests that Matrigel is a more appropriate biomaterial than collagen I at maintaining 3D trophoblast spheroid integrity. Furthermore, the additional ECM proteins present in Matrigel (*e.g.,* laminin, entactin) compared to 2D surfaces or collagen I alone may also contribute to cellular differentiation. For example, knocking out laminin (α5 subunit) led to placental abnormalities and embryonic lethality in mice [40], and silencing laminin α4 or its

receptor led to impaired trophoblastic functions (*e.g.,* decreased invasion, migration, and tube formation) in human placental trophoblast cells, suggesting unique roles among the varying ECM proteins in development and differentiation. Indeed, our thick Matrigel-driven trophoblast spheroids exhibited higher degrees of syncytial fusion and gene (*GCM1, PL, ERVWE1, CGB*) and protein (hCGβ) expression profiles indicative of a more differentiated population compared to cells grown on 2D surfaces. The lack of change seen in *CGA* mRNA levels are not particularly surprising given the known differential temporal regulation of *CGA* and *CGB* expression during pregnancy (where hCGβ normally peaks around 10-12 weeks, whereas hCGα increases gradually until term. Importantly, the extent of fusion evident in the BeWo cells cultured on thick Matrigel were visibly greater than on 2D surfaces in conjunction with increases in hCGβ secretion, collectively supporting the enhancement of cell fusion via increased ECM thickness and/or decreased stiffness. In addition to activating cellular differentiation, ECM surfaces were previously reported to activate cellular invasion [11,33,34]. During invasion, MMP expression and activity is increased to degrade collagens [41-44], which was also seen in our study. A hydrogel surface solely consisting of isolated collagen, such as collagen I, is likely to be more impacted by the degradation compared to an ECM protein cocktail-based hydrogel, like Matrigel, when faced with invasive, MMP-expressing trophoblasts [41-44]. Therefore, the lack of spheroid structures on collagen I at day 21 may be attributed to higher degrees of surface degradation over time, enabling cells to contact the coverslip and return to confluent growth, whereas

Matrigel remained more robust as a scaffold due to a more diverse ECM composition. However, supplementary studies characterizing the ECM protein composition, and actual changes to integrity and surface topography of these surfaces during and after trophoblast invasion are required to verify these speculations.

While hydrogel surface-induced placental cell aggregation was previously reported by a small number of other studies [11-13,15], our study provides a more precise definition of the surface-casting parameters (*e.g.,* surface thickness and stiffness). Our data suggests that a critical surface thickness is required for spheroid formation, and variations in thickness can regulate spheroid phenotype. Kliman and Feinberg [14] cultured primary trophoblasts and JEG3 cells on a gradual slope of Matrigel (thicknesses reported between 0-60 µm), and elegantly demonstrated variations in cell morphology across the thicknesses [14]. Although they did not report spheroid formation due to the short duration of their study (24-72 hours), they did see rounded and individually-seeded cells when cultured on 14-60 µm-thick Matrigel, which resembled a pre-spheroid state. Interestingly, their placental cells eventually entirely degraded thinner coats of Matrigel to resume growth on the underlying glass coverslip [14]. This provides a plausible explanation for why the distinct strand-like cellular formations seen in BeWo cells cultured on thin Matrigel at day 1 were not maintained over time. The thickness-dependent changes seen throughout our study also propose that the cells can grade their behaviour based on sensing the actual thickness of the surface, or perhaps by sensing another property

directly affected by thickness, such as stiffness. Indeed, crosslinking poly(ethylene) glycol networks within Matrigel to increase gel stiffness was demonstrated to alter the invasion and dispersion behaviours of mammary organoids and mesenchymal stem cells [17,45]. Others have also consistently reported increased invasive activity on ECM surfaces *in vitro* in various cell types [39,46-48]. We tested this hypothesis in our model through mechanical testing to show that ECM thickness was inversely correlated with stiffness. Moreover, the quantitative reduction in cell spreading correlates with reduction in matrix stiffness and suggests that trophoblast cells possess the ability to sense the ECM thickness via stiffness-sensing and invasion mechanisms. This was similarly seen in the work of Mullen *et al.* (2015) in osteogenic cells [16]. Interestingly, even in the absence of a traditional stimulus for invasion (*i.e.,* nutrient or oxygen gradient), small, but significant, increases in *ITGA1, ITGA5, MMP2*, and *TIMP1* mRNA levels were detected in BeWo cells cultured on both thin and thick Matrigel, likewise demonstrating that the presence of ECM is sufficient to induce expression of some underlying genes. It is understood that the integrin subunits αv, α5, α1 and/or β3 link to the actin cytoskeleton through focal adhesion kinase anchoring points, regulating MMP expression and subsequent cellular invasion via a cellular mechano-sensing pathway [49-53]. However, though capable of invasion, BeWo cells traditionally display a less invasive phenotype [54], which may explain in part why we did not observe robust changes across all the genes (*e.g., ITGAV, ITGB3, MMP9, and TIMP2*). Additional studies should investigate the effects of a stronger stimulus for

invasion (*i.e.,* nutrient or oxygen gradient) on actual spheroid invasion and whether additional invasion/migration genes (*ITGAV, ITGB3, MMP9, TIMP2, etc.*) may also change.

Spheroid formation also coincided with thickness-dependent increases in expression of several syncytialization-related genes, *GCM1, PL, CGB*, and its secreted protein product, hCGβ. While human CG is produced by several placental cell types, its main source is from syncytiotrophoblasts – the fusogenic, non-proliferative, terminally-differentiated, endocrine cells [55]. In effect, increased CG expression in our trophoblast spheroids acts as a biochemical marker of syncytiotrophoblast differentiation and fusion [32,56], thereby, providing semi-quantitative support for the increased syncytial fusion seen in immunofluorescent images of thick Matrigel-derived spheroids. Interestingly, these increases coincided with minimally-changed *ERVWE1* and decreased *ERVFRD1* mRNA levels. While the syncytins have been demonstrated to play a role in syncytial fusion, the timing of their expression and functional involvement remain unclear [57]. For example, *Syncytin-B* knock-out mice (analogous to *ERVFRD1/*syncytin-2 in humans) resulted in abnormal placentation, but the placentas still exhibited some syncytialization and the offspring were viable, suggesting compensatory mechanisms or the existence of alternative fusogenic proteins [58]. Taken together, our data suggest that the Matrigel ECM potentiates modest syncytial fusion, even in the absence of fusogenic agents such as forskolin, but future studies are required to further profile and characterize the intricate gene expression patterns underlying

these changes. This increased differentiation and syncytialization achieved further validates the importance of the ECM conditions in modelling placentation and emphasizes the benefits of spheroid formation in trophoblast cultures.

Conclusion

As the sophistication of *in vitro* research grows through the incorporation of ECM biomaterials, so does the necessity to better characterize the biological response of cells involved. Bearing in mind the collective implications on cellular organization, behaviour, and differentiation-related gene and protein expression profiles, our findings emphasize the importance of characterizing the ECM surface parameters used in spheroid/organoid-based assays and cultures. The generation of self-assembling spheroid cultures through regulation of ECM surface type and thickness also contributes to a deeper understanding of cell-ECM interactions. In consideration of the increased usage of 3D bioprinting and microfluidic "placenta-on-a-chip" devices within the last several years [5,59-61], a proper understanding and integration of ECM biomaterials will be a crucial step towards generating more *in vivo*-like models.

Acknowledgments

We thank Dr. Leo Hsu for sharing his insights on experimental design. We thank Dr. Tom Hawke, Dr. Ray Truant, and their labs, for generously providing access to microscopes. We thank Dr. Todd Hoare and his lab for generously providing access to the MicroSquisher.

References

1   Huppertz, B., Ghosh, D. & Sengupta, J. An integrative view on the physiology of human early placental villi. *Prog Biophys Mol Biol* **114**, 33-48, doi:10.1016/j.pbiomolbio.2013.11.007 (2014).

2   Red-Horse, K. *et al.* Trophoblast differentiation during embryo implantation and formation of the maternal-fetal interface. *The Journal of clinical investigation* **114**, 744-754, doi:10.1172/JCI22991 (2004).

3   Blundell, C. *et al.* A microphysiological model of the human placental barrier. *Lab Chip* **16**, 3065-3073, doi:10.1039/c6lc00259e (2016).

4   Blundell, C. *et al.* Placental Drug Transport-on-a-Chip: A Microengineered In Vitro Model of Transporter-Mediated Drug Efflux in the Human Placental Barrier. *Adv Healthc Mater* **7**, doi:10.1002/adhm.201700786 (2018).

5   Lee, J. S. *et al.* Placenta-on-a-chip: a novel platform to study the biology of the human placenta. *The Journal of Maternal-Fetal & Neonatal Medicine*, 1-9, doi:10.3109/14767058.2015.1038518 (2015).

6   Gohner, C. *et al.* The placenta in toxicology. Part IV: Battery of toxicological test systems based on human placenta. *Toxicol Pathol* **42**, 345-351, doi:10.1177/0192623313482206 (2014).

7   Tuuli, M. G., Longtine, M. S. & Nelson, D. M. Review: Oxygen and trophoblast biology--a source of controversy. *Placenta* **32 Suppl 2**, S109-118, doi:10.1016/j.placenta.2010.12.013 (2011).

8   Kolahi, K. S. *et al.* Effect of substrate stiffness on early mouse embryo development. *PloS one* **7**, e41717, doi:10.1371/journal.pone.0041717 (2012).

9   Rozario, T. & DeSimone, D. W. The extracellular matrix in development and morphogenesis: a dynamic view. *Dev Biol* **341**, 126-140, doi:10.1016/j.ydbio.2009.10.026 (2010).

10   Fennema, E., Rivron, N., Rouwkema, J., van Blitterswijk, C. & de Boer, J. Spheroid culture as a tool for creating 3D complex tissues. *Trends Biotechnol* **31**, 108-115, doi:10.1016/j.tibtech.2012.12.003 (2013).

11   Lei, T., Hohn, H. P., Behr, R. & Denker, H. W. Influences of extracellular matrix and of conditioned media on differentiation and invasiveness of trophoblast stem cells. *Placenta* **28**, 14-21, doi:10.1016/j.placenta.2006.01.020 (2007).

12   Hohn, H. P. *et al.* The role of matrix contact and of cell-cell interactions in choriocarcinoma cell differentiation. *Eur J Cell Biol* **69**, 76-85 (1996).

13   Hohn, H. P. & Denker, H. W. The role of cell shape for differentiation of choriocarcinoma cells on extracellular matrix. *Experimental cell research* **215**, 40-50, doi:10.1006/excr.1994.1312 (1994).

14   Kliman, H. J. & Feinberg, R. F. Human trophoblast-extracellular matrix (ECM) interactions in vitro: ECM thickness modulates morphology and

proteolytic activity. *Proceedings of the National Academy of Sciences of the United States of America* **87**, 3057-3061 (1990).

15   Hohn, H. P., Parker, C. R., Jr., Boots, L. R., Denker, H. W. & Hook, M. Modulation of differentiation markers in human choriocarcinoma cells by extracellular matrix: on the role of a three-dimensional matrix structure. *Differentiation* **51**, 61-70 (1992).

16   Mullen, C. A., Vaughan, T. J., Billiar, K. L. & McNamara, L. M. The effect of substrate stiffness, thickness, and cross-linking density on osteogenic cell behavior. *Biophys J* **108**, 1604-1612, doi:10.1016/j.bpj.2015.02.022 (2015).

17   Leong, W. S. *et al.* Thickness sensing of hMSCs on collagen gel directs stem cell fate. *Biochemical and biophysical research communications* **401**, 287-292, doi:10.1016/j.bbrc.2010.09.052 (2010).

18   Quibel, T. *et al.* Placental elastography in a murine intrauterine growth restriction model. *Prenat Diagn* **35**, 1106-1111, doi:10.1002/pd.4654 (2015).

19   Benton, G., Arnaoutova, I., George, J., Kleinman, H. K. & Koblinski, J. Matrigel: from discovery and ECM mimicry to assays and models for cancer research. *Adv Drug Deliv Rev* **79-80**, 3-18, doi:10.1016/j.addr.2014.06.005 (2014).

20   Rosser, J. M. *et al.* Recent Advances of Biologically Inspired 3D Microfluidic Hydrogel Cell Culture Systems. *J Cell Biol Cell Metab* **2**, 1-14 (2015).

21   Corning. Corning Matrigel Matrix: Frequently Asked Questions. (2013).

22   Orendi, K. *et al.* Placental and trophoblastic in vitro models to study preventive and therapeutic agents for preeclampsia. *Placenta* **32 Suppl**, S49-54, doi:10.1016/j.placenta.2010.11.023 (2011).

23   Orendi, K., Gauster, M., Moser, G., Meiri, H. & Huppertz, B. The choriocarcinoma cell line BeWo: syncytial fusion and expression of syncytium-specific proteins. *Reproduction* **140**, 759-766, doi:10.1530/REP-10-0221 (2010).

24   Ishikawa, A. *et al.* Cell fusion mediates dramatic alterations in the actin cytoskeleton, focal adhesions, and E-cadherin in trophoblastic cells. *Cytoskeleton (Hoboken)* **71**, 241-256, doi:10.1002/cm.21165 (2014).

25   Al-Nasiry, S., Spitz, B., Hanssens, M., Luyten, C. & Pijnenborg, R. Differential effects of inducers of syncytialization and apoptosis on BeWo and JEG-3 choriocarcinoma cells. *Hum Reprod* **21**, 193-201, doi:10.1093/humrep/dei272 (2006).

26   Borges, M., Bose, P., Frank, H. G., Kaufmann, P. & Pötgens, A. J. G. A Two-Colour Fluorescence Assay for the Measurement of Syncytial Fusion between Trophoblast-Derived Cell Lines. *Placenta* **24**, 959-964, doi:10.1016/s0143-4004(03)00173-5 (2003).

27   Krtolica, A., Ortiz de Solorzano, C., Lockett, S. & Campisi, J. Quantification of epithelial cells in coculture with fibroblasts by

fluorescence image analysis. *Cytometry* **49**, 73-82, doi:10.1002/cyto.10149 (2002).

28   Schweiger, P. J. & Jensen, K. B. Modeling human disease using organotypic cultures. *Current opinion in cell biology* **43**, 22-29, doi:10.1016/j.ceb.2016.07.003 (2016).

29   Skardal, A., Shupe, T. & Atala, A. Organoid-on-a-chip and body-on-a-chip systems for drug screening and disease modeling. *Drug Discov Today*, doi:10.1016/j.drudis.2016.07.003 (2016).

30   Clevers, H. Modeling Development and Disease with Organoids. *Cell* **165**, 1586-1597, doi:10.1016/j.cell.2016.05.082 (2016).

31   Shamir, E. R. & Ewald, A. J. Three-dimensional organotypic culture: experimental models of mammalian biology and disease. *Nature reviews. Molecular cell biology* **15**, 647-664, doi:10.1038/nrm3873 (2014).

32   Huppertz, B. & Gauster, M. Mechanisms Regulating Human Trophoblast Fusion. 203-217, doi:10.1007/978-90-481-9772-9_9 (2011).

33   LaMarca, H. L. *et al.* Three-dimensional growth of extravillous cytotrophoblasts promotes differentiation and invasion. *Placenta* **26**, 709-720, doi:10.1016/j.placenta.2004.11.003 (2005).

34   Korff, T., Krauss, T. & Augustin, H. G. Three-dimensional spheroidal culture of cytotrophoblast cells mimics the phenotype and differentiation of cytotrophoblasts from normal and preeclamptic pregnancies. *Experimental cell research* **297**, 415-423, doi:10.1016/j.yexcr.2004.03.043 (2004).

35   Robins, J. C., Morgan, J. R., Krueger, P. & Carson, S. A. Bioengineering anembryonic human trophoblast vesicles. *Reproductive sciences* **18**, 128-135, doi:10.1177/1933719110381923 (2011).

36   Muoth, C. *et al.* A 3D co-culture microtissue model of the human placenta for nanotoxicity assessment. *Nanoscale* **8**, 17322-17332, doi:10.1039/c6nr06749b (2016).

37   Evans, J., Salamonsen, L. A., Menkhorst, E. & Dimitriadis, E. Dynamic changes in hyperglycosylated human chorionic gonadotrophin throughout the first trimester of pregnancy and its role in early placentation. *Hum Reprod* **30**, 1029-1038, doi:10.1093/humrep/dev016 (2015).

38   Cole, L. A. hCG, the wonder of today's science. *Reprod Biol Endocrinol* **10**, 24, doi:10.1186/1477-7827-10-24 (2012).

39   Nguyen-Ngoc, K. V. *et al.* ECM microenvironment regulates collective migration and local dissemination in normal and malignant mammary epithelium. *Proceedings of the National Academy of Sciences of the United States of America* **109**, E2595-2604, doi:10.1073/pnas.1212834109 (2012).

40   Miner, J. H., Cunningham, J. & Sanes, J. R. Roles for Laminin in Embryogenesis: Exencephaly, Syndactyly, and Placentopathy in Mice Lacking the Laminin α5 Chain. *The Journal of cell biology* **143**, 1713-1723, doi:10.1083/jcb.143.6.1713 (1998).

41   Onogi, A. *et al.* Hypoxia inhibits invasion of extravillous trophoblast cells through reduction of matrix metalloproteinase (MMP)-2 activation in the

early first trimester of human pregnancy. *Placenta* **32**, 665-670, doi:10.1016/j.placenta.2011.06.023 (2011).

42   Bischof, P. & Campana, A. A putative role for oncogenes in trophoblast invasion? *Hum Reprod* **15 Suppl 6**, 51-58 (2000).

43   Librach, C. L. *et al.* 92-kD type IV collagenase mediates invasion of human cytotrophoblasts. *The Journal of cell biology* **113**, 437-449 (1991).

44   Isaka, K. *et al.* Expression and activity of matrix metalloproteinase 2 and 9 in human trophoblasts. *Placenta* **24**, 53-64 (2003).

45   Beck, J. N., Singh, A., Rothenberg, A. R., Elisseeff, J. H. & Ewald, A. J. The independent roles of mechanical, structural and adhesion characteristics of 3D hydrogels on the regulation of cancer invasion and dissemination. *Biomaterials* **34**, 9486-9495, doi:10.1016/j.biomaterials.2013.08.077 (2013).

46   Snir, A., Brenner, B., Paz, B., Ohel, G. & Lanir, N. The role of fibrin matrices and tissue factor in early-term trophoblast proliferation and spreading. *Thromb Res* **132**, 477-483, doi:10.1016/j.thromres.2013.08.023 (2013).

47   Zhou, Y. *et al.* Effects of Human Fibroblast-Derived Extracellular Matrix on Mesenchymal Stem Cells. *Stem Cell Rev*, doi:10.1007/s12015-016-9671-7 (2016).

48   Denecke, B. *et al.* Human endothelial colony-forming cells expanded with an improved protocol are a useful endothelial cell source for scaffold-based tissue engineering. *J Tissue Eng Regen Med* **9**, E84-97, doi:10.1002/term.1673 (2015).

49   Tarrade, A. *et al.* Characterization of human villous and extravillous trophoblasts isolated from first trimester placenta. *Lab Invest* **81**, 1199-1211 (2001).

50   Mierke, C. T. The integrin alphav beta3 increases cellular stiffness and cytoskeletal remodeling dynamics to facilitate cancer cell invasion. *New Journal of Physics* **15**, doi:10.1088/1367-2630/15/1/015003 (2013).

51   Martino, M. M. *et al.* Controlling integrin specificity and stem cell differentiation in 2D and 3D environments through regulation of fibronectin domain stability. *Biomaterials* **30**, 1089-1097, doi:10.1016/j.biomaterials.2008.10.047 (2009).

52   Cohen, M., Meisser, A. & Bischof, P. Metalloproteinases and human placental invasiveness. *Placenta* **27**, 783-793, doi:10.1016/j.placenta.2005.08.006 (2006).

53   Bae, Y. H. *et al.* A FAK-Cas-Rac-Lamellipodin Signaling Module Transduces Extracellular Matrix Stiffness into Mechanosensitive Cell Cycling. *Sci Signal* **7**, doi:ARTN ra57
10.1126/scisignal.2004838 (2014).

54   Hannan, N. J., Paiva, P., Dimitriadis, E. & Salamonsen, L. A. Models for study of human embryo implantation: choice of cell lines? *Biology of reproduction* **82**, 235-245, doi:10.1095/biolreprod.109.077800 (2010).

55   Handschuh, K. *et al.* Human chorionic gonadotropin expression in human trophoblasts from early placenta: comparative study between villous and extravillous trophoblastic cells. *Placenta* **28**, 175-184, doi:10.1016/j.placenta.2006.01.019 (2007).

56   Huppertz, B. & Gauster, M. Trophoblast fusion. *Advances in experimental medicine and biology* **713**, 81-95, doi:10.1007/978-94-007-0763-4_6 (2011).

57   Gerbaud, P. & Pidoux, G. Review: An overview of molecular events occurring in human trophoblast fusion. *Placenta* **36 Suppl 1**, S35-42, doi:10.1016/j.placenta.2014.12.015 (2015).

58   Dupressoir, A. *et al.* A pair of co-opted retroviral envelope syncytin genes is required for formation of the two-layered murine placental syncytiotrophoblast. *Proceedings of the National Academy of Sciences of the United States of America* **108**, E1164-1173, doi:10.1073/pnas.1112304108 (2011).

59   Blundell, C. *et al.* A microphysiological model of the human placental barrier. *Lab Chip*, doi:10.1039/c6lc00259e (2016).

60   Jose, R. R., Rodriquez, M. J., Dixon, T. A., Omenetto, F. G. & Kaplan, D. L. Evolution of Bioinks and Additive Manufacturing Technologies for 3D Bioprinting. *ACS Biomaterials Science & Engineering*, doi:10.1021/acsbiomaterials.6b00088 (2016).

61   Kuo, C.-Y. *et al.* Development of a 3D Printed, Bioengineered Placenta Model to Evaluate the Role of Trophoblast Migration in Preeclampsia. *ACS Biomaterials Science & Engineering*, doi:10.1021/acsbiomaterials.6b00031 (2016).

Figures and Figure Legends
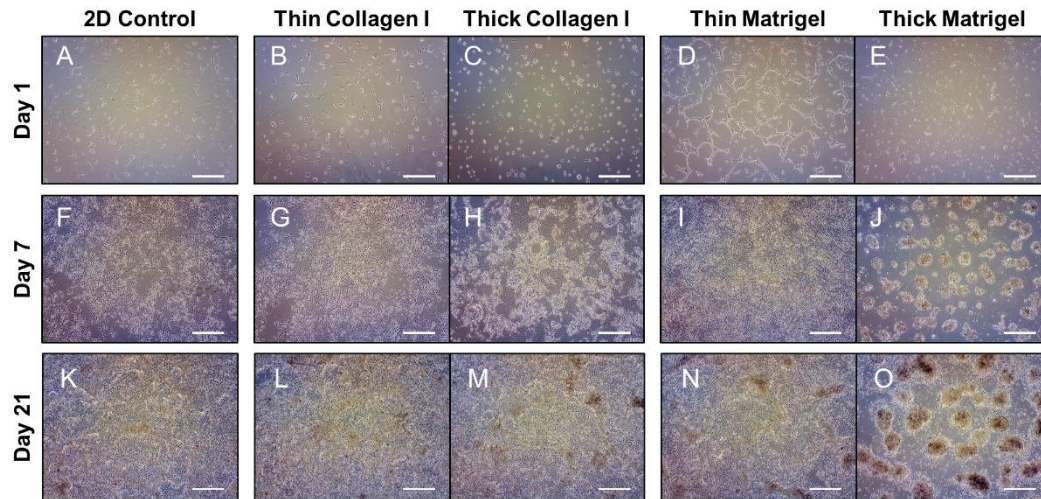
Figure 1. Thick Matrigel regulates self-assembly of trophoblast spheroids as determined by live cell imaging. BeWo cells cultured for 1 day on (A) 2D control surface, (B) thin collagen I, (C) thin Matrigel, (D) thick collagen I, and (E) thick Matrigel. BeWo cells were grown for 7 days on (F) 2D control surface, (G) thin collagen I, (H) thin Matrigel, (I) thick collagen I, and (J) thick Matrigel. BeWo cells were grown for 21 days on (K) 2D control surface, (L) thin collagen I, (M) thin Matrigel, (N) thick collagen I, and (O) thick Matrigel. All images were taken at 4x objective magnification and scale bar indicates 500 µm. n=3.
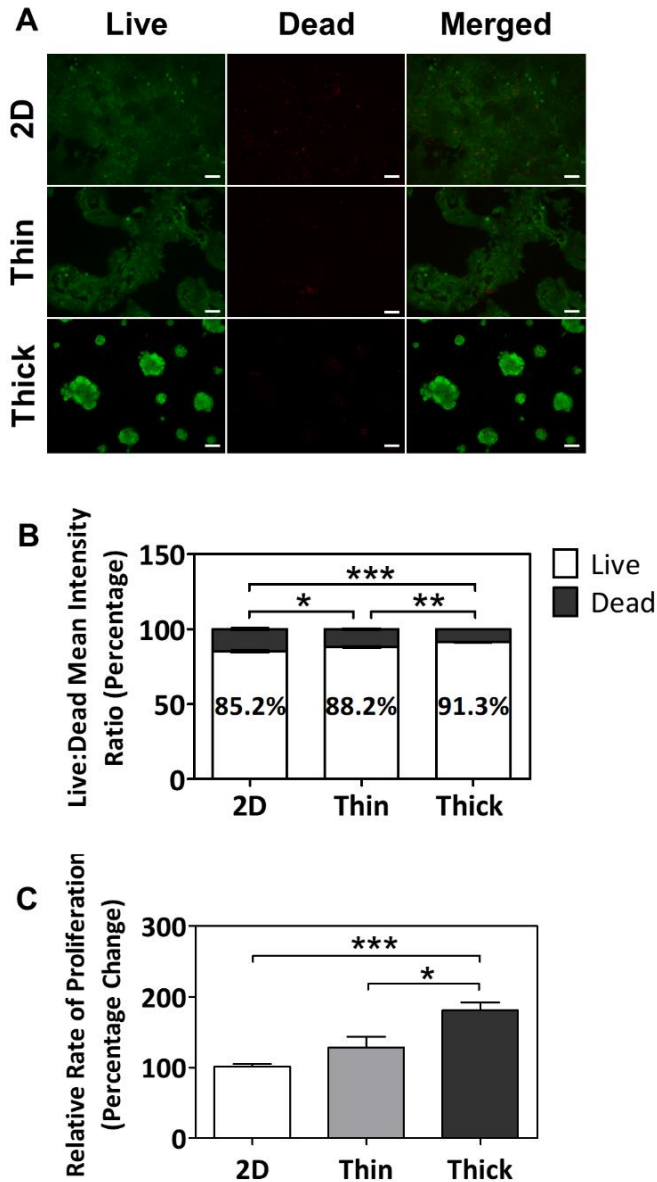
Figure 2. Thickness-dependent increases in cell viability and proliferation in BeWo cells cultured on Matrigel after 7 days. (A) Immunofluorescent images of BeWo cells stained with Calcein AM (green) and Ethidium homodimer-1 (red). All images were taken at 10x objective magnification and scale bar indicates 100 µm. (B) Percentage ratio of mean intensities of live and dead cells cultured on 2D, thin, and thick surfaces. (C) Relative rates of proliferation of cells cultured on 2D, thin, and thick surfaces as assessed via MTS assay. Significant differences between treatment groups determined by one-way ANOVA followed by Tukey's post-test; $n \geq 3$. Significant differences between means determined by post-tests were indicated by * ($p<0.05$), ** ($p<0.01$), or *** ($p<0.001$).
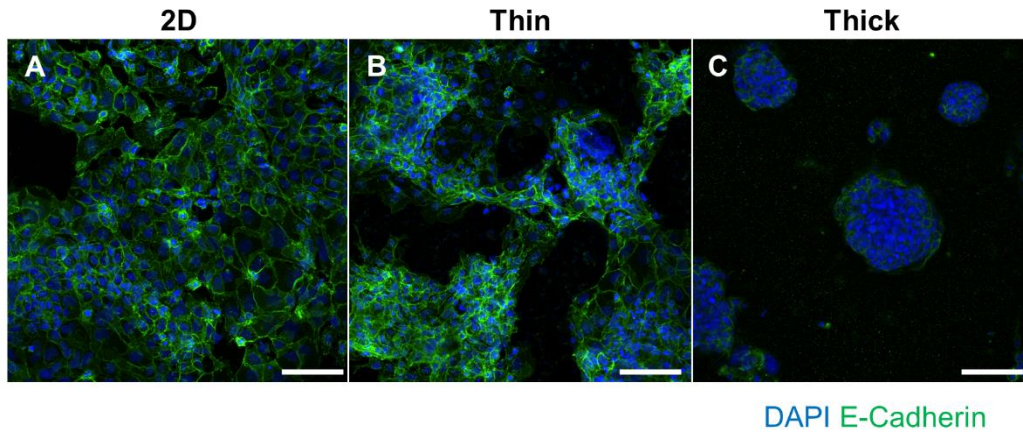
Figure 3. Immunofluorescent staining of E-Cadherin and DAPI to visualize syncytial fusion. BeWo cells grown on (A) 2D, (B) thin Matrigel, or (C) thick Matrigel surfaces. Green fluorescence indicates E-Cadherin staining and blue fluorescence indicates DAPI staining for cell nuclei. Images were taken at 20x magnification and scale bar indicates 100 µm.
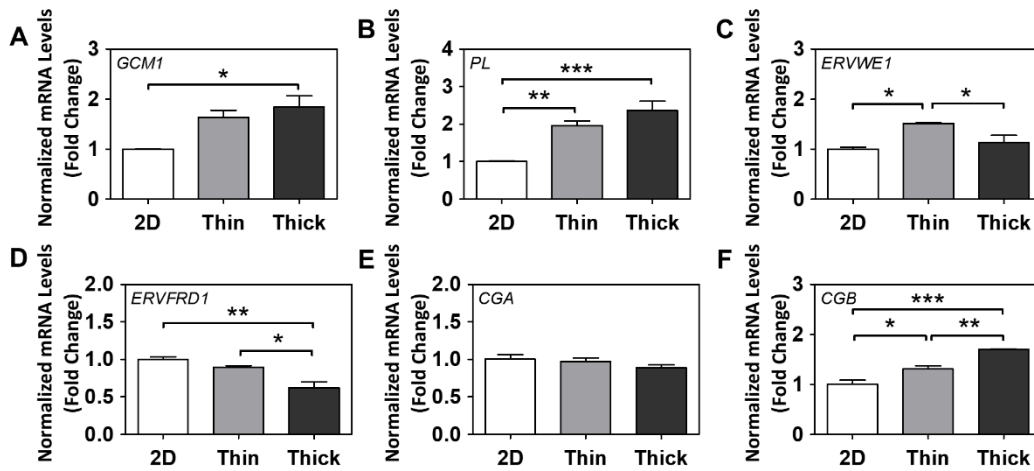
Figure 4. The effect of Matrigel thickness on gene markers of differentiation and syncytial fusion. Normalized mRNA levels of (A) *GCM1*, (B) *PL*, (C) *ERVWE1*, (D) *ERVFRD1*, (E) *CGA*, and (F) *CGB* after 7 days of growth on various surface thicknesses. (E) Normalized protein levels of secreted hCGβ in media. Significant differences between treatment groups determined by one-way ANOVA followed by Tukey's post-test; n≥3. Significant differences between means determined by post-tests were indicated by * ($p<0.05$), ** ($p<0.01$), or *** ($p<0.001$).
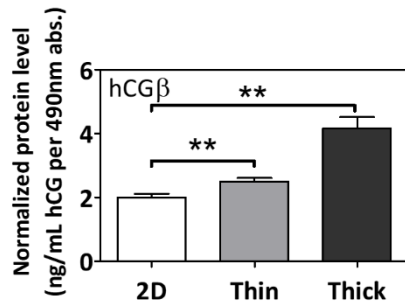
Figure 5. The effect of Matrigel thickness on the secretion of human chorionic gonadotropin β (*hCGβ*) in the cell media. Normalized protein levels of secreted hCGβ in media. Significant differences between treatment groups determined by one-way ANOVA followed by Tukey's post-test; n≥3. Significant differences between means determined by post-tests were indicated by ** (p<0.01).
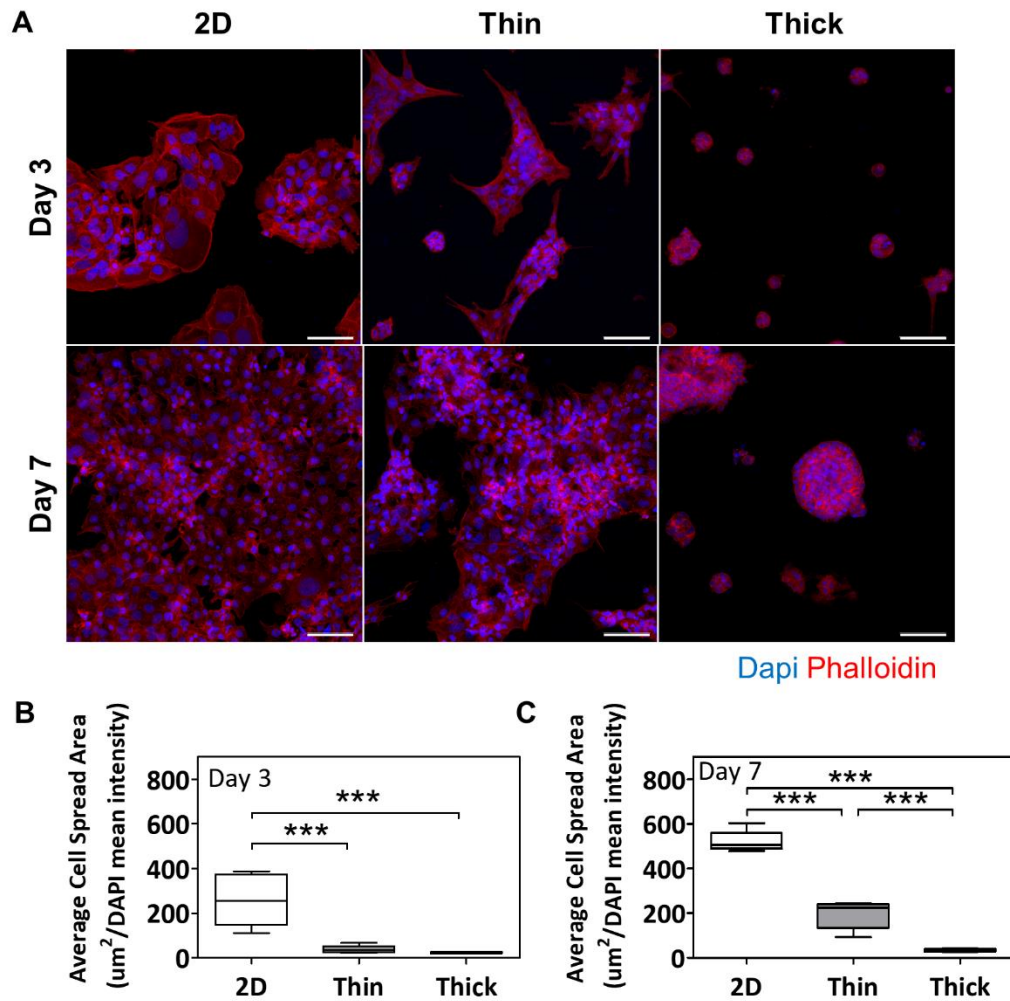
Figure 6. Thick Matrigel leads to decreased F-actin cell spread areas. (A) Immunofluorescent images of Phalloidin staining at days 3 and 7 across various surface thicknesses. Red fluorescence indicates phalloidin staining for F-actin and blue fluorescence indicates DAPI staining for cell nuclei. Images were taken at 20x magnification and scale bar indicates 100 μm. Average cell spread areas as determined by quantifying the normalized binary area of phalloidin stain at (B) day 3 and (C) day 7. Significant differences between treatment groups determined by one-way ANOVA followed by Tukey's post-test; n=3. Significant differences between means determined by post-tests were indicated by *** (p<0.001).
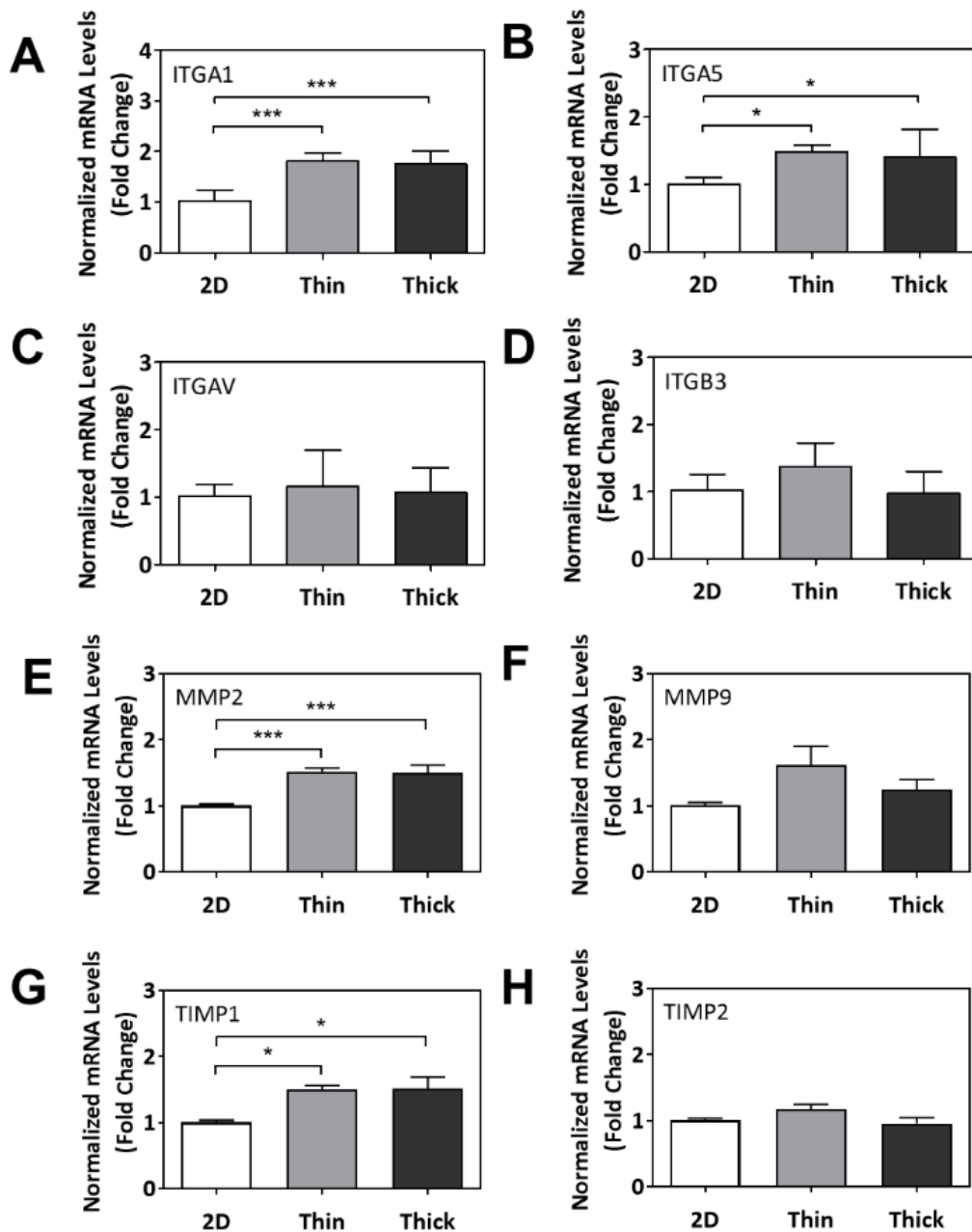
Figure 7. Gene expression profiling of cellular stiffness response to ECM surface thickness. Normalized mRNA levels of (A) *ITGA1*, (B) *ITGA5*, (C) *ITGAV*, (D) *ITGB3*, (E) *MMP2*, (F) *MMP9*, (G) *TIMP1*, and (H) *TIMP2*. Significant differences between treatment groups determined by one-way ANOVA followed by Tukey's post-test; n≥3. Significant differences between means determined by post-tests were indicated by * ($p<0.05$), ** ($p<0.01$), or *** ($p<0.001$).

Tables

Table 1. Forward and reverse sequences for the primers used for qPCR.

Gene	Forward	Reverse	GenBank
18S (RNA18S5)	CACGCCAGTACAAGATCCCA	AAGTGACGCAGCCCTCTATG	NR_003286.2
Glial Cells Missing Homolog 1 (GCM1)	CCTCTGAAGCTCATCCCTTGC	ATCATGCTCTCCCTTTGACTGG	NM_003643.3
Placental Lactogen (PL)	GCCATTGACACCTACCAG	GATTTCTGTTGCGTTTCCTC	V00573.1
Endogenous Retrovirus Group W Member 1, Envelope; Syncytin-1 (ERVWE1)	GTTAATGACATCAAAGGCACCC	CCCCATCTCAACAGGAAAACC	NM_014590
Endogenous Retrovirus Group FRD Member 1, Envelope; Syncytin-2 (ERVFRD1)	GCCTACCGCCATCCTGATTT	GCTGTCCCTGGTGTTTCAGT	NM_207582.2
Chorionic Gonadotropin, Alpha (CGA)	GCAGGATTGCCCAGAATGC	TCTTGGACCTTAGTGGAGTGG	V00518.1
Chorionic Gonadotropin, Beta (CGB)	ACCCCTTGACCTGTGAT	CTTTATTGTGGGAGGATCGG	J00117.1
Matrix Metalloproteinase (MMP) 2	TCTCCTGACATTGACCTTGGC	CAAGGTGCTGGCTGAGTAGATC	NM_004530.5
MMP9	CCGGCATTCAGGGAGACGCC	TGGAACCACGACGCCCTTGC	NM_004994.2
Tissue Inhibitor of Metalloproteinases (TIMP)1	GGGCTTCACCAAGACCTACA	TGCAGGGGATGGATAAACAG	NM_003254.2
TIMP2	GAAGAGCCTGAACCACAGGT	GGGGGAGGAGATGTAGCAC	NM_003255.4
Integrin Subunit Alpha (ITGA) 1	CAGTCTATCCACGGAGAAATG	GGCTCAAAATTCATGGTCAC	NM_181501.1
ITGA5	CCAAAAGAAGCCCCCAGCTA	TCCTTGTGTGGCATCTGTCC	NM_002205.4
ITGAV	TCACTAAGCGGGATCTTGCC	AGCACTGAGCAACTCCACAA	EF560727.1
Integrin Subunit Beta (ITGB) 3	GAAGCAGAGTGTGTCACGGA	TGCATCATTCCTCCAGCCAA	NM_000212.2

Supplemental Figures

A

Thin Gel (50µm)   Thick Gel (250µm)

B

Thin Matrigel   Thick Matrigel

C

D
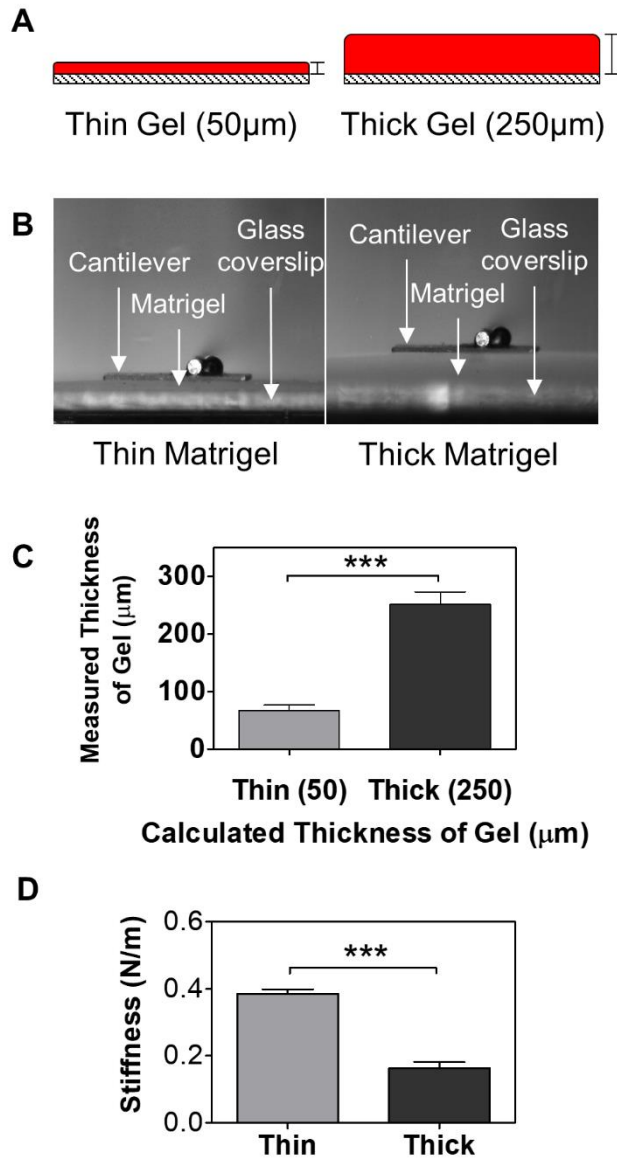
S1 Figure. Analysis of ECM surface properties. (A) Schematic representing thin and thick ECM surface samples. (B) Representative images of ECM surfaces as captured by MicroSquisher camera. (C) Measurements of actual thicknesses of ECM surface based on theoretical calculations for 50 and 250 µm. (D) Measurements of ECM surface stiffness based on surface thickness. Significant differences between means indicated by *** (p<0.001), as determined by unpaired t-Test; n=3.

CHAPTER 3: TRANSCRIPTOMIC AND FUNCTIONAL ANALYSES OF

3D PLACENTAL EXTRAVILLOUS TROPHOBLAST SPHEROIDS

Chapter Preface

This chapter is a reprint of an original article: Wong, M. K., Wahed, M., Shawky, S. A., Dvorkin-Gheva, A., & Raha, S. (2019). Transcriptomic and functional analyses of 3D placental extravillous trophoblast spheroids. Scientific reports, 9(1), 1-13. This work is licensed under the Creative Commons Attribution 4.0 International License, which permits unrestricted use, distribution, modification, and reproduction in any medium (**Appendix 1**).

By combining our ECM surface discoveries from Chapter 2 and the elegant methods used by Vinci et al. for tumour spheroids, this second model enabled the high-throughput generation of 3D extravillous trophoblast spheroids that were capable of invasion and migration. Traditional invasion assays only examined invasion of individualized cells, but our model served the advantage of also illuminating the initial migration away from the core anchoring villi and possessing greater transcriptomic similarities to extravillous trophoblasts. Lastly, we were able to assess the impact of pregnancy-relevant drugs on placental invasion (*e.g.,* Δ^9-tetrahydrocannabinol). This model provides a new platform to investigate the mechanistic underpinnings of invasion, diseases such as placental accreta, and the impact of drugs and toxins on extravillous trophoblast function.

Abstract

Placental extravillous trophoblast (EVT) invasion is essential in establishing proper blood supply to the fetus during pregnancy. However, traditional 2D *in vitro* systems do not model the *in vivo* invasion process in an anatomically-relevant manner. Our objectives were to develop a 3D spheroid model that would allow better emulation of placental invasion *in vitro* and to characterize the transcriptomic and functional outcomes. HTR8/SVneo EVT cells were self-assembled into 3D spheroids using ultra-low attachment plates. Transcriptomic profiling followed by gene set enrichment and gene ontology analyses revealed major global transcriptomic differences, with significant up-regulations in EVTs cultured as 3D spheroids in canonical pathways and biological processes such as immune response, angiogenesis, response to stimulus, wound healing, and others. These findings were further validated by RT-qPCR, showing significant up-regulations in genes and/or proteins related to epithelial-mesenchymal transition, cell-cell contact, angiogenesis, and invasion/migration. A high-throughput, spheroid invasion assay was applied to reveal the dynamic invasion of EVTs away from the spheroid core into extracellular matrix. Lastly, lipopolysaccharide, dexamethasone, or Δ^9-tetrahydrocannabinol exposure was found to impact the invasion of EVT spheroids. Altogether, we present a well-characterized, 3D spheroid model of EVT invasion and demonstrate its potential use in drug and toxin screening during pregnancy.

Introduction

The human placenta is a transient organ that forms the interface between the mother and fetus during pregnancy [1]. One of its key functions during early pregnancy is invasion and migration into the maternal decidua [2,3]. Proper invasion is critical to the remodeling of maternal spiral arteries into high capacitance, low resistance vessels that supply oxygen and nutrients to the fetus [4]. The primary placental cell type responsible for regulating invasion is the extravillous trophoblast (EVT), which bears the ability to migrate away from the solid trophoblast columns of the anchoring chorionic villi and invade into the maternal decidua [5]. This process is highly regulated by a variety of physiochemical factors (*e.g.* oxygen, growth factors, nutrients, extracellular matrix proteins), and dysregulated EVT invasion can conversely result in compromised placentation and an inability to properly support both the mother and fetus [6]. Interestingly, pregnancy-related diseases like preeclampsia and placenta accreta have been strongly associated with altered EVT invasion and spiral artery remodeling, both poorly understood pathological outcomes of impaired trophoblast function [6]. However, our ability to better understand the cellular and molecular underpinnings of these placental diseases may be limited, in part, by the unrepresentative nature of current two-dimensional (2D) *in vitro* systems.

Accumulating evidence in other organ systems and cancer models suggest that culturing cells in three-dimensions (3D) can provide more anatomically- and physiologically-relevant results compared to traditional 2D monolayer cultures [7].

While some researchers have begun to culture placental cells as 3D spheroids or organoids [8-12], our overall understanding of the transcriptomic changes and functional outcomes associated with its formation remains preliminary. Characterization studies contrasting novel 3D spheroids against 2D monolayers are especially lacking – yet, these are necessary to justify its use and advancement, as the theorized advantages (*e.g.,* enhanced cell-cell contact, physiological function, etc. [7]) are not verified in placental *in vitro* cultures. Moreover, there are no spheroid models to date that directly and specifically mimic the trophoblast column of the anchoring chorionic villi, and demonstrate functional EVT invasion and migration away from its core as seen *in vivo* [13]. To address this, we develop a self-assembling, 3D spheroid culture system of the trophoblast column and EVT invasion, and use a transcriptome-wide microarray and bioinformatics approach to characterize the global gene expression profiles against traditional 2D monolayers. We further apply a high-throughput, spheroid invasion assay to measure the actual invasion of the 3D EVT spheroids into extracellular matrix in real-time, and assess the impact of various drugs and compounds.

Results

Extravillous trophoblast cells self-assembled into 3D spheroids with high viability over eight days

HTR8/SVneo EVT cells seeded in ultra-low attachment plates at densities of 1,000, 5,000, and 10,000 cells/mL all self-assembled into spheroids within two days with average diameters of 211.1 µm, 323.7 µm, and 411.6 µm, respectively (**Figure 1a**). Spheroid diameter increased at rates of 36.05 ± 2.01, 31.26 ± 1.73 and 26.65 ± 3.47 µm/day over eight days, respective to the seeding densities, and maintained structural integrity throughout (**Figure 1a, b**). Spheroids seeded at 5,000 cells/mL were used in subsequent experiments as they maintained mean diameters of less than 500 µm over eight days, above which has been frequently characterized with necrotic cores [14]. Indeed, live and dead staining using calcein AM and ethidium homodimer-1, respectively, confirmed that spheroids maintain high viability (98.9 – 99.9% live cells) over eight days (**Figure 1c, d**). Hematoxylin and eosin (H&E) staining of cross-sections also revealed that the spheroids exhibit solid cores (**Figure 1e**), resembling the solid structural anatomy of trophoblast columns *in vivo* [15].

Distinct transcriptomic profiles in EVTs cultured as 3D spheroids and 2D monolayers

To understand how global gene expression profiles were changed in EVTs cultured as 3D spheroids compared to 2D monolayers, we analyzed 21,448 genes via Clariom S Human transcriptome profiling microarray (Thermo). A total of

4,562 gene probe sets were found to be differentially expressed in 3D spheroids compared to 2D monolayers, with 2,327 genes up-regulated and 2,235 genes down-regulated (FDR p-value < 0.05; absolute fold change ≥ 2; **Figure 2a**). Cluster dendrogram analyses demonstrated distinct grouping between samples from 3D spheroid and 2D monolayer groups and a large height distance to convergence, suggesting highly different global transcriptome profiles between the two groups (**Figure 2b**). The short height distance to convergence seen for samples within each of the two groups suggests similar transcriptome profiles within each group.

Gene set enrichment analysis of canonical pathways and biological processes

We next performed gene set enrichment analysis (GSEA) on the transcriptome microarray data to identify the enriched canonical pathways in extravillous trophoblasts cultured as 3D spheroid compared to 2D monolayers (**Figure 3a**). The top fifteen most significantly enriched canonical pathway terms in EVTs cultured as 3D spheroids included categories: "neuroactive ligand-receptor interaction", "immune processes, diseases, defensins", "signaling events", and "ECM" (FDR p<0.05; **Supplementary Table S1**). The top fifteen most significantly down-regulated pathway terms in 3D spheroids included categories: "diseases", "transcription, HIV life cycle", "cell cycle", and "cell cycle, apoptosis" (FDR p<0.05; **Supplementary Table S2**). Full list of canonical pathway modules, categories, and terms may be found in **Supplementary Table S3**.

We also performed GSEA to identify the enriched biological processes in 3D spheroids compared to 2D monolayers (**Figure 3b**). The top fifteen most

significantly enriched biological process terms in EVTs cultured as 3D spheroids included categories: "immune processes", "perception", "chemotaxis", "peptide cross linking", "systemic processes", and "response to zinc" (FDR $p<0.05$; **Supplementary Table S4**). The top fifteen most significantly down-regulated biological process terms in 3D spheroids included categories: "protein complexes", "metabolism, biosynthesis, catabolism", "cell cycle", and "transcription" (FDR $p<0.05$; **Supplementary Table S5**). Full list of biological process modules, categories, and terms may be found in **Supplementary Table S6**.

Gene ontology analysis of biological processes

In parallel, we performed gene ontology (GO) analysis on the transcriptome microarray data to elucidate the over-represented biological processes based on differential expression (**Figure 4**). The top fifteen most significantly up-regulated biological process terms in EVTs cultured as 3D spheroids compared to 2D monolayers included categories: "sensory perception", "transport", "response to stimulus, wound healing", "G-protein signaling", and "immune processes, angiogenesis, and response to stimulus" (FDR $p<0.05$; **Supplementary Table S7**). The top fifteen most significantly down-regulated biological process terms in spheroids compared to monolayers included categories: "metabolic, biosynthetic, catabolic processes", "transcription, translation, DNA replication", and "cell cycle" (FDR $p<0.05$; **Supplementary Table S8**). Full list of GO biological process categories, terms, and gene lists may be found in **Supplementary Table S9**.

Increased expression of markers related to epithelial-mesenchymal transition (EMT), cell-cell contact, angiogenesis, and invasion in EVTs cultured as 3D spheroids

We were particularly intrigued by the up-regulated biological process categories of "immune processes, angiogenesis, response to stimulus", "response to stimulus and wound healing", and "differentiation and vasculature development" in 3D spheroids, given the important role played by EVTs in placental invasion and vascular remodeling (FDR p<0.05; **Supplementary Table S9**). We first investigated changes in markers in the EMT pathway via RT-qPCR, as EMT of trophoblasts closely underlies the initiation of placental invasion[7,16]. mRNA levels of upstream EMT markers *WNT5A, TGFB1, and TGFB2* were significantly increased in 3D spheroids compared to 2D monolayers (p<0.01 for all; **Figure 5a**). Further downstream, integrin *(ITG)A2, ITGA5, ITGB1,* and vimentin (*VIM*) mRNA levels were increased in 3D spheroids compared to 2D, and occludin (*OCLN*) mRNA levels were decreased (p<0.01 for all; **Figure 5b**). Contrastingly, E-cadherin (*CDH1*) and zona occludens-1 (*TJP1)* mRNA levels were significantly increased in 3D spheroids (p<0.01 for all; **Figure 5b**), whereas they are typically repressed during EMT[16]. This may be explained in part by the fact that *CDH1* and *TJP1* were also markers of cell-cell contact and tight junction formation, which is promoted by 3D culture[7]. Claudin (*CLDN)1* and *CLDN4* mRNA levels, additional markers of tight junctions, were also significantly increased in 3D spheroids (p<0.001 for all; **Figure 5b**).

We further investigated placental angiogenesis and invasion gene markers shared across several of the biological process categories listed above. We found significant up-regulations in mRNA levels of *HIF1A*, *VEGFA*, *VEGFC*, and *MMP9* in EVTs cultured as 3D spheroids compared to 2D monolayers ($p<0.01$ for all genes; **Figure 5c**). mRNA levels of *TIMP2* remained unchanged (**Figure 5c**). Protein levels of MMP9 were also increased in EVTs cultured as 3D spheroids, and protein levels of TIMP2 decreased (**Figure 5d**; Whole blots provided in **Supplementary Fig. S1**). Altogether, this suggests that EVTs cultured as 3D spheroids exhibit enhanced expression of EMT activation, cell-cell contact, and tight junction formation in association with increased expression of angiogenesis and invasion.

EVT spheroids exhibit dynamic invasion when embedded into ECM

Considering that the spheroids expressed increased markers of invasion and angiogenesis, we next investigated their actual, functional invasiveness. We adapted and applied a novel, high-throughput spheroid invasion assay for use with our EVT spheroids [17]. Spheroids were embedded into ECM on day two, and observable invadopodia-like projections began to sprout from the spheroid core on day four, increasing in invaded area over the eight days (**Figure 6a**). Mean spheroid invasion significantly increased over time, reaching approximately 60-70% invasion at day eight ($p<0.05$; **Figure 6b**). Using F-actin and DAPI immunofluorescent staining, the invadopodia-like projections were found to be actual cells moving away from the spheroid core and into the ECM (**Figure 6c**).

Control spheroids that were not embedded in ECM did not exhibit any invadopodia-like projections and remained as round spheres over the eight days (**Figure 6c**). ECM-embedded, invasive spheroids further demonstrated significantly increased immunofluorescent staining for HIF1A protein ($p < 0.05$; **Figure 6d, f**) and MMP9 protein ($p < 0.05$; **Figure 6e, g**) compared to control spheroids.

Spheroid invasion impacted by exogenous drugs and compounds

Lastly, we were interested in testing the responsiveness of our 3D EVT spheroids to exogenous drugs and compounds. Spheroids were embedded into ECM and treated with lipopolysaccharide, dexamethasone, or THC every 48 hours for up to eight days. Lipopolysaccharide and dexamethasone have previously been shown to augment and inhibit placental invasion, respectively, thus would serve to validate the spheroids' responsiveness [18-22]. Lipopolysaccharide (1-100 ng/mL and 10,000 ng/mL) indeed significantly augmented EVT invasion by day eight compared to the vehicle control ($p < 0.05$; **Figure 7a, b**). Tube formation was observable for some LPS-treated spheroids, indicating the invasion of EVTs had extended up to the top of the ECM layer (**Figure 7b**). Dexamethasone (100-10,000 nM) significantly inhibited EVT invasion by day eight compared to the vehicle control ($p < 0.05$; **Figure 7c, d**). Given the dynamic invasive response to the validated compounds, we were interested in testing the effects of THC, a controversial, less-understood compound with early evidence to impact placental invasion [23]. THC (30 µM) significantly inhibited EVT invasion by day eight compared to the vehicle control ($p < 0.05$; **Figure 7e, f**).

Discussion

Three-dimensional spheroid and organoid cultures carry the potential to restore *in vivo*-like phenotypes in many *in vitro* organ systems [7]. Our study is the first to generate a specific 3D spheroid *in vitro* model of the trophoblast column that is capable of functional and responsive EVT invasion. We further demonstrate that 3D EVT spheroids: (1) express global transcriptomes that are distinct compared to 2D monolayers, (2) exhibit invasive and migratory gene and protein expression profiles alongside dynamic invasive behaviour when embedded into an ECM environment, and (3) may be studied by adapting the innovative spheroid invasion assay, which was originally pioneered by tumour researchers [17,24], revealing responsiveness to exogenous drugs. Moreover, the simplicity of our ultra-low attachment microplate approach, continuous real-time monitoring capability, relative low cost of materials required, and use of a well-established cell line, collectively provides an accessible and versatile tool for researchers.

The major transcriptomic differences found in the GSEA and GO analyses altogether suggest that spheroid culturing conditions alone are sufficient to drive EVTs towards expressing a unique genetic profile compared to monolayers. Spheroids possessed enhanced expression profiles of EMT, cell-cell contact, tight junction formation, invasion, and angiogenesis, suggesting they may be a useful model to study EVT invasion. The initial detachment of EVTs from the trophoblast column and continual, but highly-measured, taxis into the maternal decidua is a key phenomenon observed *in vivo* that is not emulated in traditional invasion assays [25].

One major advantage of our model is the establishment of a solid spheroid core, which mimics the microarchitecture and physiochemical driving forces present at the trophoblast column of the anchoring chorionic villi *in vivo* (*e.g.,* hypoxia/oxygen gradients, mechanical stimulation via ECM, etc.) Only EVTs that are truly invasive would be capable of detaching, invading, and migrating away from the core, whereas traditional assays use individualized cells that are primed to invade via serum-deprivation/reintroduction [25]. HIF1α, a protein known to be rapidly depleted by oxygen, was indeed augmented in our invading spheroids, suggesting the potential involvement of a hypoxia-driven mechanism [26-28]. HIF1α is a key regulator of invasion *in vivo,* and mice with *Hif1α* knocked out experience impaired placental invasion and angiogenesis compared to controls [29]. MMP9, a crucial matrix metalloproteinase in EVT invasion and known to be stimulated by hypoxia [30], was also augmented at the protein level in invading spheroids. This reveals a preliminary mechanism that is consistent with *in vivo* EVT invasion, although more work must be done to further validate this.

Spheroid cultures also enable the co-existence of proliferative, quiescent and apoptotic states within the same population due to the nature of the 3D construct and the varying depths that cells reside from nutrient and oxygen sources, which better resembles the heterogeneous cellular organization present *in vivo* [7,24]. Accordingly, it has been well-demonstrated by cancer researchers that tumour spheroids exhibit a more physiological response and resistance in drug studies compared to monolayers [24,31,32], and thus serve as more predictive *in vitro* models.

Yang, et al. [33] showed that pancreatic tumour cells cultured as spheroids exhibited greater invasive and migratory behaviour and more consistently formed tumours when injected into nude mice, compared to parental cells cultured as monolayers. Moreover, following paclitaxel chemotherapy treatment, ovarian cancer spheroids remained 20% more viable and proliferative than monolayers, which resembles a chemoresistance similarly seen in other tumours *in vivo* [32]. Following this hypothesis, our 3D EVT spheroids should also provide more a predictive response and resistance to drug exposure. For obvious ethical reasons, it was challenging to directly compare the drug responses of clinical populations given the lack of available data in pregnant women. We do, however, present novel findings that EVT spheroids are responsive to several exogenous compounds, with augmented invasion caused by lipopolysaccharide and inhibited invasion caused by dexamethasone and THC. It is well-documented that lipopolysaccharide increases cytokines like IL-6 [34,35], which in turn stimulate MMP-2/9 activity to induce invasion [18,19]; whereas dexamethasone induces the opposite effect to inhibit invasion *in vivo* and *in vitro* [20,21]. While our results with lipopolysaccharide and dexamethasone are consistent with Librach, et al. [22], there are some contrasting reports in literature that demonstrate an opposite or null effect[34-36]. This may be explained in part by the length of exposure, in which our model enables chronic exposures (eight days) compared to transwell invasion assays that must be acute (24-48 hours) [34-36]. However, this may also reveal a pitfall of transwell invasion assays as a whole, given that these studies do report a consistent downstream effect

of the drug (*e.g.,* increase and decrease in IL-6 via lipopolysaccharide and dexamethasone, respectively), but are simply unable to elicit the expected EVT invasive response [34,35]. Due to the volatility of the inflammatory response and longer-term drug exposures typically observed in clinical situations, it may be argued that our model's chronic exposures with real-time measurements are necessary to accurately study the impact of drugs on invasion *in vitro*. Lastly, significant inhibition of EVT invasion by the highest dose of THC seen in our work is consistent with *in vitro* findings by Chang, et al. [23], and may reveal a potential mechanism underlying the detrimental impact of this controversial, recreational and medicinal drug on placental and fetal development [23,37].

While drug screening applications remain limited, our knowledge of stemness and differentiation in placental spheroids and organoids was recently advanced by some exciting studies [9,11,12]. Nandi, et al. [9] demonstrated that HTR8/SVneo and primary placental cells cultured as spheroids may self-renew and differentiate down various trophoblast lineages (*e.g.,* syncytiotrophoblast). Using Matrigel® drops and organoid media, Turco, et al. [11] cultured primary cytotrophoblasts as organoids that shared high levels of transcriptomic and methylomic similarities with first trimester placental villi, and may also differentiate into invasive, HLA-G-expressing EVTs. Similarly, Haider, et al. [12] used Matrigel® and organoid media to culture primary cytotrophoblasts as stem-like organoids with comparable gene expression profiles as primary cytotrophoblasts and the capacity to differentiate. Together with our current

findings, there is accumulating evidence to support 3D culture as a useful and multifaceted model system for placental research.

In conclusion, we provide comprehensive rationale and evidence supporting the development of a microplate-based, spheroid invasion model for placental research. With enhanced invasive and angiogenic capability compared to 2D monolayer cultures and a dynamic response to exogenous compounds, we propose that our model has the potential to be further developed into a high-throughput, screening tool to preclinically assess the safety and impact of drugs and toxins on placental invasion. Given our current lack of knowledge surrounding the effects of both prescribed and illicit drug use in pregnant women, especially in Canada and the United States [38], there is a great necessity to advance the development of alternative placental models.

Methods

Cell culture

Human placental EVT-derived HTR8/SVneo cells (generously provided by Dr. Peeyush Lala, Western University) were used due to the highly-conserved characteristics and gene expression profiles with placental EVTs [39,40]. HTR8/SVneo cells were cultured at 37°C in a humidified atmosphere of 5% CO_2/95% atmospheric air in RPMI-1640 (Corning), supplemented with 5% heat-inactivated FBS (Gibco), 1% (v/v) penicillin-streptomycin (Corning) and 1% (v/v) L-glutamine (Corning).

EVT spheroid generation

96-well ultra-low attachment (ULA) plates (Corning) were used to promote the self-assembly of HTR8/SVneo cells into three-dimensional (3D) cellular spheroids. HTR8/SVneo cells were seeded at 1,000 cells/mL, 5,000 cells/mL and 10,000 cells/mL into the ultra-low attachment plates. Media was replaced every 48 hours post-seeding by aspirating 100 µL of existing media, being careful to not disturb the spheroid, and dispensing 100 µL of fresh media into each well.

Live cell imaging and analysis of spheroid size

Live images of the spheroids were captured every 48 hours post-seeding at either 4X or 10X objective magnification using an Eclipse Ti-E Inverted Microscope (Nikon). Diameter (µm) of each spheroid was quantified using a manual measurement tool on ImageJ Fiji software (National Institute of Health). Average spheroid diameters were used to generate a linear regression and slope to track the growth over time (µm/day).

Cell viability staining assay

To confirm cell viability in spheroids over the experimental period, spheroids were incubated with calcein AM (Thermo Fisher; 1:100) for green fluorescence (live cells) and ethidium homodimer-1 (Thermo Fisher; 1:100) for red fluorescence (dead cells) for 30 minutes on days 4, 6 and 8. Spheroids were imaged in 5 µm z-stacks to capture all layers throughout the spheroid using an Eclipse Ti-E Inverted Microscope (Nikon), and all steps were compiled as a z-projection image. Images were analyzed using NIS Elements software (Nikon) to quantify the

total areas covered by live or dead cells. The ratio of live to dead cells was then determined by dividing either live or dead cell area over the total area of the spheroid.

Hematoxylin and eosin (H&E) staining

Spheroids were fixed in 10% formalin within the ULA plates for 15 min at room temperature. An equal volume of liquified 2% agar was added to each well, mixed, and solidified on ice for 20 min. Solid agar pellets with spheroids were transferred into tissue cassettes, placed into 10% formalin for 48 hours, and stored in 70% ethanol. Agar pellets were then embedded in paraffin wax, sliced into 4 µm sections, stained with H&E, and imaged using an Eclipse Ti-E Inverted Microscope (Nikon).

Transcriptome-wide microarray

Total RNA was extracted from cells using TRIzol Reagent (Invitrogen) and Direct-zol RNA MiniPrep Kit (Zymo Research), following the manufacturer's protocol. RNA quality was assessed using the RNA 6000 Nano LabChip Bioanalyzer and TapeStation (Agilent), and 200 ng of RNA was processed to assess 20,000+ genes using the Clarion S Human microarray (Thermo Fisher) and GeneChip™ 3000 instrument system (Thermo Fisher), all carried out at the SickKids TCAG Microarray facility.

Transcriptomic analysis

Normalization and output file generation was performed with Affymetrix Gene Expression Console (Thermo) using the Robust Multi-Chip Analysis (RMA)

algorithm [RMA-Gene-full] [41]. Dendrogram was obtained by using all genes available on the platform excluding the control probes with the built-in *hclust* function in R. The height distance to convergence suggests the degree of similarity between the individual branches (samples). The similarity between the branches was measured based on the expression patterns exhibited by the genes in these samples.

Differential expression analysis was performed by using *limma* package in R [42,43]. Genes with FDR p-value < 0.05 were considered to be significantly regulated. Volcano plot was created using the *limma* package as well. Genes regulated with the absolute fold change ≥ 2 were used for further analyses. Examination and visualization of the significantly over-represented biological processes (Gene Ontology component) was performed by using the BINGO plugin in Cytoscape environment [44]. Gene Set Enrichment Analysis was performed by using C2, C5 and HALLMARK MSigDB collections on whole gene expression profiles [45,46]. Obtained results were further analyzed and visualized by using the EnrichmentMap plugin in Cytoscape environment [47].

Real-time quantitative polymerase chain reaction (RT-qPCR)

Total RNA (500 ng) was further reserve-transcribed to cDNA as previously described [8]. Primer sets directed against gene targets of interest were designed through National Center for Biotechnology Information's Primer-BLAST primer designing tool and synthesized at McMaster's Mobix Labs (**Table 1**). Quantitative analysis of mRNA expression was performed via qPCR using SsoAdvanced™

Universal SYBR® Green Supermix (BioRad) and CFX384 Touch Real-Time PCR

Detection System (BioRad). The cycling conditions were 95 °C for 10 min,

followed by 40 cycles of 95 °C for 10 secs and 60 °C for 10 secs and 72 °C for 15

secs. Relative fold changes were calculated using the comparative cycle times (Ct)

method, normalizing all values to the geometric mean of three endogenous control

genes (*18S, ACTB, GAPDH*). The endogenous control gene was selected based on

experimentally-determined Ct stability across all treatment groups. Given that all

primer sets had equal priming efficiency, the ΔCt values for each primer set were

calibrated to the average of all control Ct values, and the relative abundance of each

primer set compared with calibrator was determined by the formula $2^{\Delta\Delta Ct}$, in which

ΔΔCt was the normalized value.

Protein Extraction and Western Blot

Total protein was extracted from cells using RIPA buffer supplemented with

protease and phosphatase inhibitor cocktails (Roche). The solution was sonicated

for 5 sec total, 1 sec per pulse, vortexed, and quantified by colorimetric DC protein

assay (BioRad). Loading samples were prepared from fresh total protein extract,

Laemelli Sample Buffer (4X) (BioRad) and β-mercaptoethanol, and heated at 90

°C for 5 min to denature the proteins. Proteins (10 μg/well) were separated by size

via gel electrophoresis in Mini-PROTEAN® TGX Stain-Free™ 4-20%

polyacrylamide gels (BioRad), and transferred onto polyvinylidene difluoride

membranes using the Trans-Blot® Turbo™ Transfer System (BioRad). Membranes

were blocked in 1x Tris-buffered saline-Tween 20 buffer with 5% non-fat milk, and

then probed using anti-MMP9 (Abcam; ab76003; rabbit; 1:500) and anti-TIMP2 (GeneTex; GTX16392; rabbit; 1:500) antibodies diluted in the blocking solution. Donkey anti-rabbit (1:5,000) secondary antibody was used to detect the species-specific portion of the primary antibody, diluted in the blocking solution. Immuno-reactive bands were visualized using Clarity™ Western ECL Substrate (BioRad). Total protein was stained on the membrane using Amido Black and imaged to ensure even loading and transfer [48].

EVT spheroid invasion assay

EVT spheroid invasion was studied by embedding the spheroids in an extracellular matrix (ECM) inside the ultra-low attachment plate. Growth-factor reduced Geltrex® (Thermo) was used as the ECM cocktail. On day 2, after the spheroids have self-assembled inside the ULA plate, 100 µL of media was aspirated from each well and replaced with 100 µL of Geltrex® (10 mg/mL) on ice [30]. The entire plate was then centrifuged at 300 g for 3 min at 4 °C to center the spheroids at a consistent position inside the well, and incubated for 60 minutes at 37°C to allow the ECM to solidify. 100 µL of media was added on top of the solidified ECM. Brightfield images of the control and ECM-embedded spheroids were captured on days 2, 4, 6 and 8 at 4x or 10x objective magnification using an Eclipse Ti-E Inverted Microscope (Nikon) and analyzed using NIS Elements software (Nikon). Area of invasive edge of each spheroid was quantified at each time point by subtracting the average area of corresponding control spheroids from area of the invaded spheroid. Spheroid invasion percentage was then calculated as the ratio of

invasive edge area to total invaded spheroid area and used as a relative measure to compare the invasiveness between spheroids [17].

Immunofluorescence

Spheroids were fixed overnight in 4% paraformaldehyde and permeabilized for 5 minutes with 0.1% Triton X-100 in PBS. Samples were then blocked for 1 hour using 0.01% Tween-20, 10% goat serum and 1% bovine serum albumin (BSA) in PBS. Afterwards, samples were incubated with HIF1 alpha primary antibody (Abcam; ab179483; rabbit monoclonal; 1:50) or MMP9 primary antibody (Abcam; ab76003; rabbit monoclonal; 1:250) overnight at 4 degrees, and then incubated with Goat Anti-Rabbit IgG H&L Alexa Fluor® 488 secondary antibody (Abcam; ab150077; goat polyclonal; 2µg/mL) for 2 hours, as necessary. For F-actin staining, samples were incubated with CytoPainter Phalloidin-iFluor 555 reagent (Abcam; ab176756; 1:1000) for 2 hours. Samples were counterstained with 4′,6-diamidino-2-phenylindole dihydrochloride (DAPI; Santa Cruz; 1.5 µg/mL). All blocking and incubations were performed at room temperature, unless otherwise stated. Spheroids were visualized using an Eclipse Ti-E Inverted Confocal Microscope (Nikon). Z-stack images were taken in 10 µm steps to capture all layers and compiled as a z-projection image. Images were analyzed using NIS Elements software (Nikon).

Drug Treatments

Lipopolysaccharide (*Escherichia coli* serotype 055:B5; Sigma Aldrich) stock solutions were prepared from a dried powder at a concentration of 1 mg/mL

in phosphate-buffered saline (Corning), and diluted to working concentrations of 1-10,000 ng/mL in RPMI-1640 media (Corning) at time of use. Dexamethasone (Sigma Aldrich) stock solutions were prepared from a dried powder at a concentration of 1 mg/mL in 90% ethanol, and diluted to working concentrations of 1-10,000 nM in RPMI-1640 media at time of use. $\triangle^9$ – Tetrahydrocannabinol (THC) stock solutions (Sigma Aldrich) were diluted to working concentrations of 1.875-30 µM in RPMI-1640 at time of use. Cells were treated with 100 µL of media containing either the vehicle control or drug treatment every 48 hours for up to eight days.

Statistical analyses

Prism 6 software (GraphPad) was used to statistically analyze all experimental results. Results were expressed as means of the normalized values ± standard error of the mean (SEM). Data sets were assessed for statistical significance ($p<0.05$) through either an unpaired t-test, or one-way analysis of variance (ANOVA), and if significant, Tukey's *post hoc* test to perform multiple comparisons.

References

1   Burton, G. J. & Fowden, A. L. The placenta: a multifaceted, transient organ. *Philosophical transactions of the Royal Society of London. Series B, Biological sciences* **370**, 20140066, doi:10.1098/rstb.2014.0066 (2015).

2   Huppertz, B., Ghosh, D. & Sengupta, J. An integrative view on the physiology of human early placental villi. *Prog Biophys Mol Biol* **114**, 33-48, doi:10.1016/j.pbiomolbio.2013.11.007 (2014).

3   Red-Horse, K. *et al.* Trophoblast differentiation during embryo implantation and formation of the maternal-fetal interface. *The Journal of clinical investigation* **114**, 744-754, doi:10.1172/JCI22991 (2004).

4   Knofler, M. Critical growth factors and signalling pathways controlling human trophoblast invasion. *Int J Dev Biol* **54**, 269-280, doi:10.1387/ijdb.082769mk (2010).

5   Knofler, M. & Pollheimer, J. Human placental trophoblast invasion and differentiation: a particular focus on Wnt signaling. *Front Genet* **4**, 190, doi:10.3389/fgene.2013.00190 (2013).

6   Chakraborty, C., Gleeson, L. M., McKinnon, T. & Lala, P. K. Regulation of human trophoblast migration and invasiveness. *Can J Physiol Pharmacol* **80**, 116-124 (2002).

7   Fennema, E., Rivron, N., Rouwkema, J., van Blitterswijk, C. & de Boer, J. Spheroid culture as a tool for creating 3D complex tissues. *Trends Biotechnol* **31**, 108-115, doi:10.1016/j.tibtech.2012.12.003 (2013).

8   Wong, M. K. *et al.* Extracellular matrix surface regulates self-assembly of three-dimensional placental trophoblast spheroids. *PloS one* **13**, e0199632, doi:10.1371/journal.pone.0199632 (2018).

9   Nandi, P., Lim, H., Torres-Garcia, E. J. & Lala, P. K. Human trophoblast stem cell self-renewal and differentiation: Role of decorin. *Scientific reports* **8**, 8977, doi:10.1038/s41598-018-27119-4 (2018).

10   Rai, A. & Cross, J. C. Three-dimensional cultures of trophoblast stem cells autonomously develop vascular-like spaces lined by trophoblast giant cells. *Dev Biol* **398**, 110-119, doi:10.1016/j.ydbio.2014.11.023 (2015).

11   Turco, M. Y. *et al.* Trophoblast organoids as a model for maternal-fetal interactions during human placentation. *Nature* **564**, 263-267, doi:10.1038/s41586-018-0753-3 (2018).

12   Haider, S. *et al.* Self-Renewing Trophoblast Organoids Recapitulate the Developmental Program of the Early Human Placenta. *Stem Cell Reports* **11**, 537-551, doi:10.1016/j.stemcr.2018.07.004 (2018).

13   Pijnenborg, R., Dixon, G., Robertson, W. B. & Brosens, I. Trophoblastic invasion of human decidua from 8 to 18 weeks of pregnancy. *Placenta* **1**, 3-19, doi:https://doi.org/10.1016/S0143-4004(80)80012-9 (1980).

14   Hirschhaeuser, F. *et al.* Multicellular tumor spheroids: an underestimated tool is catching up again. *J Biotechnol* **148**, 3-15, doi:10.1016/j.jbiotec.2010.01.012 (2010).

15   Lee, Y. *et al.* A unifying concept of trophoblastic differentiation and malignancy defined by biomarker expression. *Hum Pathol* **38**, 1003-1013, doi:10.1016/j.humpath.2006.12.012 (2007).

16   Davies, J. E. *et al.* Epithelial-mesenchymal transition during extravillous trophoblast differentiation. *Cell Adh Migr* **10**, 310-321, doi:10.1080/19336918.2016.1170258 (2016).

17   Vinci, M., Box, C. & Eccles, S. A. Three-dimensional (3D) tumor spheroid invasion assay. *J Vis Exp*, e52686, doi:10.3791/52686 (2015).

18   Meisser, A., Cameo, P., Islami, D., Campana, A. & Bischof, P. Effects of interleukin-6 (IL-6) on cytotrophoblastic cells. *Mol Hum Reprod* **5**, 1055-1058 (1999).

19   Cohen, M., Meisser, A. & Bischof, P. Metalloproteinases and human placental invasiveness. *Placenta* **27**, 783-793, doi:10.1016/j.placenta.2005.08.006 (2006).

20   Zhou, L., Zhang, A., Wang, K., Zhou, Q. & Duan, T. Folate ameliorates dexamethasone-induced fetal and placental growth restriction potentially via improvement of trophoblast migration. *Int J Clin Exp Pathol* **8**, 3008-3014 (2015).

21   Zhang, D. *et al.* Glucocorticoid exposure in early placentation induces preeclampsia in rats via interfering trophoblast development. *Gen Comp Endocrinol* **225**, 61-70, doi:10.1016/j.ygcen.2015.09.019 (2016).

22   Librach, C. L. *et al.* Interleukin-1 beta regulates human cytotrophoblast metalloproteinase activity and invasion in vitro. *The Journal of biological chemistry* **269**, 17125-17131 (1994).

23   Chang, X. *et al.* Suppression of STAT3 Signaling by Delta9-Tetrahydrocannabinol (THC) Induces Trophoblast Dysfunction. *Cellular physiology and biochemistry : international journal of experimental cellular physiology, biochemistry, and pharmacology* **42**, 537-550, doi:10.1159/000477603 (2017).

24   Vinci, M. *et al.* Advances in establishment and analysis of three-dimensional tumor spheroid-based functional assays for target validation and drug evaluation. *BMC Biol* **10**, 29, doi:10.1186/1741-7007-10-29 (2012).

25   James, J., Tun, W. & Clark, A. Quantifying trophoblast migration: In vitro approaches to address in vivo situations. *Cell Adh Migr* **10**, 77-87, doi:10.1080/19336918.2015.1083667 (2016).

26   Pringle, K. G., Kind, K. L., Sferruzzi-Perri, A. N., Thompson, J. G. & Roberts, C. T. Beyond oxygen: complex regulation and activity of hypoxia inducible factors in pregnancy. *Hum Reprod Update* **16**, 415-431, doi:10.1093/humupd/dmp046 (2010).

27   Huppertz, B., Weiss, G. & Moser, G. Trophoblast invasion and oxygenation of the placenta: measurements versus presumptions. *J Reprod Immunol* **101-102**, 74-79, doi:10.1016/j.jri.2013.04.003 (2014).

28   Genbacev, O., Joslin, R., Damsky, C. H., Polliotti, B. M. & Fisher, S. J. Hypoxia alters early gestation human cytotrophoblast differentiation/invasion in vitro and models the placental defects that occur in preeclampsia. *The Journal of clinical investigation* **97**, 540-550, doi:10.1172/JCI118447 (1996).

29   Cowden Dahl, K. D. *et al.* Hypoxia-inducible factors 1alpha and 2alpha regulate trophoblast differentiation. *Molecular and cellular biology* **25**, 10479-10491, doi:10.1128/MCB.25.23.10479-10491.2005 (2005).

30   Wang, L., Yu, Y., Guan, H., Liu, T. & Qiao, C. 67-kDa Laminin receptor contributes to hypoxia-induced migration and invasion of trophoblast-like cells by mediating matrix metalloproteinase-9. *Clin Exp Pharmacol Physiol* **42**, 549-558, doi:10.1111/1440-1681.12389 (2015).

31   Charoen, K. M., Fallica, B., Colson, Y. L., Zaman, M. H. & Grinstaff, M. W. Embedded multicellular spheroids as a biomimetic 3D cancer model for evaluating drug and drug-device combinations. *Biomaterials* **35**, 2264-2271, doi:10.1016/j.biomaterials.2013.11.038 (2014).

32   Loessner, D. *et al.* Bioengineered 3D platform to explore cell-ECM interactions and drug resistance of epithelial ovarian cancer cells. *Biomaterials* **31**, 8494-8506, doi:10.1016/j.biomaterials.2010.07.064 (2010).

33   Yang, Z. *et al.* Transcriptome Profiling of Panc-1 Spheroid Cells with Pancreatic Cancer Stem Cells Properties Cultured by a Novel 3D Semi-Solid System. *Cellular physiology and biochemistry : international journal of experimental cellular physiology, biochemistry, and pharmacology* **47**, 2109-2125, doi:10.1159/000491479 (2018).

34   Li, L. *et al.* Effects of Lipopolysaccharide on Human First Trimester Villous Cytotrophoblast Cell Function In Vitro. *Biology of reproduction* **94**, 33, doi:10.1095/biolreprod.115.134627 (2016).

35   Anton, L., Brown, A. G., Parry, S. & Elovitz, M. A. Lipopolysaccharide induces cytokine production and decreases extravillous trophoblast invasion through a mitogen-activated protein kinase-mediated pathway: possible mechanisms of first trimester placental dysfunction. *Hum Reprod* **27**, 61-72, doi:10.1093/humrep/der362 (2012).

36   Champion, H., Innes, B. A., Robson, S. C., Lash, G. E. & Bulmer, J. N. Effects of interleukin-6 on extravillous trophoblast invasion in early human pregnancy. *Mol Hum Reprod* **18**, 391-400, doi:10.1093/molehr/gas010 (2012).

37   Khare, M., Taylor, A. H., Konje, J. C. & Bell, S. C. Delta9-tetrahydrocannabinol inhibits cytotrophoblast cell proliferation and modulates gene transcription. *Mol Hum Reprod* **12**, 321-333, doi:10.1093/molehr/gal036 (2006).

38   Vorstenbosch, S., Kant, A. & Dabekausen, Y. The Dutch Pregnancy Drug Register, a Good Idea for Canada? *J Obstet Gynaecol Can*, doi:10.1016/j.jogc.2018.10.017 (2018).

39   Weber, M., Knoefler, I., Schleussner, E., Markert, U. R. & Fitzgerald, J. S.
        HTR8/SVneo cells display trophoblast progenitor cell-like characteristics
        indicative of self-renewal, repopulation activity, and expression of
        "stemness-" associated transcription factors. *Biomed Res Int* **2013**, 243649,
        doi:10.1155/2013/243649 (2013).

40   Graham, C. H. *et al.* Establishment and characterization of first trimester
        human trophoblast cells with extended lifespan. *Experimental cell research*
        206, 204-211 (1993).

41   Irizarry, R. A. *et al.* Exploration, normalization, and summaries of high
        density oligonucleotide array probe level data. *Biostatistics* **4**, 249-264,
        doi:10.1093/biostatistics/4.2.249 (2003).

42   Phipson, B., Lee, S., Majewski, I. J., Alexander, W. S. & Smyth, G. K.
        Robust Hyperparameter Estimation Protects against Hypervariable Genes
        and Improves Power to Detect Differential Expression. *Ann Appl Stat* **10**,
        946-963, doi:10.1214/16-AOAS920 (2016).

43   Ritchie, M. E. *et al.* limma powers differential expression analyses for
        RNA-sequencing and microarray studies. *Nucleic Acids Res* **43**, e47,
        doi:10.1093/nar/gkv007 (2015).

44   Maere, S., Heymans, K. & Kuiper, M. BiNGO: a Cytoscape plugin to assess
        overrepresentation of gene ontology categories in biological networks.
        Bioinformatics **21**, 3448-3449, doi:10.1093/bioinformatics/bti551 (2005).

45   Subramanian, A. *et al.* Gene set enrichment analysis: a knowledge-based
        approach for interpreting genome-wide expression profiles. *Proceedings of
        the National Academy of Sciences of the United States of America* **102**,
        15545-15550, doi:10.1073/pnas.0506580102 (2005).

46   Mootha, V. K. *et al.* PGC-1alpha-responsive genes involved in oxidative
        phosphorylation are coordinately downregulated in human diabetes. *Nat
        Genet* **34**, 267-273, doi:10.1038/ng1180 (2003).

47   Merico, D., Isserlin, R., Stueker, O., Emili, A. & Bader, G. D. Enrichment
        map: a network-based method for gene-set enrichment visualization and
        interpretation. *PloS one* **5**, e13984, doi:10.1371/journal.pone.0013984
        (2010).

48   Aldridge, G. M., Podrebarac, D. M., Greenough, W. T. & Weiler, I. J. The
        use of total protein stains as loading controls: An alternative to high-
        abundance single-protein controls in semi-quantitative immunoblotting. *J
        Neurosci Meth* **172**, 250-254, doi:DOI 10.1016/j.jneumeth.2008.05.003
        (2008).

Author Contributions Statement

M.K.W. wrote the main manuscript text. M.K.W., S.S., and M.W. conducted all experiments. A.D. contributed to figures 2-4. M.K.W. and S.R. contributed to the experimental design. All authors reviewed the manuscript.

Competing Interests

The author(s) declare no competing interests.

Data Availability

All data generated or analyzed during this study are included in this published article (and its Supplementary Information files). Original dataset files are available in the Gene Expression Omnibus (GEO) repository [GEO accession number: GSE126844; https://www.ncbi.nlm.nih.gov/geo/query/acc.cgi?acc=GSE126844].

Figures and Figure Legends
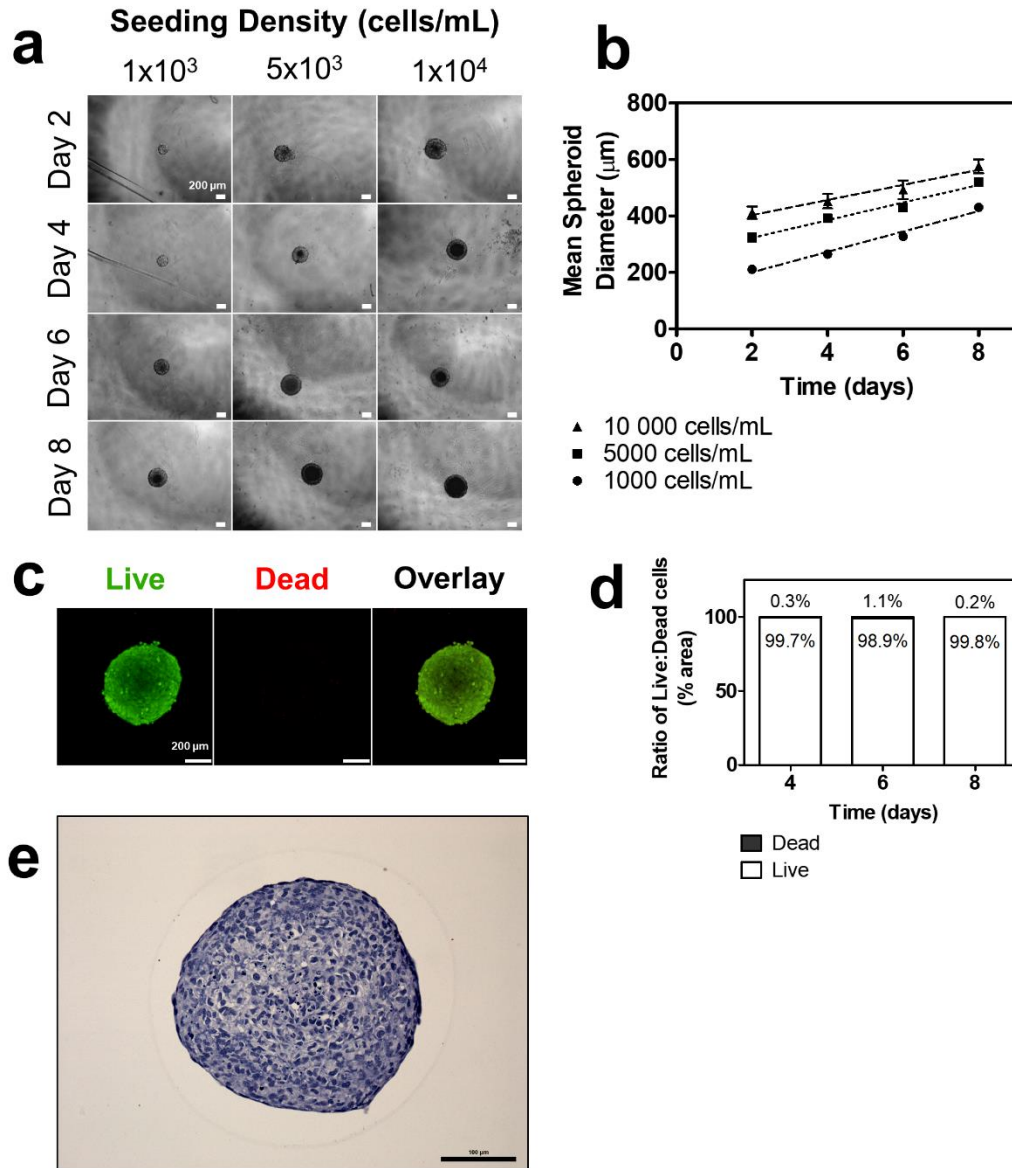
Figure 1. Self-assembly, growth, and viability of 3D EVT spheroids over eight days. (a) EVTs seeded at three different densities form spheroids that increase in size over eight days. 4x magnification. Scale bar indicates 200 µm. (b) Mean spheroid diameter over time across three seeding densities. (c) Immunofluorescent images of live and dead stain using calcein AM and ethidium homodimer-1, respectively. Green colour indicates live cells. Red colour indicates dead cells. 10x magnification. Scale bar indicates 200 µm. (d) Ratio of surface area of live to dead cells at days four, six, and eight. (e) Representative image of H&E staining of a spheroid cross-section. Scale bar indicates 100 µm. n=3.
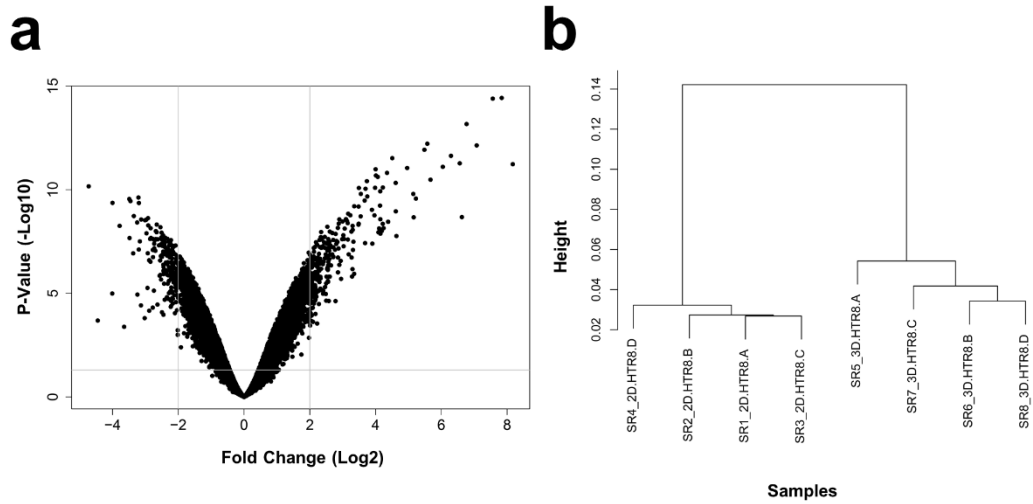
Figure 2. Transcriptome profiling of global gene expression changes in EVTs cultured as 3D spheroids compared to 2D monolayers. (a) Volcano plot comparing fold change (Log2) to p-value (-Log10) of differentially expressed genes measured using Clariom S Human microarray (Thermo). Significance determined by $p<0.05$ and absolute fold change$\geq$2. (b) Dendrogram demonstrating clustering of the samples by similarity of transcriptome profiles. Four samples were analyzed per group, with different letters at the end of the name indicating a distinct sample.
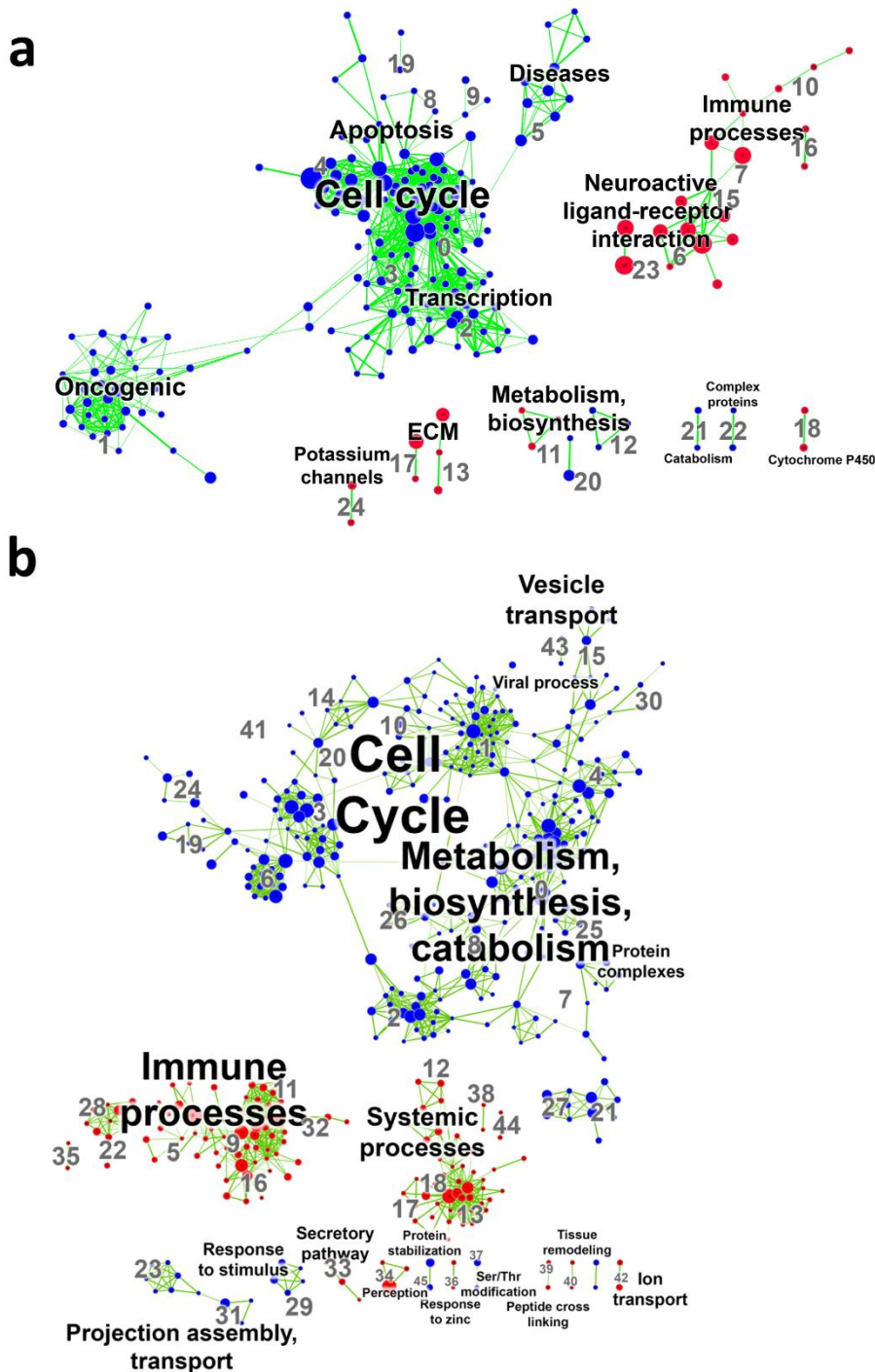
Figure 3. Enrichment maps of GSEA canonical pathways and biological processes comparing EVTs cultured as 3D spheroids and 2D monolayers. (a) Visualization of results of canonical pathway analyses and (b) biological process analyses. Every node (dot) represents a module of enriched genes in a particular pathway or process, with the size of the node representing number of genes. Red

nodes indicate up-regulation in 3D spheroids compared to 2D monolayers and blue nodes represent down-regulation. Every edge (green line) represents overlap of genes between two pathways or processes, with the thickness of the line representing number of genes overlapping. Font size of annotated classification reflects number of modules within that classification group. Significance determined by FDR p-value < 0.05 and absolute fold change ≥ 2.
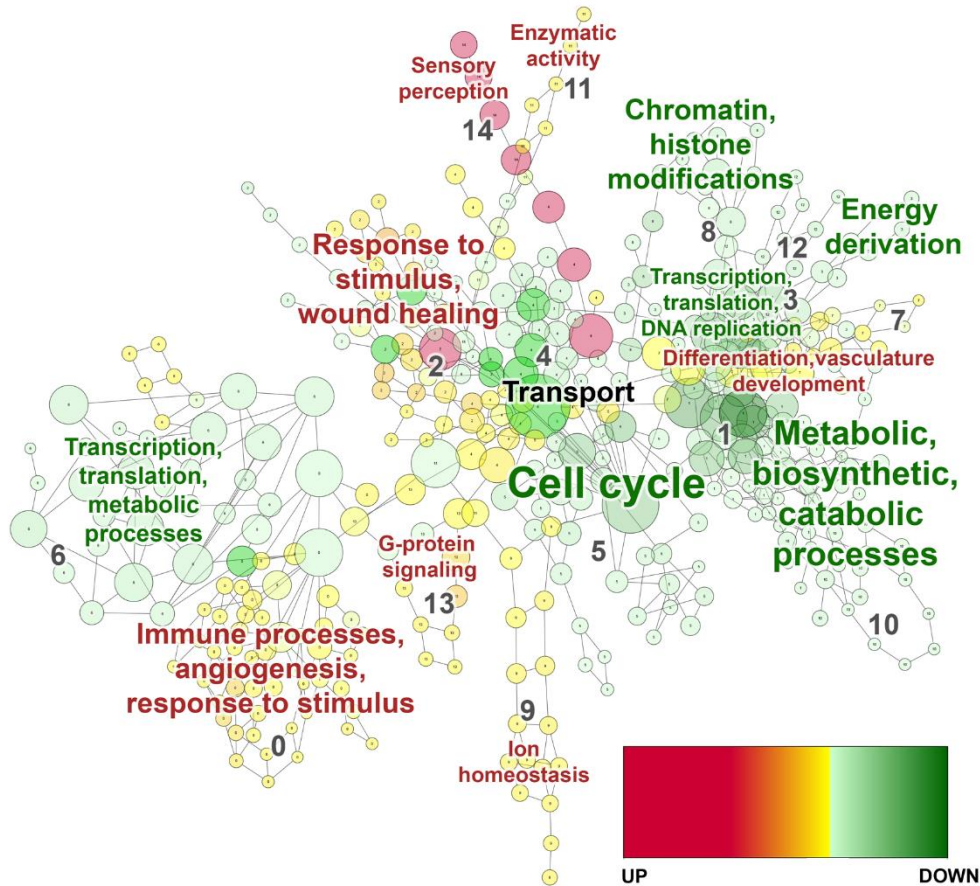
Figure 4. Gene ontology analysis map of biological processes comparing EVTs cultured as 3D spheroids and 2D monolayers. Visualization of results of biological process analyses. Every node (circle) represents a module of overrepresented genes in a particular process, with the size of the node representing number of genes. Nodes with red to yellow colour gradients indicate strong to weak up-regulation, respectively. Nodes with dark to light green colour gradients indicate strong to weak down-regulation, respectively. Every edge (line) represents overlap of genes between two pathways or processes. Red font colour indicates an up-regulated category in 3D spheroids compared to 2D monolayers, green font indicates down-regulated, and black font indicates a category with an even number of terms regulated in each direction. Font size of annotation reflects number of modules within that category. Significance determined by FDR p-value < 0.05 and absolute fold change ≥ 2.
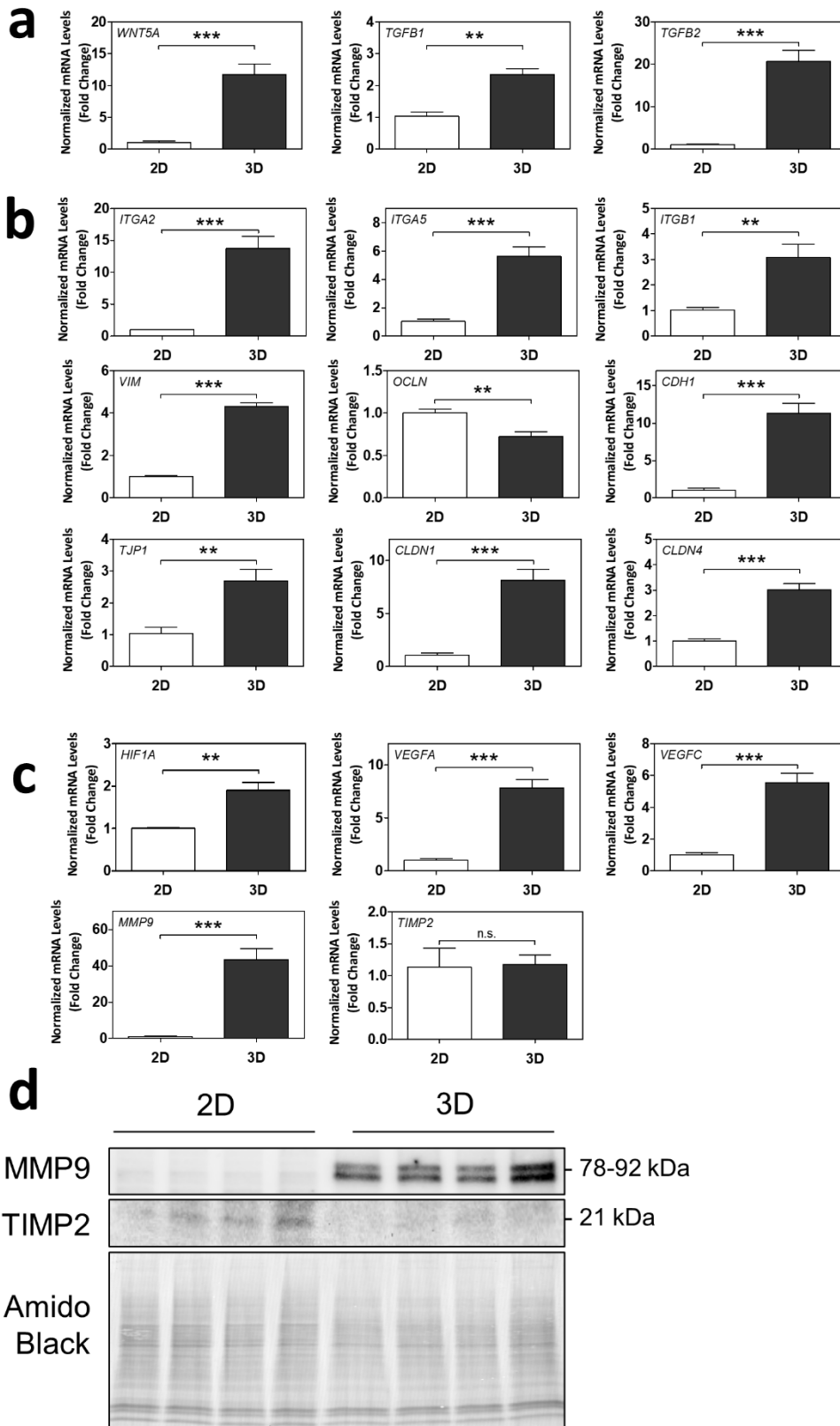
Figure 5. 3D spheroids exhibit differential mRNA and protein expression of markers of epithelial-mesenchymal transition (EMT), cell-cell contact, angiogenesis, and invasion/migration. Normalized mRNA levels of (a) *WNT5A, TGFB1, TGFB2,* (b) *ITGA2, ITGA5, ITGB1, VIM, OCLN, CDH1, TJP1, CLDN1, CLDN4,* (c) *HIF1A, VEGFA, VEGFC, MMP9,* and *TIMP2,* as measured using RT-qPCR. Significant differences between groups determined by unpaired t-test; n=4. Significant differences between means were indicated by ** ($p<0.01$) or *** ($p<0.001$). Non-significant differences indicated by n.s. (d) Cropped blots of MMP9 and TIMP2 protein bands as detected by Western blot, and Amido Black staining of total protein. n=4. Membrane was cut below 63 kDa and top half used for the MMP9 blot. Remaining membrane was cut above 25 kDa and lower half used for the TIMP2 blot. Whole blots with protein ladders found in **Supplementary Figure S1**.
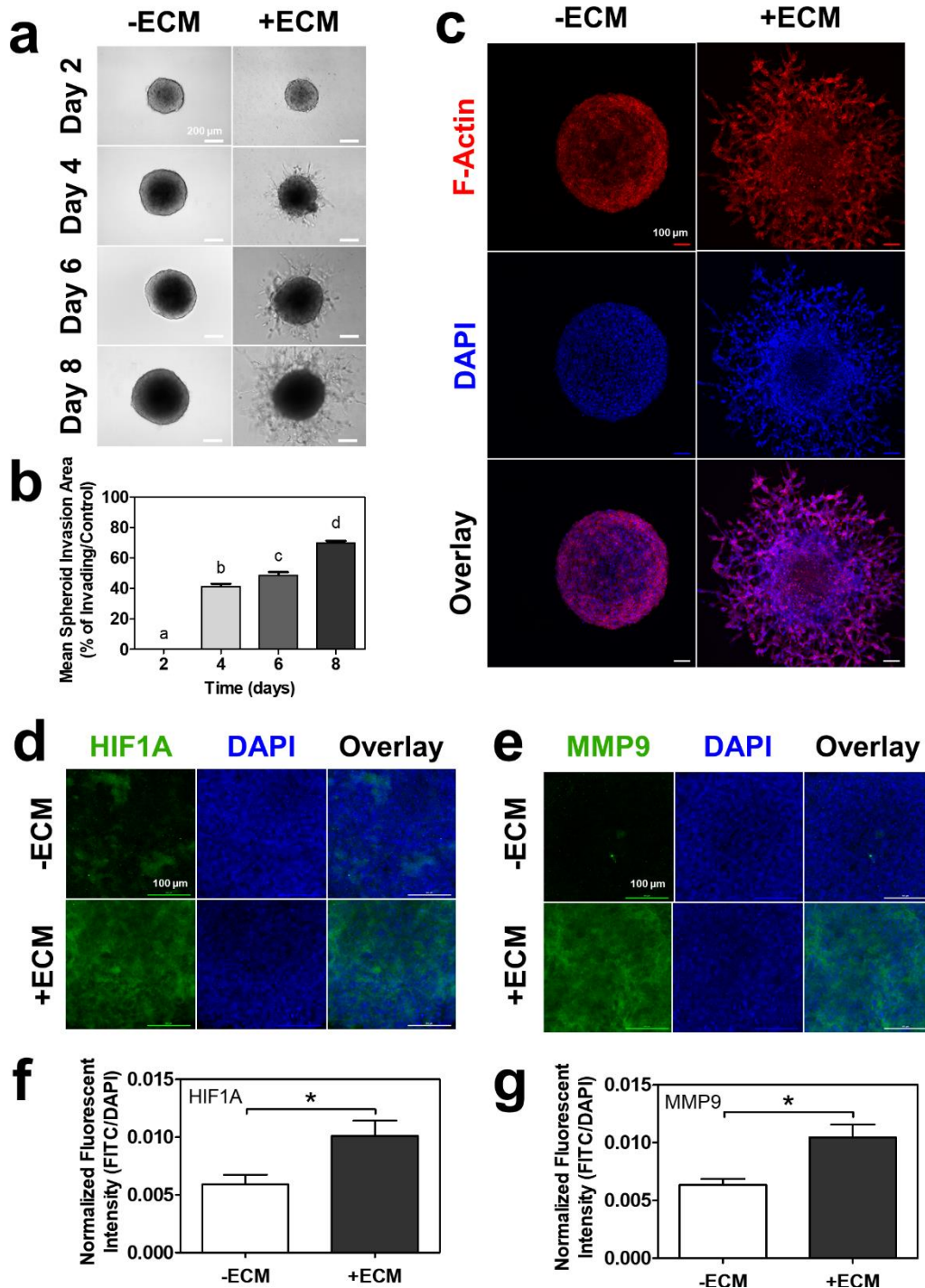
Figure 6. EVT spheroids exhibited continuous invasion into ECM over eight days. (a) Brightfield images of EVT spheroids without or with ECM over eight days. 10x magnification. Scale bar indicates 200 µm. (b) Histogram of mean spheroid invasion area percentage over eight days. Significant differences between groups determined by one-way ANOVA followed by Tukey's post-test; n=6.

Significant differences between means as determined by post-tests were indicated by different letters. (c) Immunofluorescent confocal images of EVT spheroids without or with ECM at day eight stained with phalloidin (F-Actin; green) and DAPI (blue). 10x magnification. Scale bar indicates 100 µm. Immunofluorescent confocal images of EVT spheroids without or with ECM at day eight stained with (d) HIF1A (green) or (e) MMP9 (green), and DAPI (blue). 20x magnification, imaged at center of spheroid. Scale bar indicates 100 µm. Histogram of mean fluorescent intensity of FITC normalized to area of DAPI-positive nuclei for (f) HIF1A and (g) MMP9. Significant differences between groups determined by unpaired t-test; n=3. Significant differences between means were indicated by * (p<0.05).
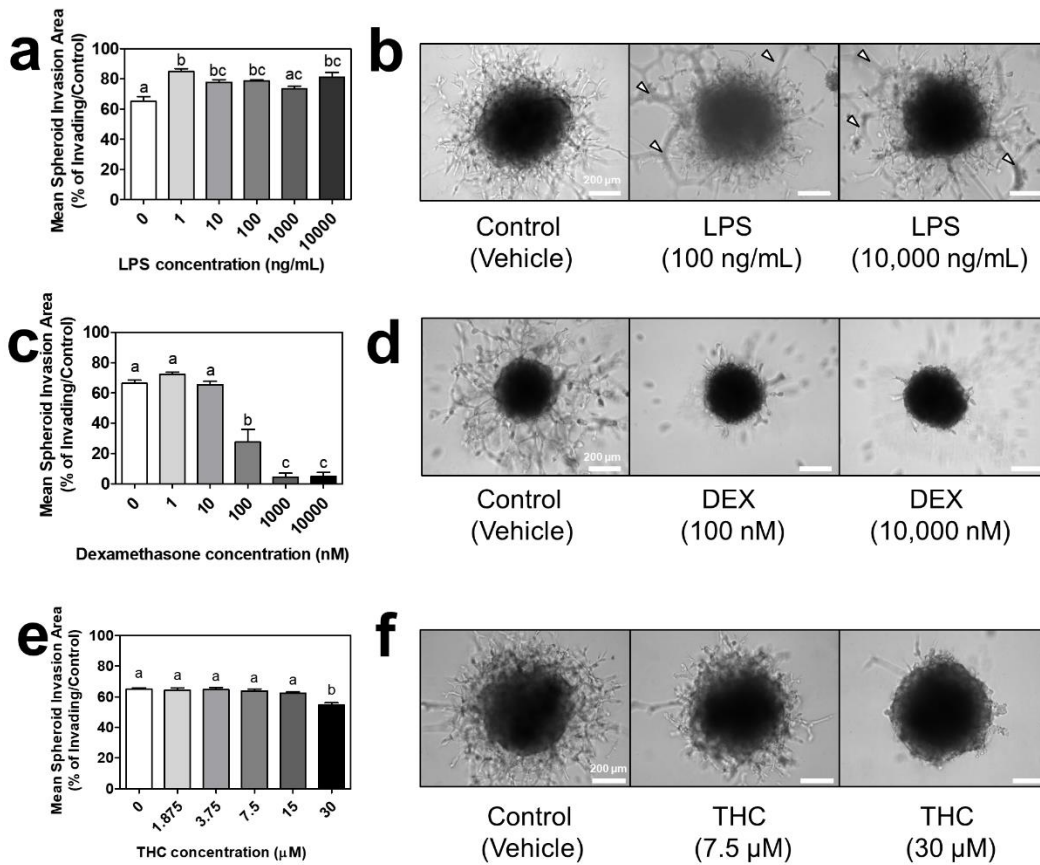
Figure 7. Impact of lipopolysaccharide, dexamethasone, or $\triangle^9$ **– tetrahydrocannabinol on spheroid invasion.** (a) Mean spheroid invasion areas of EVT spheroids treated with 1-10,000 ng/mL lipopolysaccharide (LPS) on day eight. (b) Brightfield images of EVT spheroids in ECM treated with the vehicle control, 100 ng/mL LPS, or 10,000 ng/mL LPS (three representative doses selected along curve to demonstrate effect). White arrows indicate examples of tube formation of EVTs that have invaded to surface of ECM. (c) Mean spheroid invasion areas of EVT spheroids treated with 1-10,000 nM dexamethasone (DEX) on day eight. (d) Brightfield images of EVT spheroids in ECM treated with the vehicle control, 100 nM DEX, or 10,000 nM DEX. (e) Mean spheroid invasion areas of EVT spheroids treated with 1.875-30 µM $\triangle^9$ – tetrahydrocannabinol (THC) on day eight. (f) Brightfield images of EVT spheroids in ECM treated with the vehicle control, 7.5 µM THC, or 30 µM THC. Significant differences between groups determined by one-way ANOVA followed by Tukey's post-test; n≥3. Significant differences between means as determined by post-tests were indicated by different letters. Images taken at 10x objective magnification. Scale bar represents 200 µm.

Tables

Table 1. Forward and reverse sequences for the primers used for RT-qPCR.

Gene	Forward	Reverse	GenBank
18S (RNA18S5)	CACGCCAGTAC AAGATCCCA	AAGTGACGCAGC CCTCTATG	NR_003286.2
ACTB	TTACAGGAAGT CCCTTGCCATC	GCAATGCTATCA CCTCCCCTG	NM_001101.5
GAPDH	TCACCATCTTCC AGGAGCGA	ATGACGAACATG GGGGCATC	NM_0013579 43.1
HIF1A	CAGCAACGACA CAGAAACTGA	TTGGGTGAGGGG AGCATTAC	AF208487.1
VEGFA	GGCAGAATCAT CACGAAGTGG	GGTCTCGATTGG ATGGCAGT	NM_0011716 23.1
VEGFC	CCAATCACACT TCCTGCCGA	GCCTGACACTGT GGTAGTGTT	NM_005429.4
WNT5A	CTTGAGCACGA CGAAGCAAC	GGAGGTTGGAGA CAAAGGGG	NM_003392.4
TGFB1	CTCCCGCAAAG ACTTTTCCC	GAATAGGGGATC TGTGGCAGG	NM_000660.7
TGFB2	TGCACCATGCTT TGGCTTTC	CTGGCTGGCTCA GCAACTAT	NM_0011355 99.3
CDH1	ACACTGGTGCC ATTTCCACT	TTAGGGCTGTGT ACGTGCTG	AH006175.2
OCLN	TCGACCAATGC TCTCTCAGC	CTCCTGGAGGAG AGGTCCAT	U49184.1
TJP1	TCTGAGCCTGT AAGAGAGGACT	GCTTGCTGCTTAC CTGTTGAG	AF169196.1
ITGA2	CGGTTATTCAG GCTCACCGA	ACCTACCAAGAG CACGTCTG	NM_002203.4
ITGA5	CCAAAAGAAGC CCCCAGCTA	TCCTTGTGTGGCA TCTGTCC	NM_002205.4
ITGB1	AAGCGAAGGCA TCCCTGAAA	GTCTACCAACAC GCCCTTCA	NM_002211.4
VIM	GCAAAGACAGG CTTTAGCGAG	TTCAAGTCTCAG CGGGCTC	NM_003380.5
CLDN1	CTGTCATTGGG GGTGCGATA	CTGGCATTGACT GGGGTCAT	NM_021101.5
CLDN4	CCACTCGGACA ACTTCCCAA	ACTTCCGTCCCTC CCCAATA	NM_001305.4
MMP9	CCGGCATTCAG GGAGACGCC	TGGAACCACGAC GCCCTTGC	NM_004994.2
TIMP2	GAAGAGCCTGA ACCACAGGT	GGGGGAGGAGAT GTAGCAC	NM_003255.4

Supplementary Figures and Tables

Supplementary Figure S1. Whole blots for Western blots of (a) MMP9 and (b) TIMP2 protein. A single gel was run and protein transferred onto a PVDF membrane. Membrane was then cut below 63kDa and the top half used for the MMP9 blot. Same membrane was cut just above 25 kDa was used for the TIMP2 blot. Remaining, unused portion of membrane was disposed.
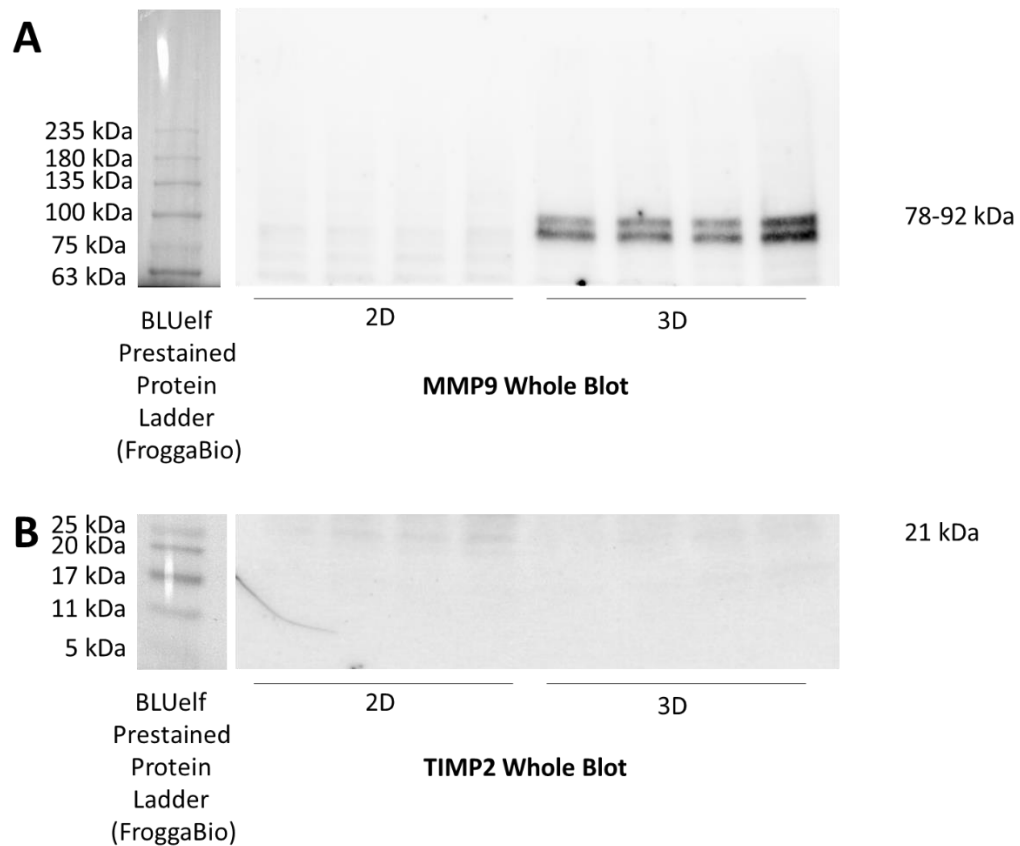
Supplementary Table S1. Most significantly up-regulated GSEA canonical pathways in EVTs cultured as 3D spheroids.

Module	Category	Canonical Pathway Term	NES	FDR p-value
23	Neuroactive ligand-receptor interaction	Olfactory Signaling Pathway	-3.0542696	0
23	Neuroactive ligand-receptor interaction	Olfactory Transduction	-2.966659	0
6	Neuroactive ligand-receptor interaction	Class A1 Rhodopsin Like Receptors	-2.5756402	0
16	Immune processes, diseases, defensins	Defensins	-2.4561152	0
6	Neuroactive ligand-receptor interaction	GPCR Ligand Binding	-2.439125	0
16	Immune processes, diseases, defensins	Beta Defensins	-2.4266376	0
6	Neuroactive ligand-receptor interaction	Neuroactive Ligand Receptor Interaction	-2.3954382	0
15	Signaling events	Peptide Ligand Binding Receptors	-2.3515468	0
7	Immune processes, diseases, defensins	Chemokine Receptors Bind Chemokines	-2.2149904	0
6	Neuroactive ligand-receptor interaction	Amine Ligand Binding Receptors	-2.1915238	9.33E-05
7	Immune processes, diseases, defensins	Cytokine-Cytokine Receptor Interaction	-2.1703234	8.48E-05
7	Immune processes, diseases, defensins	Cytosolic DNA Sensing Pathway	-2.162791	7.77E-05
15	Signaling events	G Alpha I Signaling Events	-2.142522	7.17E-05
7	Immune processes, diseases, defensins	Secreted Factors	-2.0940683	2.38E-04
13	ECM	ECM Regulators	-2.0885324	2.22E-04

Supplementary Table S2. Most significantly down-regulated GSEA canonical pathways in EVTs cultured as 3D spheroids

Module	Category	Canonical Pathway Term	NES	FDR p-value
5	Diseases	Respiratory Electron Transport	2.80283	0
5	Diseases	Respiratory Electron Transport ATP Synthesis by Chemiosmotic Coupling and Heat Production by Uncoupling Proteins	2.735257	0
5	Diseases	TCA Cycle and Respiratory Electron Transport	2.715474	0
2	Transcription, HIV life cycle	RNA Pol II Transcription	2.701939	0
2	Transcription, HIV life cycle	Late Phase of HIV Life Cycle	2.638732	0
0	Cell cycle, apoptosis	DNA Replication	2.581079	0
2	Transcription, HIV life cycle	mRNA Processing	2.567776	0
2	Transcription, HIV life cycle	RNA Pol II Pre-Transcription Events	2.557952	0
0	Cell cycle, apoptosis	Mitotic M-M/G1 Phases	2.541292	0
3	Cell cycle	DNA Repair	2.527595	0
0	Cell cycle, apoptosis	Activation of ATR In Response to Replication Stress	2.509505	0
2	Transcription, HIV life cycle	Transcription Coupled Nucleotide Excision Repair	2.504607	0
3	Cell cycle	Nucleotide Excision Repair	2.501146	0
3	Cell cycle	Nucleotide Excision Repair	2.485817	0
2	Transcription, HIV life cycle	mRNA Splicing	2.484428	0

Supplementary Table S3. Full list of GSEA canonical pathways in EVTs cultured as 2D monolayers and 3D spheroids. Please see excel document entitled "Supplementary Table S3 - GSEA Canonical Pathway 2D and 3D" at https://www.nature.com/articles/s41598-019-48816-8#Sec25.

Supplementary Table S4. Most significantly up-regulated GSEA biological processes in EVTs cultured as 3D spheroids

Module	Category	Biological Process Term	NES	FDR p-value
34	Perception	Sensory Perception of Chemical Stimulus	-2.9727	0
9	Chemotaxis	Chemokine Mediated Signaling Pathway	-2.23976	3.86E-04
16	Immune Processes	Positive Regulation of Inflammatory Response	-2.23484	2.58E-04
n/a	n/a	Phospholipase C Activating G Protein Coupled Receptor Signaling Pathway	-2.23057	1.93E-04
39	Peptide cross linking	Peptide Cross Linking	-2.2077	1.55E-04
11	Immune Processes	Positive Regulation of Leukocyte Chemotaxis	-2.20589	1.29E-04
11	Immune Processes	Regulation of Leukocyte Chemotaxis	-2.16591	4.43E-04
11	Immune Processes	Positive Regulation of Leukocyte Migration	-2.16474	3.88E-04
5	Immune Processes	Defense Response to Bacterium	-2.15508	4.31E-04
17	Systemic process	Regulation of Neurological System Process	-2.12934	9.29E-04
11	Immune Processes	Regulation of Leukocyte Migration	-2.12286	9.85E-04
36	Response to zinc	Cellular Response to Zinc Ion	-2.12121	9.03E-04
16	Immune Processes	Regulation of Heat Generation	-2.10755	0.001011
16	Immune Processes	Positive Regulation of Acute Inflammatory Response	-2.09269	0.001104
28	Immune Processes	Natural Killer Cell Activation Involved in Immune Response	-2.09089	0.001185

Supplementary Table S5. Most significantly down-regulated GSEA biological processes in EVTs cultured as 3D spheroids

Module	Category	Biological Process Term	NES	FDR p-value
25	Protein complexes	Mitochondrial Translation	3.070361	0
25	Protein complexes	Translational Termination	2.97231	0
25	Protein complexes	Translational Elongation	2.886832	0
2	Metabolism, biosynthesis, catabolism	Electron Transport Chain	2.729035	0
1	Cell cycle	Nucleotide Excision Repair	2.713833	0
2	Metabolism, biosynthesis, catabolism	Oxidative Phosphorylation	2.685758	0
1	Cell cycle	Transcription Coupled Nucleotide Excision Repair	2.676514	0
2	Metabolism, biosynthesis, catabolism	Mitochondrial Respiratory Chain Complex I Biogenesis	2.666465	0
2	Metabolism, biosynthesis, catabolism	Mitochondrial Respiratory Chain Complex Assembly	2.661326	0
1	Cell cycle	DNA-Dependent DNA Replication	2.659598	0
4	Transcription	DNA-Templated Transcription Termination	2.611477	0
2	Metabolism, biosynthesis, catabolism	Cellular Respiration	2.577143	0
25	Protein complexes	Cellular Protein Complex Disassembly	2.53722	0
0	Metabolism, biosynthesis, catabolism	tRNA Metabolic Process	2.504275	0
4	Transcription	RNA Splicing via Transesterification Reactions	2.479853	1.21E-04

Supplementary Table S6. Full list of GSEA biological processes in EVTs cultured as 2D monolayers and 3D spheroids. Please see excel document entitled "Supplementary Table S6 - GSEA Biological Processes 2D and 3D" at https://www.nature.com/articles/s41598-019-48816-8#Sec25.

Supplementary Table S7. Most significantly up-regulated GO biological processes in EVTs cultured as 3D spheroids. GO-ID may be used to cross-reference category and term to find full gene list provided in Supplementary Table S9.

Category	GO-ID	Biological Process Term	FDR p-value
Sensory perception	7608	Sensory Perception of Smell	2.97E-65
Sensory perception	7606	Sensory Perception of Chemical Stimulus	1.36E-63
Sensory perception	7600	Sensory Perception	4.10E-48
Transport	50877	Neurological System Process	5.62E-47
Sensory perception	50890	Cognition	3.54E-46
Transport	3008	System Process	9.63E-46
Response to stimulus, would healing	50896	Response to Stimulus	7.50E-40
Transport	32501	Multicellular Organismal Process	1.74E-34
Response to stimulus, would healing	6952	Defense Response	2.11E-13
Response to stimulus, would healing	7626	Locomotory Behavior	1.73E-10
G-protein signaling	7186	G-Protein Coupled Receptor Protein Signaling Pathway	8.83E-10
Response to stimulus, would healing	42330	Taxis	3.71E-09
Response to stimulus, would healing	6935	Chemotaxis	3.71E-09
Transport	40011	Locomotion	8.68E-09
Immune processes, angiogenesis, response to stimulus	32101	Regulation of Response to External Stimulus	4.36E-08

Supplementary Table S8. Most significantly down-regulated GO biological processes in EVTs cultured as 3D spheroids. GO-ID may be used to cross-reference category and term to find full gene list provided in Supplementary Table S9.

Category	GO-ID	Biological Process Term	FDR p-value
Metabolic, biosynthetic, catabolic processes	44237	Cellular Metabolic Process	8.46E-37
Metabolic, biosynthetic, catabolic processes	8152	Metabolic Process	1.16E-24
Transcription, translation, DNA replication	44260	Cellular Macromolecule Metabolic Process	3.94E-23
Metabolic, biosynthetic, catabolic processes	44238	Primary Metabolic Process	1.19E-19
Metabolic, biosynthetic, catabolic processes	34641	Cellular Nitrogen Compound Metabolic Process	1.50E-18
Cell cycle	6996	Organelle Organization	9.17E-18
Metabolic, biosynthetic, catabolic processes	6139	Nucleobase, Nucleoside, Nucleotide and Nucleic Acid Metabolic Process	2.32E-17
Cell cycle	9987	Cellular Process	4.64E-16
Metabolic, biosynthetic, catabolic processes	6807	Nitrogen Compound Metabolic Process	5.82E-16
Transcription, translation, DNA replication	43170	Macromolecule Metabolic Process	1.04E-15
Cell cycle	16043	Cellular Component Organization	9.53E-15
Transcription, translation, DNA replication	90304	Nucleic Acid Metabolic Process	1.05E-14
Metabolic, biosynthetic, catabolic processes	44249	Cellular Biosynthetic Process	1.27E-14
Transcription, translation, DNA replication	44267	Cellular Protein Metabolic Process	4.32E-13
Metabolic, biosynthetic, catabolic processes	9058	Biosynthetic Process	5.54E-13

Supplementary Table S9. Full list of GO biological processes in EVTs cultured as 2D monolayers and 3D spheroids. Please see excel document entitled "Supplementary Table S9 - GO Biological Processes 2D and 3D" at https://www.nature.com/articles/s41598-019-48816-8#Sec25.

CHAPTER 4: ESTABLISHMENT OF AN IN VITRO PLACENTAL BARRIER MODEL CULTURED UNDER PHYSIOLOGICALLY-RELEVANT OXYGEN LEVELS

Chapter Preface

This chapter is a manuscript currently in revisions at a peer-reviewed journal. There are no copyright restrictions that we are aware of. Contributors to this manuscript include Michael K. Wong, Edward W. Li, Mohamed Adam, Ponnambalam R. Selvaganapathy, and Sandeep Raha.

Any substance that passes between the mother or fetus must be exchanged at the placental barrier of the terminal chorionic villi. In this third model, we built an *in vitro* platform of the placental barrier that supported co-culturing of trophoblast and endothelial cells, underwent syncytial fusion, and demonstrated size-specificity in maternal-fetal transport. We further performed culture under an oxygen environment (3-8%) that is relevant to what the placenta experiences *in vivo*. Proper oxygenation of cell culture is likely one of the most misapplied or ignored factors in placental research to date. Importantly, we attempted to evaluate secretion and barrier selectivity under these representative oxygen levels. In summary, we developed and characterized a platform that will allow future researchers to better study maternal-fetal transport at the placental barrier *in vitro*.

Abstract

The human placental barrier facilitates many key functions during pregnancy, most notably, the exchange of all substances between the mother and fetus. However, preclinical models of the placental barrier often lacked the multiple cell layers, syncytialization of the trophoblast cells, and the low oxygen levels that are present within the body. Therefore, we aimed to design and develop an *in vitro* model of the placental barrier that would reinstate these factors and enable improved investigations of barrier function. BeWo placental trophoblastic cells and human umbilical vein endothelial cells (HUVECs) were co-cultured on contralateral sides of an extracellular matrix-coated transwell insert to establish a multilayered barrier. Epidermal growth factor and forskolin led to significantly increased multi-nucleation of the BeWo cell layer and increased biochemical markers of syncytial fusion (*e.g.,* ERVWE1, hCGβ). Our *in vitro* placental barrier possessed size-specific permeability to molecules of different sizes, with 4,000 Da molecules experiencing greater transport and a lower apparent permeability coefficient than 70,000 Da molecules. We further demonstrated that the BeWo layer had greater resistance to smaller molecules compared to the endothelial layer. Chronic, physiologically-low oxygen exposure (3-8%) increased expression of HIF1α and ERVWE1, further increased multi-nucleation of the BeWo cell layer, and decreased barrier permeability only against smaller molecules (457/4,000 Da). In conclusion, we built a novel *in vitro* co-culture model of the placental barrier that possessed size-specific permeability and could function under physiologically-low oxygen

levels. Importantly, this will enable future researchers to better study the maternal-fetal transport of nutrients and drugs during pregnancy.

Introduction

The human placental barrier is a complex and dynamic interface that facilitates substance exchange, hormone secretion, and barrier protection between the mother and fetus during pregnancy [1]. The placental barrier mainly consists of a thin, multi-nucleated layer of syncytiotrophoblast and vascular endothelial cells, alongside variable populations of cytotrophoblasts, other placental and immune cell types, and extracellular matrix (ECM) proteins [2,3]. The fused, multi-nucleated syncytiotrophoblast layer is immersed in maternal blood, while the vascular endothelial cells line the blood vessels within the chorionic villi containing fetal blood [2,3]. Like many physiological barriers within the body, the placental barrier is of great clinical relevance because of its central role in modulating not only the transfer of beneficial nutrients, but also drugs, toxins, and other agents between mother and fetus. Clinical tragedies, like thalidomide-induced teratogenesis, could perhaps have been avoided by a deeper understanding of what can and cannot cross the placental barrier [4].

While progress has been made, there is still much work to be done in recapitulating the anatomy and function of the placental barrier into preclinical models, and elucidating the many factors that dictate its physiology, such as syncytialization, multiple cell layers, and the oxygen environment. BeWo or

primary cytotrophoblast mono-culture transwell models have been well-used in the past [5-7], but the fetal vascular endothelial layer is a crucial component of the placental barrier that cannot be excluded in the study of maternal-fetal transport [8,9]. Recently, several BeWo-endothelial co-culture transwell models have also been published [10-15], but these models did not include syncytialization of the trophoblast layer. Syncytialization is a crucial feature in emulating the placental barrier phenotype *in vivo* since the syncytiotrophoblast layer has been shown to possess altered expression of specific nutrient and drug transporters [16]. Advances in these areas will create more predictive testing platforms and unlock new discoveries for prominent pregnancy-related diseases. The low oxygen environment under which placental development and trophoblast syncytialization commences *in vivo* is also of particular importance. Physiological oxygen levels in the human placenta range from around 20 – 60 mmHg (~3 – 8%) depending on the trimester [1,17-21]. Yet, the majority of *in vitro* research is conducted under atmospheric air (21% oxygen), an environment which should be extremely hyperoxic for placental cells [22]. Such observations raise questions and concerns about past studies that classify placental trophoblasts in the low oxygen group (<3%) as the "pathological, hypoxic group", and atmospheric air (21%) as the "healthy, normoxic group" [23,24]. With all the knowledge we have today regarding the fundamental role of low oxygen in mediating early trophoblast processes such as proliferation and differentiation [25,26], and its dynamic, sub-atmospheric alterations from 3-8% following key events like spiral artery remodeling [1,21], modern *in vitro* approaches must incorporate

physiological levels into experimental design and characterize the impact accordingly.

Therefore, in the present study, we aim to develop an *in vitro* model of the human placental barrier by co-culturing syncytialized trophoblastic cells and vascular endothelial cells on contralateral sides of ECM-coated transwell inserts. Moreover, we aim to investigate how chronic, physiologically-low oxygen tension (3-8%) may impact trophoblast syncytialization, placental barrier development, and transport of molecules of varying sizes.

Materials and Methods

Cell culture

BeWo placental trophoblastic cells (ATCC) were cultured at 37 $^{\circ}$C in 95% room air/5% CO_2 in F-12K media (Corning) supplemented with 10% heat-inactivated fetal bovine serum, 1% L-glutamine, and 1% penicillin-streptomycin. BeWo cells were transfected with EGFP-N1 vector (Addgene; plasmid # 54767; a gift from Dr. Michael Davidson; http://n2t.net/addgene:54767; RRID:Addgene_54767) using FuGENE 6 Transfection Reagent (Promega), similar to previously described [27]. After 24 hours, transfected cells (EGFP-BeWo) underwent 14 days of selection in media with G418 (Thermo). Bright, fluorescent EGFP-BeWo were confirmed using fluorescent microscopy and expanded for experimentation. Cells between the passages of 10-20 were used for all experiments, and seeded at a density of 1×10^5 cells/cm^2. Red fluorescent protein-

transfected human umbilical vein endothelial cells (RFP-HUVEC; Angio-Proteomie) were cultured at 37 $^{\circ}$C in 95% room air/5% CO_2 in EGM-2 Endothelial Cell Growth Medium-2 BulletKit (Lonza). Cells between the passages of 4-8 were used for all experiments, and seeded at a density of $1x10^6$ cells/cm^2. Low oxygen (3-8%) culturing was performed in the Xvivo System Model X3 (BioSpherix), which allowed long-term cell incubation and handling under specific, constant oxygen levels.

Transwell insert co-culture model

On Day 0, polyester transwell inserts (Falcon; 12-well, 0.4 µm pores) were placed upside-down and the basolateral sides of the membranes were coated with fibronectin (0.1 mg/mL) for 2 hours at 37 degrees to promote cellular attachment (**Figure 1A**). In the "BeWo only" and "Co-Culture" groups, EGFP-BeWo cells were seeded onto the basolateral side of the transwell insert at $1x10^5$ cells/cm^2 and incubated at 37 degrees for 3 hours to allow attachment. For the "HUVEC only" and "No Cell" groups, an equal volume of cell-free, F-12K media was added to the basolateral side of the transwell insert. All transwell inserts were then reversed and inserted into a multi-well plate filled with F-12K media. On Day 1, to induce BeWo syncytial fusion, F-12K media with epidermal growth factor (EGF; 50 ng/mL) was added to the basolateral chamber for 48 hours, and F-12K media with EGF (50 ng/mL) and forskolin (50 µM) was added to the basolateral chamber for another 48 hours. In experiments that included control, unfused BeWo cell groups, F-12K media with an equal volume of vehicle solution was added instead (phosphate-

buffered saline instead of EGF, dimethyl sulfoxide instead of forskolin). On Day 5, in the "HUVEC only" and "Co-Culture" groups, RFP-HUVEC cells were seeded at 1×10^6 cells/cm^2 onto the apical side of the transwell insert and allowed to reach confluence over 48 hours. In the "BeWo only" and "No Cell" groups, an equal volume of cell-free, EGM-2 media was added to the apical chamber.

Cell concentration

BeWo cells were detached from the growth surface using Trypsin solution (Corning; 0.025%), and cell concentration (cells/mL) was calculated using trypan blue solution (Thermo) and the Countess Automated Cell Counter (Thermo), as per the manufacturer's instructions.

Transport experiments

457 Da Lucifer Yellow (10 µM; Sigma), 4,000 Da fluorescein-dextran (10 µM; Sigma), or 70,000 Da fluorescein-dextran (10 µM; Sigma) were introduced into the basolateral side of the transwell system, whereas fresh media was introduced into the apical side. 50 µL of media was taken from both apical and basolateral sides at 0, 1, 2, 8, 24, and 48 hours. Fluorescent intensities of media samples collected were measured at 485 nm excitation/528 nm emission using a Synergy Plate Reader (BioTek). The "fetal chamber amount" was calculated by normalizing the fluorescent intensity measured in the fetal chamber to the total fluorescence measured in both fetal and maternal chambers. The apparent permeability coefficient was calculated as follows: Apparent permeability coefficient (cm/s) = $(d\text{Q}/d\text{t})/(\text{A}\times\text{C}_0)$, Where dQ is the change in fluorescent

intensity compared to the initial fluorescent intensity in the fetal chamber; dt is the change in time; A the surface area of the transwell insert membrane; C_0 is the initial fluorescent intensity in the maternal chamber (adapted from Huang, et al. [6]).

Live cell imaging

Live, fluorescent images were captured using an Eclipse Ti-E Inverted Confocal Microscope (Nikon) under 4x or 10x objective magnification. FITC channel was used to capture images of EGFP-BeWo cells and TRITC channel was used to capture images of RFP-HUVECs, both from the basal side. 1 μm, z-stack images of co-cultures were captured and 3D-rendered using NIS Elements software (Nikon) to allow X-Z visualization of the cell layers on the transwell insert.

Immunofluorescence

Cells were fixed for 10 minutes in ice-cold methanol (100%) and permeabilized for 5 minutes with Triton X-100 in PBS (0.1%). Immunofluorescence was performed as previously described [28,29]. In brief, samples were incubated with either anti-E-Cadherin primary antibody (1:500; Abcam; ab40772) or anti-hCG primary antibody (1:1000; Meridian; MAF05-019) overnight at 4 degrees and then incubated with goat anti-rabbit IgG H&L Alexa Fluor® 488 secondary antibody (2 μg/mL; Abcam; ab150077) or goat anti-mouse IgG H&L Alexa Fluor® 488 secondary antibody (1:1000; Abcam; ab150117) for 1 hour. Samples were counterstained with 4′,6-diamidino-2-phenylindole dihydrochloride (DAPI; 1.5 μg/mL; Santa Cruz) and mounted onto glass slides using Fluoromount™ Aqueous Mounting Medium (Sigma-Aldrich). Slides were

visualized using an Eclipse Ti-E Inverted Fluorescence Microscope (Nikon). To assess syncytial fusion, E-Cadherin was visualized to identify cell borders (as E-Cadherin is localized to the plasma membrane [30]) and DAPI to identify nuclei. The relative syncytial fusion percentage was then calculated as follows (adapted from Orendi, et al. [31]): Fusion Percentage (%) = (Number of nuclei in syncytia / Total number of nuclei) * 100%, where syncytia may be defined as having two or more nuclei.

RNA Extraction and Real-Time Quantitative Polymerase Chain Reaction (qPCR)

Total RNA (500 ng) was isolated using Direct-zol RNA Miniprep Kit (Zymo Research) and reserve-transcribed to cDNA using High-Capacity cDNA Reverse Transcription Kit (Applied Biosystems), as previously described [29]. In brief, primer sets directed against gene targets of interest were designed through National Center for Biotechnology Information's Primer-BLAST primer designing tool and synthesized at McMaster's Mobix Labs (**Table I**). Quantitative analysis of mRNA expression was performed via qPCR using SsoAdvanced™ Universal SYBR® Green Supermix (BioRad) and CFX384 Touch Real-Time PCR Detection System (BioRad). The cycling conditions were 95 $^\circ$C for 10 min, followed by 40 cycles of 95 $^\circ$C for 10 secs and 60 $^\circ$C for 10 secs and 72 $^\circ$C for 15 secs. Relative fold changes were calculated using the comparative cycle times (Ct) method, normalizing all values to the geometric mean of three endogenous control genes (*18S, ACTB, GAPDH*). The endogenous control gene was selected based on experimentally-determined Ct stability across all treatment groups. Given that all

primer sets had equal priming efficiency, the ΔCt values for each primer set were calibrated to the average of all control Ct values, and the relative abundance of each primer set compared with calibrator was determined by the formula $2^{\Delta\Delta Ct}$, in which ΔΔCt was the normalized value.

Protein Extraction and Western Blot

Total protein was extracted from cells using RIPA buffer supplemented with protease and phosphatase inhibitor cocktails (Roche), as previously described [28]. The solution was sonicated for 5 sec total, 1 sec per pulse, vortexed, and quantified by colorimetric DC protein assay (BioRad). Loading samples were prepared from fresh total protein extract, Laemelli Sample Buffer (4X) (BioRad) and β-mercaptoethanol, and heated at 90 °C for 5 min to denature the proteins. Proteins (20 μg/well) were separated by size via gel electrophoresis in Mini-PROTEAN® TGX Stain-Free™ 4-20% polyacrylamide gels (BioRad), and transferred onto polyvinylidene difluoride membranes using the Trans-Blot® Turbo™ Transfer System (BioRad). Membranes were cut into sections based on predicted molecular weight of target protein, as guided by ladder standard (FroggaBio). Membrane sections were then blocked in 1x Tris-buffered saline-Tween 20 buffer with 5% non-fat milk, and then probed using HIF1α (1:1000; Abcam; ab179483), hCG (1:20000; Dako; A0231), and ERVWE1 (1:200; Abcam; ab71115) antibodies diluted in the blocking solution. Anti-rabbit (1:5,000; GE Healthcare; NA9340) secondary antibody was used to detect the species-specific portion of the primary antibody, diluted in the blocking solution. Immuno-reactive bands were visualized

using Clarity™ Western ECL Substrate (BioRad). Total protein was stained on the membrane using Amido Black and imaged to ensure even loading and transfer [32]. Full, raw blots may be found in **Supplemental Figure S1.**

Enzyme-Linked Immunosorbent Assay (ELISA)

Cell media was collected and protein levels of secreted hCGβ and PLGF were analyzed via ELISA kits (Abcam), as described by the manufacturer. Secreted protein levels were normalized against total BeWo intracellular protein per well using colorimetric DC protein assay (BioRad).

Statistical Analysis

All statistical analyses were performed using Prism 5 software (GraphPad). Results were expressed as means of normalized values ± standard error of the mean (SEM). Experiments were replicated at least three times (n≥3), unless otherwise specified. The significance of differences ($p<0.05$) between normalized mean values were then evaluated using unpaired, two-tailed t-test or one-way analysis of variance (ANOVA) followed by Tukey's post-test, as appropriate.

Results

Formation of an in vitro placental barrier model

We established our *in vitro* placental barrier model by contralaterally co-culturing BeWo trophoblastic cells and human umbilical vein endothelial cells (HUVECs) on opposing sides of fibronectin-coated transwell inserts (**Figure 1A**). Both BeWo and HUVECs could be grown up to around 93% confluency in co-

culture by day 7 (**Figure 1B, C**). Syncytial fusion of the BeWo layer via epidermal growth factor (50 mg/mL) and forskolin (50 µM) did not impact overall surface area confluency of either layers, although the augmentation of fluorescent intensity at certain regions suggest increased clustering of BeWo cells (**Figure 1B-C**). 1 µm, z-stack images of co-cultures were captured and 3D-rendered to allow X-Z axis visualization of the cell layers on the transwell insert (**Figure 1D**). Distinct cell layers may be seen on contralateral sides of the membrane, revealing maintained adjacency of the co-culture in both control and syncytial fusion groups. Overall, the establishment of our co-culture placental barrier model allows us to emulate the critical maternal blood- and fetal blood-facing layers that constitute the human placental barrier *in vivo* [2].

To characterize the syncytial fusion of the BeWo layer, we performed immunofluorescent staining for E-Cadherin protein, which visualizes the plasma membrane borders between cells. BeWo cells that received the fusion treatment exhibited larger and fewer nuclei, and increased multi-nucleation as shown through decreased E-Cadherin expression between nuclei (**Figure 2A**). Control BeWo cells had a fusion percentage of 8.56±0.40%, whereas BeWo cells that received the fusion treatment had a significantly increased fusion percentage of 30.58±1.49% (p<0.001; **Figure 2A**). Furthermore, human chorionic gonadotropin (hCG) was found to be increased in BeWo cells that received the fusion treatment, as seen through immunofluorescent staining (**Figure 2B**) and Western blot (p<0.0001; **Figure 2C**). ERVWE1/Syncytin-1, a protein responsible for facilitating syncytial

fusion, was also found to be significantly increased in BeWo cells that received the fusion treatment compared to controls (p=0.0242; **Figure 2D**). Collectively, these results suggest that the BeWo cell layer in our placental barrier model may be driven towards a syncytialized phenotype *in vitro* through our fusion treatment.

BeWo layer of placental barrier exhibits size-specific permeability to various molecules

We were next interested in determining how syncytial fusion of the BeWo cell layer might impact the permeability of our placental barrier system to molecules of varying sizes. The use of fluorescein-dextran molecules and other dyes to assess barrier permeability, integrity, and size-specificity has been well-established in various *in vitro* organ systems [6,33,34]. Two fluorescein-dextran molecules (4,000 Da and 70,000 Da) were introduced into the BeWo-facing, "maternal chamber" of the transwell insert, and the resultant intensity of fluorescent signal accumulated in the "fetal chamber" was measured and normalized to the total fluorescence in both maternal and fetal chambers. Lower fluorescent intensity indicated lower number of molecules that passively transported into the fetal chamber, and thus, greater barrier permeability, and vice versa [6,34]. Syncytial fusion of the BeWo layer (FUS) did not cause any significant differences in the amount of both 4,000 Da and 70,000 Da molecules that crossed into the fetal chamber compared to the unfused control group (CON) at all time points (**Figure 3A, B**). We calculated the apparent permeability coefficients of the 4,000 Da and 70,000 Da molecules at 48 hours in order to compare the permeability of the BeWo layer

to each molecule. Significantly lower permeability coefficients were found for the 70,000 Da molecules compared to 4,000 Da molecules in both unfused and fused BeWo groups at 48 hours ($p < 0.0001$; **Figure 3C**), demonstrating that smaller molecules more readily permeate the BeWo layer.

BeWo and HUVEC layers differentially regulate barrier permeability

We were next interested in determining the individual and joint contributions of the BeWo and vascular endothelial cell layers in regulating the permeability of the barrier. All BeWo cells from this point onwards received the syncytial fusion treatment. The BeWo only and Co-Culture groups had significantly less 4,000 Da fluorescein dextran molecules cross into the fetal chamber compared to the No Cell group at 2, 8, 24, and 48 hours, and compared to the HUVEC only group at 48 hours ($p < 0.05$; **Figure 3D**). The HUVEC only group also had significantly less 4,000 Da molecule cross into the fetal chamber compared to the No Cell group at 2, 8, and 24 hours ($p < 0.05$; **Figure 3D**). All groups had significantly less 70,000 Da molecules cross into the fetal chamber compared to the No Cell group at 2, 8, 24, and 48 hours ($p < 0.01$; **Figure 3E**). The Co-Culture group also had significantly less 70,000 Da molecule cross into the fetal chamber compared to the HUVEC only group at 48 hours ($p < 0.01$; **Figure 3E**). We calculated the apparent permeability coefficients of both molecules at 48 hours to compare the permeability of the molecules across each layer of the barrier. Significantly lower permeability coefficients were found for the 70,000 Da molecule than for the 4,000 Da molecule in all groups ($p < 0.001$; **Figure 3F**),

suggesting both BeWo and HUVEC layers contribute to the size-specific permeability. Furthermore, the ratio between the apparent permeability coefficients of BeWo only and HUVEC only layers is lower for the 4,000 Da molecule (0.678 ± 0.061) than for the 70,000 Da molecule (0.789 ± 0.040; p=0.0589), suggesting the BeWo layer may play a more substantial role in the size-exclusion and resistance of smaller molecules across the barrier.

Low oxygen tension impacts growth patterns and syncytial fusion

To evaluate the impact of physiologically-low oxygen tension (3-8%) on syncytial fusion of the trophoblastic layer and barrier exchange, BeWo cells were seeded under 21% oxygen for 48 hours, transferred into chronic 21%, 8%, or 3% oxygen tension to acclimatize for 24 hours, and induced to syncytialize under the respective oxygen tensions for another 48 hours. Hypoxia-inducible factor 1α (HIF1α) protein levels were significantly increased in a dose-dependent manner when BeWo cells were fused under 3% and 8% oxygen compared to 21% oxygen, confirming the cells' responsiveness to a low oxygen environment (p<0.05; **Figure 4A, B**). The α-subunit of HIF1 is constitutively expressed under low oxygen conditions, but rapidly degraded in the presence of oxygen, making it a useful sensor for relative oxygen levels [35,36]. Placental growth factor (PLGF) is known to decrease under low oxygen, thus may be used as a second marker to verify the cellular response [37]. Indeed, secreted PLGF protein levels were significantly decreased in a dose-dependent manner (p<0.05; **Figure 4C**). *HIF1A* mRNA levels were consistently increased at 3% oxygen compared to 21% and 8% oxygen

(p<0.05; **Figure 4D**), and *PLGF* mRNA levels were decreased in an oxygen-dependent manner (p<0.001; **Figure 4E**). Furthermore, BeWo cell concentration did not significantly change across 7 days under 3% oxygen, whereas BeWo cell concentration significantly increased under 21% oxygen (p<0.001; **Figure 4F**).

Live cell imaging of the co-cultures revealed relatively less BeWo cell growth at 3% and 8% oxygen compared to 21% based on fluorescent intensity (**Figure 5A**), which is consistent with the inhibition of proliferation demonstrated above (**Figure 4F**). The HUVEC layer of the co-culture appeared more abundant at 3% and 8% oxygen compared to 21% (**Figure 5A**). E-Cadherin immunofluorescent staining revealed significantly increased syncytial fusion percentages in an oxygen-dependent manner, as BeWo cells were cultured under 21% oxygen (28.57±2.68% fusion), 8% oxygen (38.86±6.29% fusion), and 3% oxygen (50.44±4.68% fusion) (p<0.05 for all; **Figure 5B**). BeWo cells also appeared to grow more evenly and organized under 3% with fewer instances of clustering. ERVWE1 protein levels were significantly increased under 3% and 8% oxygen compared to 21% oxygen (p<0.001; **Figure 5C, D**). However, both intracellular and secreted protein levels of hCGβ were significantly decreased in a dose-dependent manner in 3% and 8% oxygen compared to 21% oxygen (p<0.05; **Figure 5C, E, F**). *ERVWE1* (p<0.001; **Figure 5G**) and *CGB* mRNA levels (p<0.05; **Figure 5H**) were also decreased at 3% and 8% oxygen compared to 21%.

Low oxygen tension increases specificity of permeability across placental barrier

Given the impact of low oxygen tension on syncytial fusion of the BeWo trophoblastic layer, we were next interested in investigating the effects on barrier permeability. Three fluorescent molecules of varying sizes (457 Da Lucifer Yellow, 4,000 Da fluorescein-dextran, and 70,000 Da fluorescein-dextran) were introduced into the "maternal chamber", and the resultant intensity of fluorescent signal in the "fetal chamber" was measured as described above. The Co-Culture group had significantly fewer 457 Da molecules from 2 – 48 hours, 4,000 Da molecules from 1 – 48 hours, and 70,000 Da molecules from 24 – 48 hours cross into the fetal chamber, compared to the No Cell control under all oxygen levels ($p<0.05$; **Figure 6A-C**). We further calculated the apparent permeability coefficients for each molecule at 48 hours to compare the differences across oxygen levels. The apparent permeability coefficient of the 457 Da molecule was significantly lower in the placental barrier under 8% oxygen compared to 21% oxygen and 3% oxygen ($p<0.01$; **Figure 6D**). The apparent permeability coefficient of the 4,000 Da molecule was significantly lower under 3% and 8% oxygen compared to 21% oxygen ($p<0.01$; **Figure 6D**). There were no significant differences in the apparent permeability coefficient of the 70,000 Da molecule (**Figure 6D**).

Discussion

Stronger preclinical models of the placental barrier are key towards advancing our understanding of the effects of maternal drug and toxin exposure on the fetus. In the current study, we designed and characterized a new approach to modelling the placental barrier *in vitro*, where BeWo trophoblastic cells and HUVECs may be co-cultured on contralateral sides of an ECM-coated transwell insert. Our approach was novel in the following ways: Firstly, by seeding the BeWo cells on the basolateral side of the transwell insert, we were able to induce syncytial fusion without exposing the HUVECs to forskolin, which is unique compared to many past transport models that do not attempt to induce syncytial fusion at all (Aengenheister *et al.* , 2019, Aengenheister *et al.* , 2018, Bode *et al.* , 2006). Secondly, we demonstrated that our placental barrier model can exhibit size-specific barrier permeability to various fluorescent molecules (457 Da Lucifer Yellow, 4,000 Da fluorescein-dextran, and 70,000 Da fluorescein-dextran). Lastly, we profiled the response of our placental barrier to physiologically-low oxygen environments (3-8%) and the impact on syncytial fusion and barrier permeability. Through use of readily-accessible tools (such as transwell inserts) and well-characterized cell lines (BeWo and HUVEC), our approach is also very practical for other placental researchers to adopt.

The low oxygen environment (3-8%) under which placental development occurs within the body is an important factor that has been controversially ignored in many *in vitro* systems to date [17-19]. Our results, however, show that the BeWo

cell layer is responsive to altered environmental oxygen levels. This is important as oxygen-sensitive transcription factors, such as HIF1, control the expression of many development-related genes and proteins [36,38,39], and the disruption of its signalling can lead to impaired placental development and cellular differentiation [40]. Thus, placental cultures performed under atmospheric air, which we demonstrated to indeed have degraded HIF1α protein levels compared to low oxygen cultures, are expected to lead to markedly altered HIF1-dependent transcriptomic and functional phenotypes [36,38,39]. Low oxygen has also been demonstrated to lead to membrane-to-cytoplasm translocation and reduced expression of connexin43 in trophoblastic cells, which may be a potential molecular mechanism underlying the altered barrier permeability in low oxygen given the role of gap junction formation in intercellular exchange of small molecules [41,42].

Past studies have reported controversial interpretations regarding the impact of oxygen on syncytial fusion, where many assumed a priori that low oxygen should be a deleterious treatment group for trophoblast culture *in vitro* when compared to atmospheric air [23,24]. Yet, pregnancy pathologies like preterm birth and intrauterine growth restriction have been found at times to be associated with hyperoxia, not hypoxia [43,44].While pathological hypoxia and ischemia may be undoubtedly harmful in the body, the use of atmospheric air as the "healthy, normal group" in placental experiments may be confounding and misleading, given the weak evidence for hypoxia in the etiology of placental diseases [1,22]. Moreover, it does not reflect the chronic, low oxygen tension experienced within the placenta throughout

gestation, especially during trophoblast syncytialization [22-24,45-47]. Furthermore, placental explants cultured under 8% oxygen reported better tissue structure and RNA quality than those cultured under atmospheric air [48]. While there is some evidence suggesting that BeWo cells have a similar response to changes in oxygen as primary trophoblasts (*e.g.,* decreased PlGF gene expression reported in both primary trophoblasts and BeWo cells when exposed to 2% vs. 20% oxygen, but no change seen in HTR8/SVneo cells) [37], there may also be differences as BeWo cells have been inappropriately cultured at atmospheric air for many generations. Thus, some caution must be taken in interpreting these findings, but it nonetheless emphasizes the need to better define the oxygen environment in future experimental and model designs.

The increased presence of multi-nucleated cells and elevated ERVWE1/Syncytin-1 protein expression under 8% and 3% oxygen provided evidence supporting our hypothesis for improved syncytialization under low oxygen. Furthermore, the selectively decreased permeability only to the smaller particles (457 and 4,000 Da) at low oxygen would suggest increased barrier specificity. However, lower oxygen also led to decreased levels in some traditional markers of syncytialization (*e.g.,* hCG protein, *CGB* and *ERVWE1* mRNA), which is consistent with findings by others [49]. To help interpret this, Diaz, et al. [50] also found that hCG expression and secretion was decreased in placental explants with established, intact syncytiotrophoblast layers cultured under 6% oxygen compared to similar explants cultured under 21% oxygen. These findings alongside expert

opinions by Huppertz and Gauster [51] suggest that the state of syncytial fusion does not always correlate to hCG levels, and that oxygen may even directly regulate hCG expression [50]. Furthermore, JEG-3 cells, a non-fusogenic, trophoblastic cell line, may also exhibit augmented hCG expression under certain experimental conditions without any incidence of fusion [52,53]. Thus, changing levels of hCG and other classical mRNA or protein markers can help indicate syncytial fusion, but must be supported by additional tests (*e.g.,* plasma membrane visualization via E-Cadherin [54]), especially when assessing experiments involving changes in oxygen.

While BeWo cells have some limitations as a choriocarcinoma cell line, the forskolin-induced model is well-validated with controlled, predictable rates of fusion, allowing precise study of barrier permeability and response to low oxygen tension [27,30]. Primary trophoblast cells would have been challenging and perhaps disadvantageous to use in this study, given their spontaneous, uncontrollable fusion events and unpredictable rates across donors [51,55]. In fact, another BeWo co-culture model was recently demonstrated to study barrier permeability to nanoparticles [11]. However, these authors cultured BeWo cells on the apical side and HUVECs on basal side, and did not attempt to induce fusion in the BeWo cells [11]. Syncytial fusion is a crucial phenotype required to emulate the human placental barrier, and our novel approach to reverse-culturing BeWo cells on the basal side of the transwell insert enables the selective induction of syncytial fusion prior to seeding the endothelial cell layer. While we did not demonstrate any changes in barrier permeability to fluorescein dextran molecules after syncytial fusion, there are many

other specific transporters expressed on the placental barrier for functional molecules (*e.g.,* ATP-binding cassette transporter (ABC) A1, ABCG2, glucose transporter (GLUT) 1) that may change in expression and function after syncytialization or low oxygen exposure [6,56]. Therefore, there is much promise for future studies to build upon and apply our current model to explore the impact of oxygen and/or syncytial fusion on transport of specific, functional molecules.

In conclusion, we established a multi-layered, *in vitro* model of the human placental barrier that may undergo syncytial fusion, exhibit size-specific barrier permeability, and function under physiologically-low oxygen. These findings will contribute vital biological insights to the advancement of future micro-physiological placental systems, such as the placenta-on-a-chip or bio-printed models, ultimately, progressing our understanding of maternal-fetal exchange during pregnancy.

Acknowledgements

Authors' Roles

MKW wrote the main manuscript text. MKW, EL, and MA conducted all experiments and analyses. PRS and SR contributed to the experimental design. All authors reviewed the manuscript.

Funding

Conflict of Interest

None to declare.

References

1   Huppertz, B., Weiss, G. & Moser, G. Trophoblast invasion and oxygenation of the placenta: measurements versus presumptions. *J Reprod Immunol* **101-102**, 74-79, doi:10.1016/j.jri.2013.04.003 (2014).

2   Huppertz, B., Ghosh, D. & Sengupta, J. An integrative view on the physiology of human early placental villi. *Prog Biophys Mol Biol* **114**, 33-48, doi:10.1016/j.pbiomolbio.2013.11.007 (2014).

3   Rubinchik-Stern, M. & Eyal, S. Drug Interactions at the Human Placenta: What is the Evidence? *Front Pharmacol* **3**, 126, doi:10.3389/fphar.2012.00126 (2012).

4   Vargesson, N. Thalidomide-induced teratogenesis: history and mechanisms. *Birth Defects Res C Embryo Today* **105**, 140-156, doi:10.1002/bdrc.21096 (2015).

5   Heaton, S. J. *et al.* The use of BeWo cells as an in vitro model for placental iron transport. *American journal of physiology. Cell physiology* **295**, C1445-1453, doi:10.1152/ajpcell.00286.2008 (2008).

6   Huang, X. *et al.* Establishment of a confluent monolayer model with human primary trophoblast cells: novel insights into placental glucose transport. *Mol Hum Reprod* **22**, 442-456, doi:10.1093/molehr/gaw018 (2016).

7   Li, H., van Ravenzwaay, B., Rietjens, I. M. & Louisse, J. Assessment of an in vitro transport model using BeWo b30 cells to predict placental transfer of compounds. *Arch Toxicol* **87**, 1661-1669, doi:10.1007/s00204-013-1074-9 (2013).

8   Boss, A. L., Chamley, L. W. & James, J. L. Placental formation in early pregnancy: how is the centre of the placenta made? *Hum Reprod Update* **24**, 750-760, doi:10.1093/humupd/dmy030 (2018).

9   Elad, D., Levkovitz, R., Jaffa, A. J., Desoye, G. & Hod, M. Have we neglected the role of fetal endothelium in transplacental transport? *Traffic* **15**, 122-126, doi:10.1111/tra.12130 (2014).

10   Aengenheister, L. *et al.* Investigating the accumulation and translocation of titanium dioxide nanoparticles with different surface modifications in static and dynamic human placental transfer models. *Eur J Pharm Biopharm* **142**, 488-497, doi:10.1016/j.ejpb.2019.07.018 (2019).

11   Aengenheister, L. *et al.* An advanced human in vitro co-culture model for translocation studies across the placental barrier. *Scientific reports* **8**, 5388, doi:10.1038/s41598-018-23410-6 (2018).

12   Bode, C. J. *et al.* In vitro models for studying trophoblast transcellular transport. *Methods Mol Med* **122**, 225-239 (2006).

13   Yin, F. *et al.* A 3D human placenta-on-a-chip model to probe nanoparticle exposure at the placental barrier. *Toxicology in vitro : an international journal published in association with BIBRA* **54**, 105-113, doi:10.1016/j.tiv.2018.08.014 (2019).

14   Pemathilaka, R. L., Caplin, J. D., Aykar, S. S., Montazami, R. & Hashemi, N. N. Placenta-on-a-Chip: In Vitro Study of Caffeine Transport across Placental Barrier Using Liquid Chromatography Mass Spectrometry. *Global Challenges* **3**, doi:10.1002/gch2.201800112 (2019).

15   Lee, J. S. *et al.* Placenta-on-a-chip: a novel platform to study the biology of the human placenta. *The Journal of Maternal-Fetal & Neonatal Medicine*, 1-9, doi:10.3109/14767058.2015.1038518 (2015).

16   Liu, L. & Liu, X. Contributions of Drug Transporters to Blood-Placental Barrier. *Advances in experimental medicine and biology* **1141**, 505-548, doi:10.1007/978-981-13-7647-4_11 (2019).

17   Miller, R. K. *et al.* Human placental explants in culture: approaches and assessments. *Placenta* **26**, 439-448, doi:10.1016/j.placenta.2004.10.002 (2005).

18   Lackman, F., Capewell, V., Gagnon, R. & Richardson, B. Fetal umbilical cord oxygen values and birth to placental weight ratio in relation to size at birth. *American journal of obstetrics and gynecology* **185**, 674-682, doi:10.1067/mob.2001.116686 (2001).

19   Andrade, P. Z. *et al.* Ex vivo expansion of cord blood haematopoietic stem/progenitor cells under physiological oxygen tensions: clear-cut effects on cell proliferation, differentiation and metabolism. *J Tissue Eng Regen Med* **9**, 1172-1181, doi:10.1002/term.1731 (2015).

20   Rodesch, F., Simon, P., Donner, C. & Jauniaux, E. Oxygen measurements in endometrial and trophoblastic tissues during early pregnancy. *Obstet Gynecol* **80**, 283-285 (1992).

21   Jauniaux, E. *et al.* Onset of Maternal Arterial Blood Flow and Placental Oxidative Stress. *The American journal of pathology* **157**, 2111-2122, doi:10.1016/s0002-9440(10)64849-3 (2000).

22   Tuuli, M. G., Longtine, M. S. & Nelson, D. M. Review: Oxygen and trophoblast biology--a source of controversy. *Placenta* **32 Suppl 2**, S109-118, doi:10.1016/j.placenta.2010.12.013 (2011).

23   Kudo, Y., Boyd, C. A. R., Sargent, I. L. & Redman, C. W. G. Hypoxia alters expression and function of syncytin and its receptor during trophoblast cell fusion of human placental BeWo cells: implications for impaired trophoblast syncytialisation in pre-eclampsia. *Biochimica et Biophysica Acta (BBA) - Molecular Basis of Disease* **1638**, 63-71, doi:10.1016/s0925-4439(03)00043-7 (2003).

24   Alsat, E. *et al.* Hypoxia impairs cell fusion and differentiation process in human cytotrophoblast, in vitro. *J Cell Physiol* **168**, 346-353, doi:10.1002/(SICI)1097-4652(199608)168:2<346::AID-JCP13>3.0.CO;2-1 (1996).

25   Genbacev, O., Zhou, Y., Ludlow, J. W. & Fisher, S. J. Regulation of human placental development by oxygen tension. *Science* **277**, 1669-1672, doi:10.1126/science.277.5332.1669 (1997).

26   Zhou, S., Xie, Y., Puscheck, E. E. & Rappolee, D. A. Oxygen levels that optimize TSC culture are identified by maximizing growth rates and minimizing stress. *Placenta* **32**, 475-481, doi:10.1016/j.placenta.2011.03.013 (2011).

27   Wang, R. *et al.* Live cell imaging of in vitro human trophoblast syncytialization. *Biology of reproduction* **90**, 117, doi:10.1095/biolreprod.113.114892 (2014).

28   Wong, M. K., Wahed, M., Shawky, S. A., Dvorkin-Gheva, A. & Raha, S. Transcriptomic and functional analyses of 3D placental extravillous trophoblast spheroids. *Scientific reports* **9**, 12607, doi:10.1038/s41598-019-48816-8 (2019).

29   Wong, M. K. *et al.* Extracellular matrix surface regulates self-assembly of three-dimensional placental trophoblast spheroids. *PloS one* **13**, e0199632, doi:10.1371/journal.pone.0199632 (2018).

30   Ishikawa, A. *et al.* Cell fusion mediates dramatic alterations in the actin cytoskeleton, focal adhesions, and E-cadherin in trophoblastic cells. *Cytoskeleton (Hoboken)* **71**, 241-256, doi:10.1002/cm.21165 (2014).

31   Orendi, K., Gauster, M., Moser, G., Meiri, H. & Huppertz, B. The choriocarcinoma cell line BeWo: syncytial fusion and expression of syncytium-specific proteins. *Reproduction* **140**, 759-766, doi:10.1530/REP-10-0221 (2010).

32   Aldridge, G. M., Podrebarac, D. M., Greenough, W. T. & Weiler, I. J. The use of total protein stains as loading controls: An alternative to high-abundance single-protein controls in semi-quantitative immunoblotting. *J Neurosci Meth* **172**, 250-254, doi:DOI 10.1016/j.jneumeth.2008.05.003 (2008).

33   Schwabe, T., Bainton, R. J., Fetter, R. D., Heberlein, U. & Gaul, U. GPCR signaling is required for blood-brain barrier formation in drosophila. *Cell* **123**, 133-144, doi:10.1016/j.cell.2005.08.037 (2005).

34   Matsukawa, Y., Lee, V. H., Crandall, E. D. & Kim, K. J. Size-dependent dextran transport across rat alveolar epithelial cell monolayers. *Journal of pharmaceutical sciences* **86**, 305-309, doi:10.1021/js960352x (1997).

35   Huang, L. E., Arany, Z., Livingston, D. M. & Bunn, H. F. Activation of Hypoxia-inducible Transcription Factor Depends Primarily upon Redox-sensitive Stabilization of Its Subunit. *Journal of Biological Chemistry* **271**, 32253-32259, doi:10.1074/jbc.271.50.32253 (1996).

36   Lee, J. W., Bae, S. H., Jeong, J. W., Kim, S. H. & Kim, K. W. Hypoxia-inducible factor (HIF-1)alpha: its protein stability and biological functions. *Experimental & molecular medicine* **36**, 1-12, doi:10.1038/emm.2004.1 (2004).

37   Fujii, T. *et al.* Enhanced HIF2alpha expression during human trophoblast differentiation into syncytiotrophoblast suppresses transcription of placental growth factor. *Scientific reports* **7**, 12455, doi:10.1038/s41598-017-12685-w (2017).

38   Breckenridge, R. A. *et al.* Hypoxic regulation of hand1 controls the fetal-neonatal switch in cardiac metabolism. *PLoS Biol* **11**, e1001666, doi:10.1371/journal.pbio.1001666 (2013).

39   Rath, G., Aggarwal, R., Jawanjal, P., Tripathi, R. & Batra, A. HIF-1 Alpha and Placental Growth Factor in Pregnancies Complicated With Preeclampsia: A Qualitative and Quantitative Analysis. *J Clin Lab Anal*, doi:10.1002/jcla.21819 (2014).

40   Fryer, B. H. & Simon, M. C. Hypoxia, HIF and the placenta. *Cell Cycle* **5**, 495-498, doi:10.4161/cc.5.5.2497 (2006).

41   Otto, T. *et al.* Oxygen Sensitivity of Placental Trophoblast Connexins 43 and 46: A Role in Preeclampsia? *J Cell Biochem* **116**, 2924-2937, doi:10.1002/jcb.25240 (2015).

42   Knerr, I. *et al.* Stimulation of GCMa and syncytin via cAMP mediated PKA signaling in human trophoblastic cells under normoxic and hypoxic conditions. *FEBS Lett* **579**, 3991-3998, doi:10.1016/j.febslet.2005.06.029 (2005).

43   Sibley, C. P. *et al.* Pathogenesis of intrauterine growth restriction (IUGR)-conclusions derived from a European Union Biomed 2 Concerted Action project 'Importance of Oxygen Supply in Intrauterine Growth Restricted Pregnancies'-a workshop report. *Placenta* **23 Suppl A**, S75-79, doi:10.1053/plac.2002.0796 (2002).

44   Kakogawa, J., Sumimoto, K., Kawamura, T., Minoura, S. & Kanayama, N. Noninvasive monitoring of placental oxygenation by near-infrared spectroscopy. *Am J Perinatol* **27**, 463-468, doi:10.1055/s-0030-1247600 (2010).

45   Genbacev, O., McMaster, M. T., Zdravkovic, T. & Fisher, S. J. Disruption of oxygen-regulated responses underlies pathological changes in the placentas of women who smoke or who are passively exposed to smoke during pregnancy. *Reproductive toxicology* **17**, 509-518, doi:10.1016/s0890-6238(03)00094-7 (2003).

46   Knerr, I. *et al.* Transcriptional effects of hypoxia on fusiogenic syncytin and its receptor ASCT2 in human cytotrophoblast BeWo cells and in ex vivo perfused placental cotyledons. *American journal of obstetrics and gynecology* **189**, 583-588, doi:10.1067/s0002-9378(03)00538-6 (2003).

47   Genbacev, O., Joslin, R., Damsky, C. H., Polliotti, B. M. & Fisher, S. J. Hypoxia alters early gestation human cytotrophoblast differentiation/invasion in vitro and models the placental defects that occur in preeclampsia. *The Journal of clinical investigation* **97**, 540-550, doi:10.1172/JCI118447 (1996).

48   Brew, O. *et al.* Quality of placental RNA: Effects of explant size and culture duration. *Placenta* **46**, 45-48, doi:10.1016/j.placenta.2016.08.083 (2016).

49   Strohmer, H. *et al.* Hypoxia downregulates continuous and interleukin-1-induced expression of human chorionic gonadotropin in choriocarcinoma cells. *Placenta* **18**, 597-604, doi:10.1016/0143-4004(77)90016-9 (1997).

50   Diaz, P., Sibley, C. P. & Greenwood, S. L. Oxygen-Sensitive K+ Channels Modulate Human Chorionic Gonadotropin Secretion from Human Placental Trophoblast. *PloS one* **11**, e0149021, doi:10.1371/journal.pone.0149021 (2016).

51   Huppertz, B. & Gauster, M. in *Cell Fusions*   Ch. Chapter 9, 203-217 (2011).

52   Rothbauer, M. *et al.* A comparative study of five physiological key parameters between four different human trophoblast-derived cell lines. *Scientific reports* **7**, 5892, doi:10.1038/s41598-017-06364-z (2017).

53   Vargas, A., Moreau, J., Le Bellego, F., Lafond, J. & Barbeau, B. Induction of trophoblast cell fusion by a protein tyrosine phosphatase inhibitor. *Placenta* **29**, 170-174, doi:10.1016/j.placenta.2007.10.012 (2008).

54   Borges, M., Bose, P., Frank, H. G., Kaufmann, P. & Pötgens, A. J. G. A Two-Colour Fluorescence Assay for the Measurement of Syncytial Fusion between Trophoblast-Derived Cell Lines. *Placenta* **24**, 959-964, doi:10.1016/s0143-4004(03)00173-5 (2003).

55   Poidatz, D. *et al.* Trophoblast syncytialisation necessitates mitochondrial function through estrogen-related receptor-gamma activation. *Mol Hum Reprod* **21**, 206-216, doi:10.1093/molehr/gau102 (2015).

56   Francois, L. N. *et al.* Down-regulation of the placental BCRP/ABCG2 transporter in response to hypoxia signaling. *Placenta* **51**, 57-63, doi:10.1016/j.placenta.2017.01.125 (2017).

Figures and Figure Legends
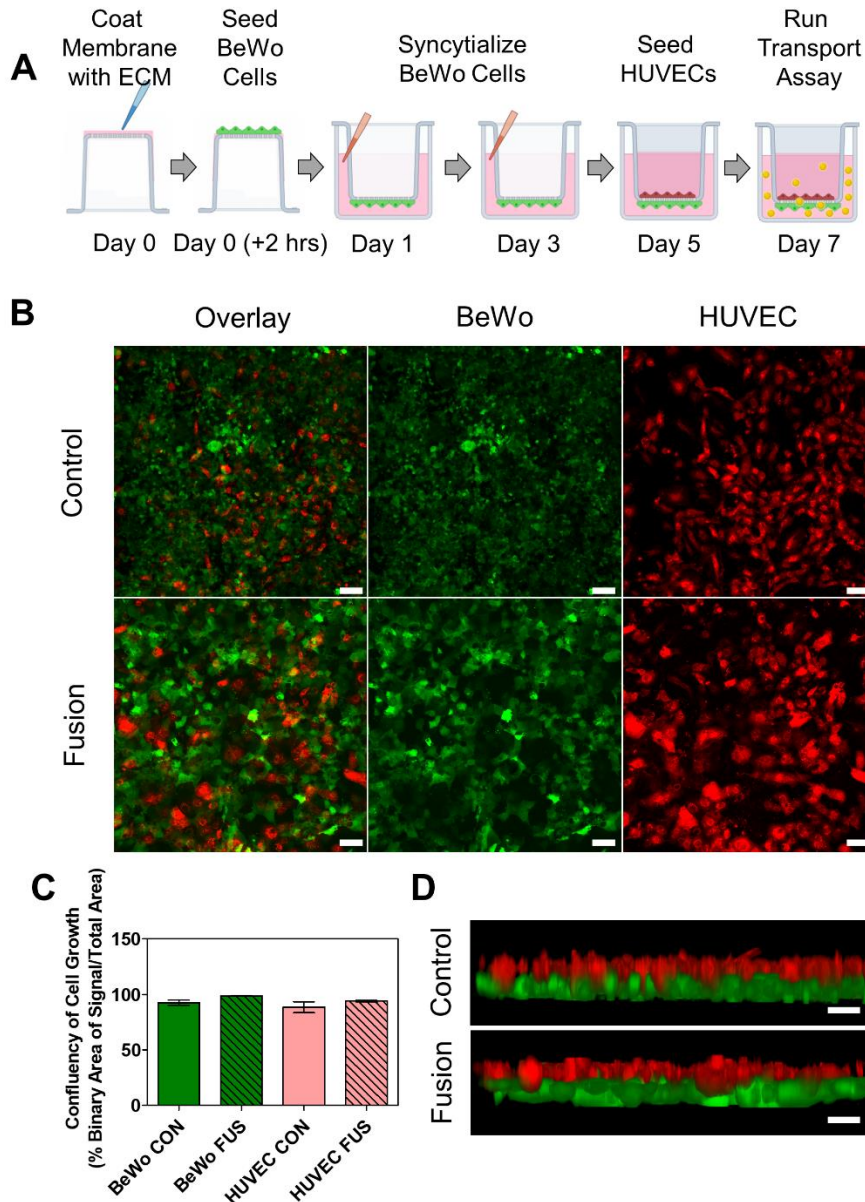
Figure 1. BeWo and HUVECs co-cultured on contralateral sides of a transwell insert for up to 7 days. (A) Schematic of co-culture method to establish *in vitro* placental barrier model. **(B)** Live, immunofluorescent images of BeWo and HUVECs in co-culture. Green colour indicates BeWo cells and red colour indicates HUVECs. Scale bar indicates 100 μm. **(C)** Confluency of growth of all cell groups, as determined by the surface area of fluorescent signal normalized to the total surface area of field of view. One-way ANOVA was used to assess significant differences between the groups. **(D)** 3D-rendered images of the X-Z axis of BeWo and HUVECs cultured on the transwell insert at day 7.
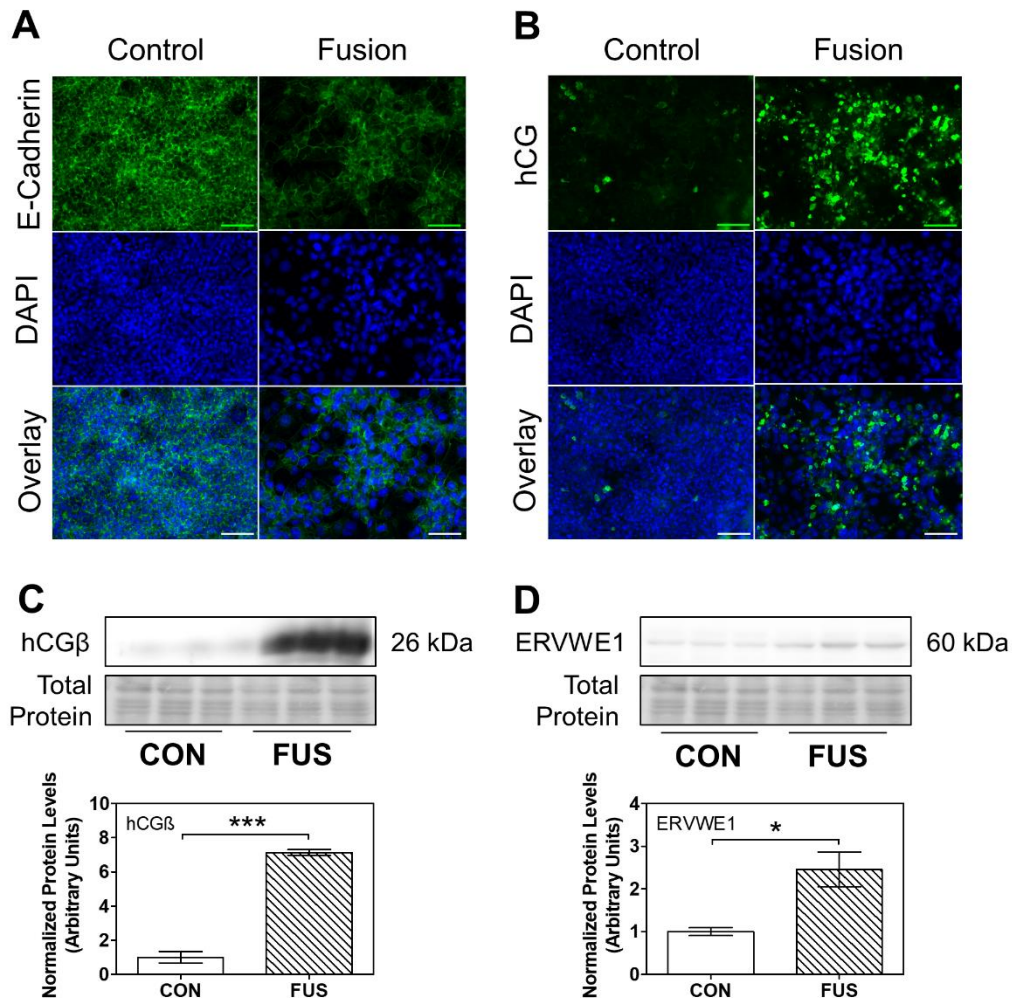
Figure 2. BeWo trophoblastic cells treated with epidermal growth factor (50 ng/mL) and forskolin (50 μM) express increased markers of syncytial fusion. (**A**) Immunofluorescent staining for E-Cadherin protein of BeWo cells in the control and fusion treatment groups. (**B**) Immunofluorescent staining for hCG protein and nuclei (DAPI). Scale bar indicates 100 μm. Western blots and densitometry quantifications of (**C**) hCGβ and (**D**) ERVWE1 protein. Densitometric quantification of relative protein expression based on band intensity. All arbitrary values were expressed as means normalized to Amido black ± SEM. Significant differences between treatment groups determined by t-test; n ≥ 3. Significant differences between means indicated by *, p<0.05 or ***, p<0.0001.
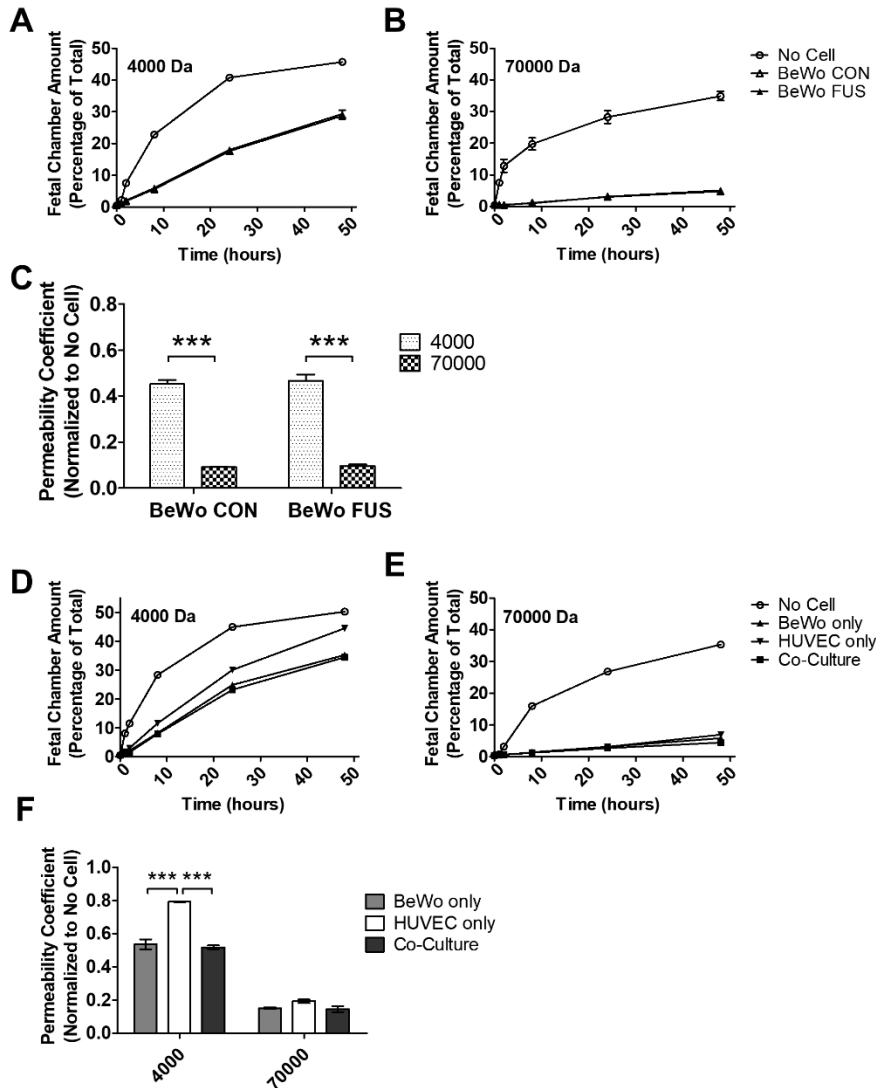
Figure 3. Placental barrier exhibits size-specific permeability to 4,000 Da and 70,000 Da molecules. Percentage of fluorescent intensity measured in fetal chamber normalized to total fluorescent intensity in both maternal and fetal chambers in the No Cell, unfused BeWo (CON), or fused BeWo (FUS) groups for (**A**) 4,000 Da fluorescein-dextran molecules or (**B**) 70,000 Da fluorescein-dextran molecules. (**C**) Apparent permeability coefficients of 4,000 Da and 70,000 Da molecules in BeWo control and fusion groups at 48 hours normalized to the No Cell control group. Percentage of fluorescent intensity measured in fetal chamber normalized to total fluorescent intensity in the No Cell, BeWo only, HUVEC only, or Co-Culture groups for (**D**) 4,000 Da or (**E**) 70,000 Da. (**F**) Apparent permeability coefficients of 4,000 Da and 70,000 Da molecules in BeWo only, HUVEC only, and Co-Culture groups at 48 hours. Significant differences between treatment groups determined by two-way ANOVA; n ≥ 3. Significant differences between means indicated by ***, $p < 0.001$.
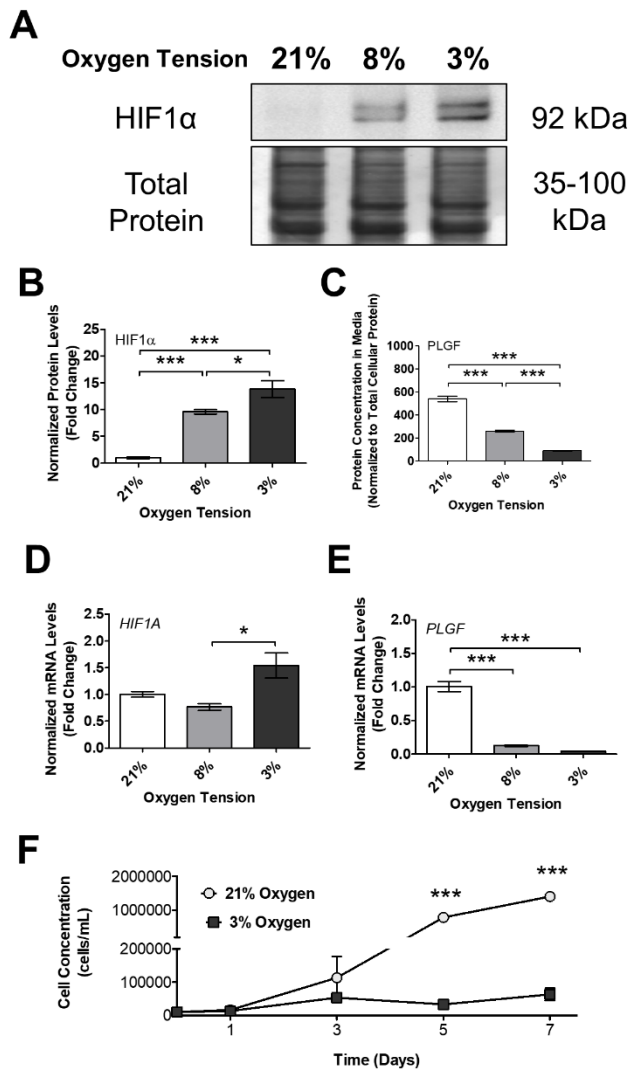
Figure 4. Low oxygen tension impacts expression of various protein markers of hypoxia in BeWo cells. (**A**) Protein levels of HIF1α, as determined by Western blot. Full, raw blot may be found in **Supplemental Figure S1**. (**B**) Densitometric quantification of relative protein expression based on band intensity. All arbitrary values were expressed as means normalized to total protein ± SEM. (**C**) Secreted protein levels of PLGF, as determined by ELISA. All arbitrary values were expressed as means normalized to total intracellular protein ± SEM. mRNA levels of (**D**) *HIF1* and (**E**) *PLGF,* as determined by RT-qPCR. All arbitrary values were expressed as means normalized to the geometric mean of housekeeping genes ± SEM. (**F**) Cell concentration of BeWo cells cultured in 21% or 3% oxygen for up to 7 days. Significant differences between means indicated by *, $p < 0.05$, **, $p < 0.01$, or ***, $p < 0.001$.
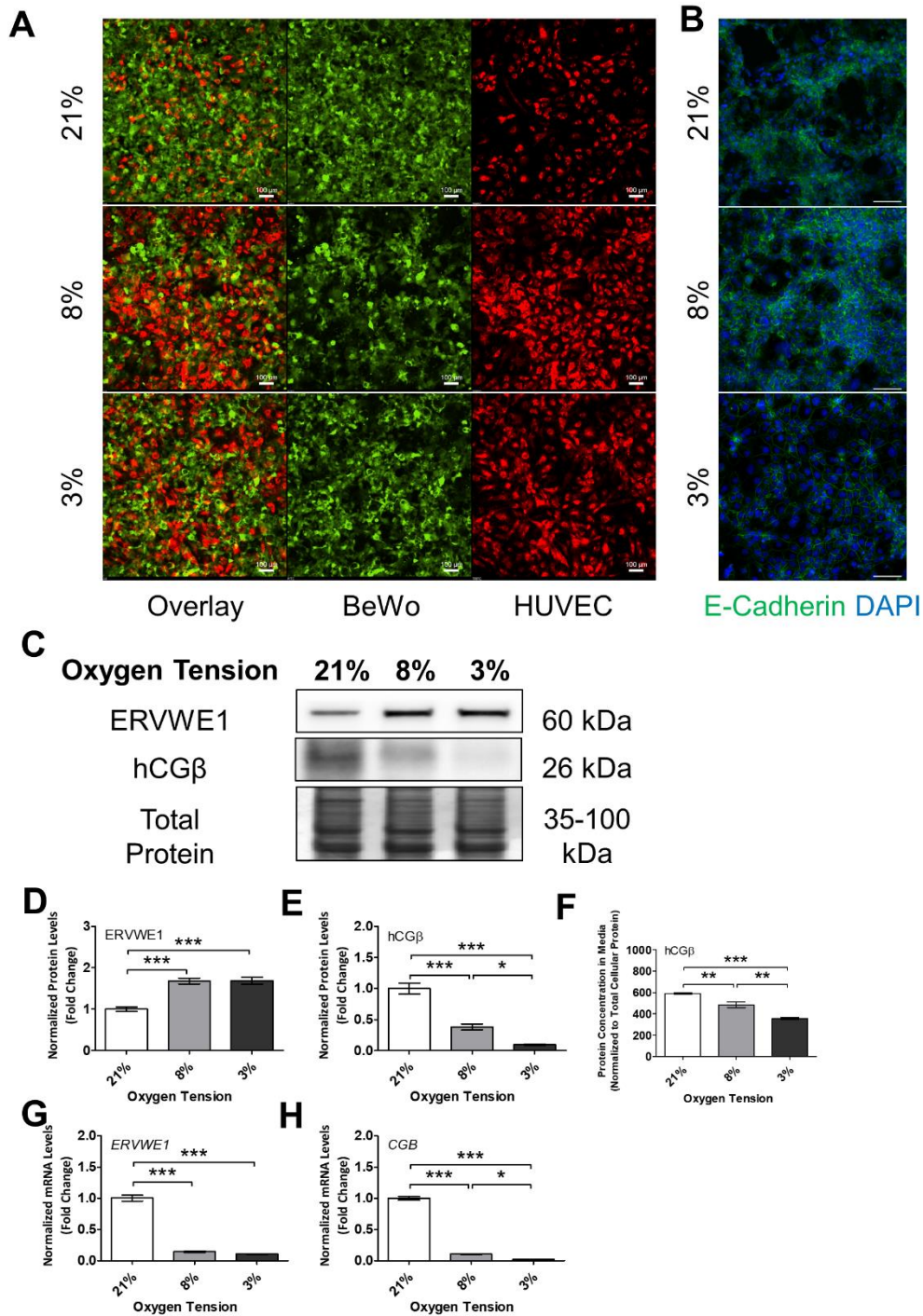
Figure 5. Low oxygen tension impacts morphology and expression of various markers of syncytial fusion. (**A**) Live cell imaging of EGFP-BeWo (green) and RFP-HUVECs (red). Images were taken at 10x magnification and scale bar indicates 100 µm. (**B**) Immunofluorescent staining of E-Cadherin and DAPI. Green fluorescence indicates E-Cadherin staining and blue fluorescence indicates DAPI

staining for cell nuclei. Images were taken at 20x magnification and scale bar indicates 100 µm. (**C**) Protein levels of ERVWE1 and hCGβ as determined by Western blot. Densitometric quantification of (**D**) ERVWE1 and (**E**) hCGβ relative protein expression based on band intensity. Full, raw blots may be found in **Supplemental Figure S1**. (**F**) Secreted protein levels of hCGβ, as determined by ELISA. All arbitrary values were expressed as means normalized to total intracellular protein ± SEM. mRNA levels of (**G**) *ERVWE1* and (**H**) *CGB*, as determined by RT-qPCR. All arbitrary values were expressed as means normalized to the geometric mean of housekeeping genes ± SEM. Significant differences between means indicated by *, $p < 0.05$, **, $p < 0.01$, or ***, $p < 0.001$.
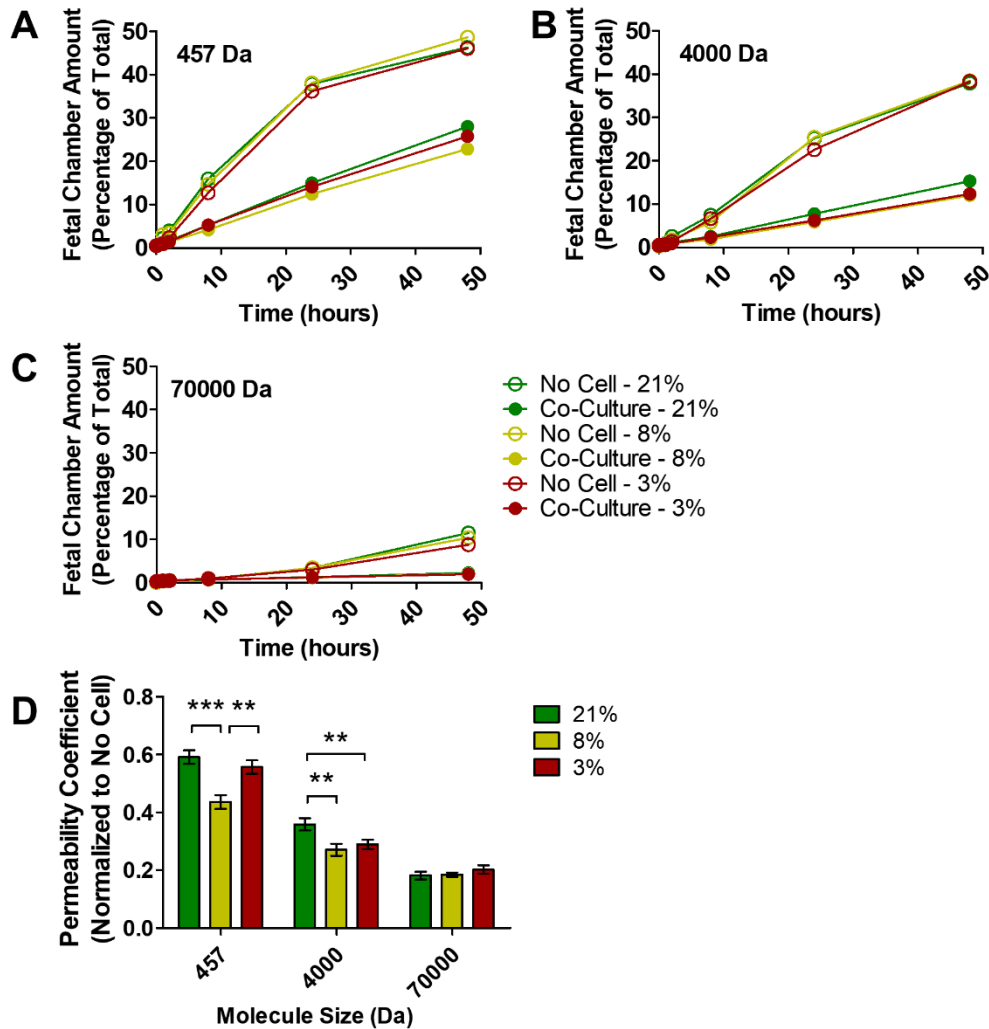
Figure 6. Permeability of *in vitro* placental barrier to various molecules under 21%, 8%, and 3% oxygen levels. Percentage of fluorescent intensity measured in fetal chamber normalized to total fluorescent intensity in both maternal and fetal chambers in the No Cell and Co-Culture groups cultured under 21%, 8%, and 3% oxygen levels for (**A**) 457 Da Lucifer Yellow molecules, (**B**) 4,000 Da fluorescein-dextran molecules or (**C**) 70,000 Da fluorescein-dextran molecules. (**D**) Apparent permeability coefficients of 457, 4,000, and 70,000 Da molecules in the Co-Culture group under 21%, 8%, and 3% oxygen levels at 48 hours normalized to the No Cell control group. Significant differences between treatment groups determined by two-way ANOVA; n ≥ 4. Significant differences between means indicated by **, $p<0.01$ or ***, $p<0.001$.

Tables

Table 1. Forward and reverse sequences for the primers used for RT-qPCR.

Gene	Forward	Reverse	GenBank
18S (RNA18S5)	CACGCCAGTACA AGATCCCA	AAGTGACGCAGC CCTCTATG	NR_00328 6.2
ACTB	TTACAGGAAGTC CCTTGCCATC	GCAATGCTATCA CCTCCCCTG	NM_0011 01.5
GAPDH	TCACCATCTTCC AGGAGCGA	ATGACGAACATG GGGGCATC	NM_0013 57943.1
HIF1A	CAGCAACGACAC AGAAACTGA	TTGGGTGAGGGG AGCATTAC	AF208487 .1
PLGF	ACCCTCAGGAAT TCAGTGCCTTCA	GGCCACGTGTCT TGCTTCTTTCAA	X54936.1
ERVWE1	GTTAATGACATC AAAGGCACCC	CCCCATCTCAAC AGGAAAACC	NM_0145 90
CGB	ACCCCTTGACCT GTGAT	CTTTATTGTGGG AGGATCGG	J00117.1

Supplementary Figures

A

HIF1α Whole Blot

B

ERVWE-1 Whole Blot

C

hCG Whole Blot
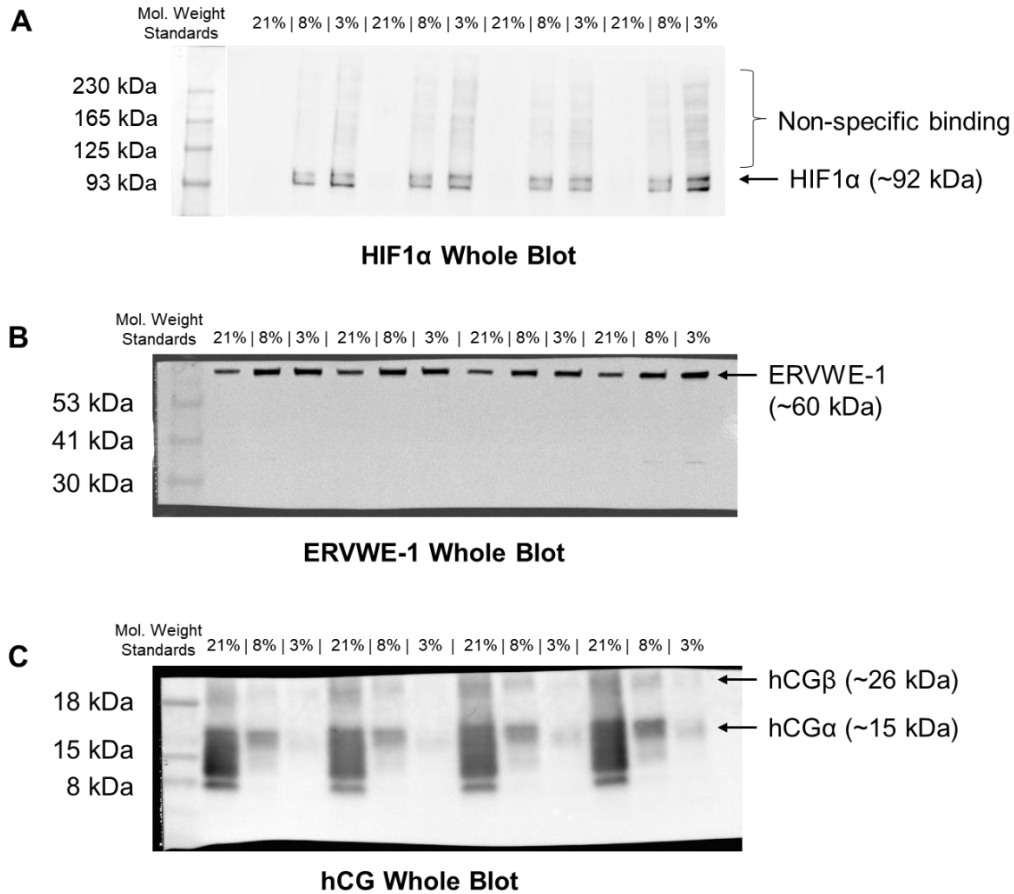
Supplemental Figure S1. Full, raw blots for Western blots of **(A)** HIF1α, **(B)** ERVWE1 and **(C)** hCGβ protein overlaid with ladder channel. A single gel was run and protein transferred onto a PVDF membrane. Membrane was then cut at around 75 kDa and 25 kDa to be used for immunoblotting for the three protein targets. Antibody used for hCG detected both α and β subunits, but only the β subunit was selected for analysis. Mol = molecular.

CHAPTER 5: CONCLUSIONS AND FUTURE DIRECTIONS

Summary and Impact

This doctoral thesis was inspired by the central hypothesis that the design of more anatomically- and physiologically-relevant *in vitro* platforms would enable improved investigations of placental biology and function compared to classical approaches. With the creation and comprehensive characterization of three, unique microphysiological models that displayed more robust, placental-specific performance compared to traditional models, we conclude that our objectives were met and the hypothesis was overall supported.

One of our primary intentions in creating these models was to reintegrate essential biological elements that had been missing in past studies, yet known to be critical for trophoblast cell behaviour and function. These included elements like extracellular matrices (ECM), low oxygen environments, co-culturing of multiple cell types, and dynamic, self-assembly of 3D cellular constructs. We first discovered that manipulating the thickness and stiffness of the ECM can promote the self-assembly of trophoblast cells into three-dimensional (3D) spheroidal aggregates that exhibit increased genetic and functional markers of syncytial fusion (**Figure 1A**)[1]. We further established a high-throughput platform to generate 3D trophoblast spheroids that expressed transcriptomic profiles redolent of the extravillous trophoblast phenotype (*e.g.,* angiogenesis, response to stimulus, immune response, wound healing, etc.), dynamically invaded away from its core

when embedded in ECM, and responded to various drugs and toxins relevant to pregnancy (*e.g.,* Δ^9-tetrahydrocannabinol) (**Figure 1B**) [2]. Lastly, we developed a trophoblast-endothelial cell co-culture model of the placental barrier which underwent syncytial fusion, exhibited size-specific barrier permeability to molecules of varying sizes (457-70,000 Da), and functioned under physiologically-low oxygen tensions (3-8%; **Figure 1C**).

Our models may also serve as valuable tools for researchers to address new questions in placental biology. For example, shear wave elastography revealed that preeclamptic women typically have stiffer placentae (3-71 kPa) than healthy, pregnant women (1.5-14 kPa) [3]. What are the underlying cellular mechanisms altered by this change in stiffness? Using our first model [1], future research may manipulate the ECM surface stiffness to match the diseased and healthy states *in vitro*, investigate the trophoblastic cellular pathways underlying the disease phenotype, and potentially develop targeted therapeutics to treat the disease. Our second model was used to test the effects of dexamethasone, lipopolysaccharide, and Δ^9-tetrahydrocannabinol, but future work could screen hundreds of compounds in parallel to profile the independent and synergistic pharmacological effectors of placental EVT invasion [2]. This is very clinically important as aberrant EVT invasion is implicated in intrauterine growth restriction, placenta accreta, and other pregnancy-related diseases, yet, there are very few placental drugs and treatments available [4,5]. Our model could enable the first large-scale preclinical drug screen for invasion-modulating compounds to improve placental disease outcomes. Our third

model of the placental barrier similarly holds promise as a tool for drug screening. More specifically, it may be used to investigate the transplacental passage of beneficial therapeutics to the developing fetus. Targeted drug delivery to the developing fetus is a severely understudied and tabooed topic, but there are many fetal disorders that require time-sensitive treatment during pregnancy, as they may lead to miscarriage (*e.g.,* aneuploidy) or significant early-life pathology (*e.g.,* cleft lip and palate, osteogenesis imperfecta) [6,7]. The success of fetal-targeting therapies will be contingent on the ability of the therapeutic to traverse the placental barrier, and our model can serve as a useful preclinical platform to optimize delivery.

Limitations and Next Steps

Our model development efforts, like all other areas of science, are not exempt from limitations and caveats. In this next section, I will discuss the major limitations of our work and how recent and future research efforts can be directed to overcome them.

Trophoblastic cell lines and the human trophoblast stem cell

The first limitation is the use of carcinoma or immortalized cell lines. A more extensive background on the strengths and weaknesses of cell lines may be found in Chapter 1, but the general limitation is that they possess phenotypes that may have deviated in some way from their non-cancerous predecessor. However, we employed several strategies to mitigate this caveat. Firstly, cells were only passaged a limited number of times within any given project (*e.g.,* maximum of 5-

10 passages) to minimize risk of introducing new, confounding mutations [8,9]. Secondly, only well-characterized placental cell lines (BeWo and HTR8/SVneo) were used such that we had a reasonable grasp of their strengths and weaknesses. Thirdly, for placental processes that had greater immediate relevance to cancer phenotypes (*e.g.,* invasion and migration), we used non-cancerous, immortalized HTR8/SVneo cells instead.

To offer a contrasting opinion, research may suggest that placental function can be validly studied using a placental carcinoma cell line given the close evolutionary link that was recently discovered between placentation and cancer [10]. The functional and biological parallels between placentae and tumours have been compared for several years, with notable similarities in invasion and vascular remodeling, epithelial-to-mesenchymal transition processes, host immune modulation, low oxygen functionality, and a preference for glycolytic metabolism [11-13]. Thus, the cancerization of a placental cell may not be as confounding as we once thought, although there is much more work required to verify this hypothesis.

Interestingly, human trophoblast stem cells were recently derived by Okae, et al. [14], offering a new alternative to model the trophoblast cell. By treating primary first-trimester placental cytotrophoblasts with epidermal growth factor, a Wnt activator, and inhibitors of TGFβ, ROCK/Rho kinase, and histone deacetylase, they could maintain the trophoblast cells in a stem-like state and induce differentiation into cytotrophoblasts, syncytiotrophoblasts, and extravillous trophoblasts. Their trophoblast stem cells further fulfilled the four trophoblast criteria established by

Lee, et al. [15] (protein expression of GATA3, KRT7, TFAP2C; HLA class I profile; hypomethylation of the ELF5 promoter; and expression of chromosome 19 microRNA cluster). While the anatomical location of trophoblast stem cells is unclear in the human placenta *in vivo*, they may still serve as a phenotypically-accurate and renewable source of cells for model development in the future.

Emulating the human placental ECM

A second limitation is the use of Matrigel and Geltrex, a mouse sarcoma-derived extracellular matrix cocktail, to represent the human placental ECM in Chapters 2 and 3. Matrigel and Geltrex consists of laminin (60%), collagen IV (30%), entactin (8%), and other proteins and growth factors (Corning). In comparison, early immunofluorescence experiments of the human placenta similarly revealed laminin, collagens, entactins, fibronectin, and proteoglycans [16]. Recent proteomic analysis of solubilized, decellularized placental ECM further revealed protein families (and peptide fractions) of laminin (0.44), collagen vi, xii, xiv, and xv (0.14), fibronectin (0.11), heparin sulfate proteoglycan (0.09), fibrinogen (0.09), and nidogen subunits (0.02), which would suggest that Matrigel and Geltrex may share some similarities with human placental ECM [17]. Strangely, analysis of placental ECM proteins from a second publication from the same lab reported protein families (and peptide fractions) of laminin (0.222), myosin (0.110), collagen (0.082), fibrinogen (0.075), fibronectin (0.068), tropomyosin (0.061), annexin (0.055), filamin (0.054), complement protein (0.041), and keratin (0.041), suggesting there could be very high sample-to-sample variability [18]. Thus, while

Matrigel and Geltrex possess some of the same ECM proteins as human placental ECM (*e.g.,* laminin, collagen, entactins), there may be differing proportions of these proteins in the native, placental ECM. Furthermore, we don't fully understand the discrepant interactions that may occur between human cells and mouse ECM proteins. While human-derived ECM alternatives are commercially-available, they are often cost-prohibitive. Advancing approaches to proportionately isolate ECM proteins from decellularized placentas that are consistent across samples will open valuable avenues for use in cell culture [19-21].

Inducing syncytial fusion in trophoblastic cell lines

The biochemical-induced fusion approach in BeWo trophoblastic cells has served to provide valuable insights on the trophoblast syncytial fusion process [22]. However, these *in vitro* syncytial fusion approaches remain low in efficiency, with only 15-40% of the population undergoing fusion at best as seen in our work (~20-25%) and others [23-26]. This is problematic as some speculate that the syncytiotrophoblast layer lining the chorionic villi may be entirely fused *in vivo* [4]. Furthermore, all reported syncytialization events *in vivo* post-establishment of the primitive syncytium occurs through cytotrophoblasts fusing into the syncytiotrophoblast layer, not through cytotrophoblasts into other cytotrophoblasts – although the depth of our understanding in these events remains shallow [27]. Nonetheless, no one to our knowledge has successfully induced anywhere near 100% fusion rates to date in trophoblastic cell lines *in vitro.*

In my doctoral work, we established a biochemical protocol to induce syncytial fusion using epidermal growth factor and forskolin, which was further improved through exposure to varying ECM surface thicknesses and physiologically-low oxygen [1]. In fact, we demonstrated that culturing BeWo cells on a thick surface of ECM (250 µm) alone was sufficient to induce high levels of syncytial fusion within trophoblast aggregates [1]. This is noteworthy as BeWo cells have traditionally depended on forskolin and other biochemical means for fusion induction. Our biophysical approach was further supported by a recent study using micropatterned, adhesive surfaces to promote syncytial fusion [28]. Miura, et al. [29] also demonstrated that fluid shear stress alone in their microfluidic placenta-on-a-chip model could induce syncytial fusion and microvilli formation in BeWo cells. McConkey, et al. [30] revealed that 3D culture on Cytodex-3 beads in a rotating wall vessel bioreactor could even drive the non-fusogenic JEG-3 trophoblastic cell line to undergo syncytial fusion, providing shocking but powerful evidence for the great potential of biophysical manipulation. Other efforts have been directed towards elucidating the transcriptomic, epigenomic, and proteomic signatures underlying syncytial fusion in fusogenic trophoblastic cell lines (*e.g.,* BeWo) compared to non-fusogenic trophoblastic cell lines (*e.g.,* JEG-3) [22,31-35]. For example, genetically knocking-out SIK1 via CRISPR-Cas9 was demonstrated to abolish syncytial fusion in BeWo cells, thus one might imagine that there are genes that could be conversely knocked-in or enhanced to achieve an *in vivo*-like, fully syncytialized layer [31].

Progress is being made, but these limitations in fusion must be resolved in order for fusogenic trophoblast cell lines to remain relevant in the future.

Validating in vitro models with human in vivo data

Lastly, the scarcity of causal data from live, *in vivo* human placenta, especially from the second and third trimester, is a major hindrance in the proper validation of experimental *in vitro* models. This caveat is particularly challenging to overcome, as the limited mechanistic scope of *in vivo* human models are part of the rationale justifying the development of *in vitro* models – yet, *in vitro* models cannot be definitively validated unless *in vivo* models provide sufficient data to confirm the emulations of biological processes. Due to ethical restrictions, there are many processes that simply cannot be probed in human populations (*e.g.*, temporal, cellular-level changes in syncytial fusion events at the placental barrier over the course of pregnancy.)

While this currently leaves scientists in a bit of a chicken-or-egg stand-off, advances in real-time imaging and sampling approaches will surely resolve this limitation in the future. Farhadi, et al. [36] elegantly designed "acoustic reporter genes" that would induce the proportionate formation of non-toxic, nano-sized gas vesicles inside transfected cells and animals as the specifically paired gene-of-interest was expressed. The more highly a gene was expressed, the greater number of gas vesicles would form inside the cell. These intracellular gas vesicles could then be quantitated via ultrasound imaging, enabling non-invasive, live tracking of gene expression. This method has yet to be applied to placental research. Friesen-

Waldner, et al. [37] demonstrated incredible innovations with magnetic resonance imaging technology for study of *in vivo* placental metabolism. By using a variation of the technique known as hyperpolarized [1-^{13}C] pyruvate MRI, they observed fetoplacental metabolism and transport of pyruvate in pregnant guinea pigs [37]. These advancements in non-invasive monitoring provide great promise for accurate and safe data collection on the mechanisms underlying placentation throughout human pregnancy.

Design and Fabrication of a Placenta-on-a-Chip Platform

In addition to the three models presented in this thesis, we also engaged in the collaborative development of a placenta-on-a-chip device, which currently remains in progress. I will discuss in this next section some of our efforts to date and the outstanding challenges (full methods may be found in **Appendix 2**).

Device design and fabrication

We custom designed 3D-printed molds of the maternal and fetal channels for imprinting polydimethylsiloxane (PDMS; **Figure 2A, B**). Following from our placental barrier model, the apical "maternal" channel was intended to culture placental trophoblast cells and a basal "fetal" channel for vascular endothelial cells. There were two major channel design prototypes: (1) circular, maternal channel and a straight, narrow fetal channel, which better represented the spacious, maternal intervillous space and narrow fetal vasculature, respectively (**Figure 2A**), and (2) straight maternal and fetal channels, which offered greater simplicity and resembled

the majority of past prototypes [38-40] (**Figure 2B**). A polyester membrane (0.4 μm

pore) was used as the surface for cell adhesion and separated the two channels.

Establishing proper bonding between all the materials comprising the

placenta-on-a-chip device was crucial for proper culture and function. There were

two major methods that we tested for bonding: (1) Kapton tape adhesive (**Figure

2C**) and (2) Plasma-activated bonding using a BD-20AC Laboratory Corona

Treater (**Figure 2D**). Kapton tape is a highly stable, polyimide-based, double-sided

adhesive that may be used to bond many types of materials. Plasma-activated

bonding involves bombarding the surface of interest with oxygen ions, which

"activates" the surface. Surfaces may then be pressed together, forming a covalent

bond. After ultraviolet light sterilization, fibronectin (0.1 mg/mL) was infused into

device channels and incubated at 37°C for >4 hours to promote cell adherence.

Fluorescently-tagged BeWo cells and HUVECs were then seeded into the maternal

and fetal channels respectively, given time to adhere to the surface, and connected

to a syringe pump flow system at 100 μL/hr (see **Figure 7** in Chapter 1).

Preliminary findings

While a more sophisticated circular maternal channel was described above

(**Figure 2A**), current experiments were conducted using the straight maternal and

fetal channels for the sake of simplicity (**Figure 2B)**. Our initial observations were

that Kapton tape was very easy to handle and effective in sealing the channels to

prevent leakage, but it was challenging to accurately cut the Kapton tape to

precisely fit the channel (even when using a machine cutter). As a result, alignment

was imperfect and the Kapton tape created an unintended para-channel around the main channels, which caused uneven seeding, as cells could leak into the para-channel (**Figure 3**). BeWo and HUVEC cells seeded and maintained viability for the first several days, but the BeWo channel declined in viability by day 7 (**Figure 3**). Furthermore, confluence was uneven, which is problematic for transport studies.

In attempts to incorporate a bonding technique that allowed for greater channel boundary precision, we explored the use of plasma-activation to bond our PDMS slabs with the membrane. Similar to Kapton tape, plasma-activated surfaces bond together very effectively without any channel leakage. A major advantage was that the PDMS is able to bond directly to the polycarbonate membrane, enabling precise channel boundaries compared to the Kapton tape method (**Figure 4**). Seeding was more even and the cells experienced better confluence at day 1 compared to when the device was bonded with Kapton tape. However, viability again declined by day 7, especially for the BeWo cells.

We suspected that this loss of viability may be due in part to uncontrolled, shear stress experienced by the cells in the channel from the syringe pump. To overcome this, we tested the commercially-available, OrganoPlate 3-lane (Mimetas) which similarly has two cell-culturing straight channels to represent maternal and fetal channels, but also contains a third, middle channel that may be filled with Geltrex (10 µg/mL) to separate the two cell populations (instead of a polyester membrane). The OrganoPlate further uses "gravity flow" for media delivery, which involves the use of a rocker to circulate media back and forth

between two reservoirs. The maternal and fetal channels were then either left unseeded as a control, seeded with green fluorescent protein-transfected BeWo (GFP-BeWo) cells alone, or seeded with GFP-BeWo cells and red fluorescent protein-transfected HUVECs (**Figure 5**). After seeding, transport experiments were run by infusing the maternal channel with 70,000 Da fluorescein-dextran molecules (10 µM) and observing transport across to the fetal channel via fluorescent microscopy for up to 24 hours. When no cells were seeded in the channels, a substantial amount of 70,000 Da molecules permeated the ECM barrier into the fetal channel (**Figure 5**). However, substantially fewer molecules crossed when BeWo cells were present, and virtually no molecules crossed into the fetal channel when both cell types were present (**Figure 5**). These findings collectively suggest that the cells may form a successful barrier within the OrganoPlate to prevent the passage of large molecules, similar to what we observed in our transwell placental barrier model in Chapter 4.

In summary, we optimized the in-house device fabrication of a two-channel, placenta-on-a-chip microfluidic device and made some progress in co-culturing placental trophoblast and vascular endothelial cells. However, the technical challenges with long-term confluent growth and viability must be overcome in order to achieve utility for placental barrier modelling. We also established a trophoblast-endothelial co-culture within the Mimetas OrganoPlate, and demonstrated strong inhibition of 70,000 Da fluorescein-dextran transport. The OrganoPlate may be a useful microfluidic platform to model the placental barrier,

but must undergo further transport testing with various molecules and for longer timepoints to validate its utility. Furthermore, microfluidic device construction and usage is not a common skillset among biologists and clinicians, thus in-house fabrication and handling remains a large barrier-to-entry unless collaborations with engineering partners are possible. In the meantime, the three models presented in this thesis may serve as accessible, useful, and well-characterized tools for placental researchers.

Pioneering the Next Generation of Placental Models

In this final section, I will discuss the implications of our findings in the context of other current placental model development efforts, and predict the outlook of the next generation of models. 3D spheroid and organoid cultures have been demonstrated by us and others to be excellent at enabling placental cells to self-assemble and differentiate into complex tissues on dynamic, biological surfaces [1,2,41-43]. Yet, current 3D culture platforms do not enable dynamic media flow or vascularization, and are limited in the customizability of the platform (*e.g.,* integration of biosensors, channels, read-outs, etc.) [44]. Without vascularization, there is an upper limit in the size of the organoid before the core undergoes necrosis [45]. On the other hand, organ-on-a-chip microfluidic devices possess the advantages of having versatile control over design of platform features (*e.g.,* size of channels, shape of culture area), flow and vascularization, and capacity for built-in readouts (*e.g.,* biosensors for glucose, oxygen, etc.) [46]. Yet, organ-on-chips remain restricted

mostly to 2D growth on synthetic materials, basic cell-to-cell and cell-to-ECM interactions, relatively low differentiation potential, and minimal demonstrations of cell-driven organization into complex tissues – which are important features in advancing into the next stages of clinical translatability [44,47,48]. One potential solution to overcoming the current caveats of each independent system is through the integration into a synergized system that some are calling the "organoid-on-a-chip" [44,48].

Placental barrier organoid-on-a-chip

To date, the "*placental* organoid-on-a-chip" remains a figment of scientific imagination. To achieve this goal would involve the incorporation of 3D organoid culture of placental trophoblast cells (with 3D growth conditions driving the self-assembly of the stem-like, cytotrophoblast population into a more differentiated, functional population with anatomical fidelity) and microfluidic approaches (that enable effective vascularization and perfusion of the entire system.) The meaningful establishment of the placental organoid-on-a-chip must be validated through the use of transcriptomic or proteomic profiling, alongside demonstrations of biological functions native to the differentiated cellular population(s) of interest.

A placental phenomena that the placental organoid-on-a-chip approach could help study is the dynamic maintenance of the syncytiotrophoblast layer via apical syncytial fusion of cytotrophoblast cells *in vivo* [49]. This is a key biological function of the placental barrier, but has not been simulated by any of the current placenta-on-a-chip prototypes [38-40,50-52]. The closest attempt to model this was

through the incorporation of a bioprinted hydrogel layer with interspersed cytotrophoblasts in between monolayers of cytotrophoblasts and endothelial cells in a 3D-bioprinted model [18,53]. Yet, the authors did not develop an apical syncytiotrophoblast layer (only a monolayer of cytotrophoblast), nor were there any functional contributions demonstrated from the middle layer of interspersed cytotrophoblast cells. By combining our past work, future studies could be directed to advance this into an organoid-on-a-chip of the placental barrier.

Firstly, stem-like cytotrophoblast cells may be seeded onto an ECM-coated basal side of transwell insert (with the ECM surface coating at the correct thickness or stiffness to induce syncytial fusion as we have previously demonstrated [1]), resulting in self-assembly into syncytiotrophoblast organoids. Mononuclear cytotrophoblast cells interspersed within a hydrogel could then be 3D-bioprinted onto the apical side of the transwell insert, immediately adjacent to the syncytiotrophoblast organoid layer. Transfection of different fluorescent proteins colours prior to seeding could enable the identification of the separate cytotrophoblast populations. To study the specific fusion event of the underlying cytotrophoblasts into the syncytiotrophoblast organoid above, we could track the mixing of fluorescent colours [23]. Once the hydrogel cures, vascular endothelial cells could lastly be seeded apical to the cytotrophoblast layer and self-assembled into tubes [54], or bioprinted as functional, hollow tubes to form the fetal vasculature [55,56]. The advantage of 3D-bioprinting the blood vessels is that we will be able to recreate actual blood vessel architecture, functionality, and manipulate the vessel size,

length, and shape [56]. Nutrients, drugs, or toxins may be introduced into the stagnant, maternal chamber facing the syncytiotrophoblast organoid layer, and their transport could be observed through the multiple layers into the flowing, fetal channels.

While this is undoubtedly an ambitious design, all the required techniques have been separately reported as described above. Its synergy into a placental barrier organoid-on-a-chip would enable highly intricate studies of transport and permeability through microvilli-laden syncytiotrophoblasts [29,39], the factors that may stimulate fusion of mononucleated cytotrophoblasts into the syncytiotrophoblast, and the dynamic flow of media through the fetal vasculature.

Extravillous trophoblast organoid-on-a-chip

Another placental phenomenon that has historically been difficult to study *in vitro* is the extravillous trophoblast remodeling of uterine spiral arteries. The best example to date is a 3D-bioprinted model of a central hollow tube (representing a spiral artery) using gelatin methacrylate infused with placental ECM proteins [17,57]. In a recent paper, the authors bioprinted a human umbilical vein endothelial cell (HUVEC) layer adjacent to the lumen of the hollow tube with HTR8 EVT cells interspersed in a second hydrogel layer surrounding the HUVEC layer [58]. They further demonstrated invasion and interdigitation of the EVTs into the HUVEC layer, and the induction of apoptosis of the HUVECs [58]. This was an important research milestone as trophoblast-directed replacement of the vascular endothelium is a critical step in the endovascular EVT invasion pathway [59]. However, this approach has the potential of additionally modelling the earlier developmental

stage, where EVTs migrate away from the cell column and locate the spiral arteries. This could be accomplished through the integration of organoids or spheroids, as we and others have previously demonstrated [2,42,43].

Firstly, the trophoblast organoid could be formed in ultra low-attachment plates and transferred onto the surface upon which the endothelial cell-lined hollow tube (which represents the spiral artery) is 3D-bioprinted. Perfusion of the endothelial cell-lined hollow tube with fresh media could create an oxygen and nutrient gradient between the organoid and the tube. This will theoretically serve to drive the invasion and migration of EVTs away from the solid core organoid towards the tube, replacing the endothelial cells, and remodeling the tube to expand its diameter. Furthermore, scalable multi-axial microfluidic extrusion nozzle techniques, as developed by Attalla, et al. [60], may enable bi- and tri-cell-layered bioprinting of hollow channels (*e.g.,* fibroblast, smooth muscle, and vascular endothelial cells). This could enable the fabrication of complex, multicellular blood vessels capable of dilating, constricting, and importantly, undergoing remodeling [55]. Interesting endpoint measurements from this model could include changes in media flow from the hollow tube as spiral artery remodeling progresses, elucidations of the mechanisms by which trophoblast cells replace the endothelial cells, changes in transcriptomic or proteomic profiles of the EVTs following endothelial replacement, and the formation of trophoblast plugs in the lumen. This could also enable us to distinguish our investigations between the two extravillous trophoblast lineages *in vitro*: (i) endovascular extravillous trophoblasts as described

above and (ii) interstitial extravillous trophoblasts, which are responsible for inducing vascular smooth muscle cell apoptosis and degrading the arterial media of the spiral arteries (provided these additional factors are incorporated into the bioprinted model) [61]. This level of dynamism is required of *in vitro* models we evolve in our abilities in scientific experimentation and discovery.

Ethical Implications

Ethical concerns had recently surfaced surrounding the development of brain organoids, with the argument that neural mini-tissues have the potential of progressing into human sentience or consciousness [62,63]. The ethical quandaries became even more apparent with the successful transplantation of human brain organoids into adult mice brains, resulting in hybrid species neural integration, vascularization, and graft-to-host synaptic connectivity [64]. We imagine similar ethical concerns may be raised against placental trophoblast organoids given the placenta's intimate roles in embryonic and fetal development and reproduction. Could placental organoids become so efficient and functional that they entirely replace the need for human reproduction in the future? Could placental organoids derive embryonic tissues *de novo* and be used to create new "life"? Could placental organoids engraft fetuses created outside of the body, or even enable human men to experience pregnancy? These questions seem unrealistic and impossible at the moment, yet no one would have expected the successful creation of the extrauterine system, or "artificial womb", that could support fetal development of premature

lambs outside of the body [65]. The authors even speculated during an interview that the first-in-human trials could begin around 2020 [66].

It is important to emphasize that while controversial applications of science are possible, the future does not have to be dystopian. The artificial womb has the potential to rescue premature births, which is a major global health issue [65]. In the same way, placental microphysiological models such as organoid will undoubtedly find ethically-sound applications in drug testing that will aid in establishment of safety and efficacy profiles of new medicines. In fact, the development of cellular models with greater predictiveness may even help reduce the volume of animal testing and reduce the risk on human subjects at the clinical stages [67]. All-in-all, researchers must remain at the forefront of ethical discussions to provide society with accurate information that is tempered to the scope, limitations, and potential of the science.

Conclusion

The complexity and elegance of human placental function is one of the greatest biological discoveries to emerge from modern science. Substantial progress has been made since its early classification as the accompanying "after-birth" into our current knowledge of its multifaceted roles in early development and programming of later-life health and disease [68,69]. We contributed to this field by establishing and characterizing three, unique microphysiological models of the human placenta that demonstrated improved anatomical- and physiological-

relevance compared to traditional systems. Moreover, our models provide useful tools for other scientists to use and conduct research with, innovative approaches to further the development of preclinical placental models, and novel evidence that deepens our understanding and appreciation of this sophisticated organ.

References

1   Wong, M. K. *et al.* Extracellular matrix surface regulates self-assembly of three-dimensional placental trophoblast spheroids. *PloS one* **13**, e0199632, doi:10.1371/journal.pone.0199632 (2018).

2   Wong, M. K., Wahed, M., Shawky, S. A., Dvorkin-Gheva, A. & Raha, S. Transcriptomic and functional analyses of 3D placental extravillous trophoblast spheroids. *Scientific reports* **9**, 12607, doi:10.1038/s41598-019-48816-8 (2019).

3   Kilic, F. *et al.* Shear wave elastography of placenta: in vivo quantitation of placental elasticity in preeclampsia. *Diagn Interv Radiol* **21**, 202-207, doi:10.5152/dir.2014.14338 (2015).

4   Huppertz, B. Placental origins of preeclampsia: challenging the current hypothesis. *Hypertension* **51**, 970-975, doi:10.1161/HYPERTENSIONAHA.107.107607 (2008).

5   Sibley, C. P. Treating the dysfunctional placenta. *The Journal of endocrinology* **234**, R81-R97, doi:10.1530/JOE-17-0185 (2017).

6   Zhang, J. *et al.* Non-invasive prenatal sequencing for multiple Mendelian monogenic disorders using circulating cell-free fetal DNA. *Nat Med* **25**, 439-447, doi:10.1038/s41591-018-0334-x (2019).

7   Kohli, S. S. & Kohli, V. S. A comprehensive review of the genetic basis of cleft lip and palate. *J Oral Maxillofac Pathol* **16**, 64-72, doi:10.4103/0973-029X.92976 (2012).

8   Kim, M. *et al.* Passage-dependent accumulation of somatic mutations in mesenchymal stromal cells during in vitro culture revealed by whole genome sequencing. *Scientific reports* **7**, 14508, doi:10.1038/s41598-017-15155-5 (2017).

9   Hughes, P., Marshall, D., Reid, Y., Parkes, H. & Gelber, C. The costs of using unauthenticated, over-passaged cell lines: how much more data do we need? *Biotechniques* **43**, 575, 577-578, 581-572 passim, doi:10.2144/000112598 (2007).

10   Kshitiz *et al.* Evolution of placental invasion and cancer metastasis are causally linked. *Nature ecology & evolution*, doi:10.1038/s41559-019-1046-4 (2019).

11   Costanzo, V., Bardelli, A., Siena, S. & Abrignani, S. Exploring the links between cancer and placenta development. *Open Biol* **8**, doi:10.1098/rsob.180081 (2018).

12   Beaman, K. D. *et al.* Pregnancy is a model for tumors, not transplantation. *Am J Reprod Immunol* **76**, 3-7, doi:10.1111/aji.12524 (2016).

13   Burton, G. J., Jauniaux, E. & Murray, A. J. Oxygen and placental development; parallels and differences with tumour biology. *Placenta* **56**, 14-18, doi:10.1016/j.placenta.2017.01.130 (2017).

14   Okae, H. *et al.* Derivation of Human Trophoblast Stem Cells. *Cell Stem Cell* **22**, 50-63 e56, doi:10.1016/j.stem.2017.11.004 (2018).

15   Lee, C. Q. *et al.* What Is Trophoblast? A Combination of Criteria Define Human First-Trimester Trophoblast. *Stem Cell Reports* **6**, 257-272, doi:10.1016/j.stemcr.2016.01.006 (2016).

16   Kisalus, L. L., Herr, J. C. & Little, C. D. Immunolocalization of extracellular matrix proteins and collagen synthesis in first-trimester human decidua. *The Anatomical Record* **218**, 402-415 (1987).

17   Kuo, C. Y. *et al.* Placental basement membrane proteins are required for effective cytotrophoblast invasion in a three-dimensional bioprinted placenta model. *J Biomed Mater Res A* **106**, 1476-1487, doi:10.1002/jbm.a.36350 (2018).

18   Arumugasaamy, N., Gudelsky, A., Hurley-Novatny, A., Kim, P. C. W. & Fisher, J. P. Model Placental Barrier Phenotypic Response to Fluoxetine and Sertraline: A Comparative Study. *Adv Healthc Mater* **8**, e1900476, doi:10.1002/adhm.201900476 (2019).

19   Kakabadze, Z. *et al.* Decellularized human placenta supports hepatic tissue and allows rescue in acute liver failure. *Hepatology* **67**, 1956-1969, doi:10.1002/hep.29713 (2018).

20   Choi, J. S., Kim, J. D., Yoon, H. S. & Cho, Y. W. Full-thickness skin wound healing using human placenta-derived extracellular matrix containing bioactive molecules. *Tissue Eng Part A* **19**, 329-339, doi:10.1089/ten.TEA.2011.0738 (2013).

21   Flynn, L., Semple, J. L. & Woodhouse, K. A. Decellularized placental matrices for adipose tissue engineering. *J Biomed Mater Res A* **79**, 359-369, doi:10.1002/jbm.a.30762 (2006).

22   Orendi, K., Gauster, M., Moser, G., Meiri, H. & Huppertz, B. The choriocarcinoma cell line BeWo: syncytial fusion and expression of syncytium-specific proteins. *Reproduction* **140**, 759-766, doi:10.1530/REP-10-0221 (2010).

23   Kudo, Y. *et al.* Quantifying the syncytialisation of human placental trophoblast BeWo cells grown in vitro. *Biochimica et Biophysica Acta (BBA) - Molecular Cell Research* **1640**, 25-31, doi:10.1016/s0167-4889(03)00004-1 (2003).

24   Wang, R. *et al.* Live cell imaging of in vitro human trophoblast syncytialization. *Biology of reproduction* **90**, 117, doi:10.1095/biolreprod.113.114892 (2014).

25   Poidatz, D. *et al.* Trophoblast syncytialisation necessitates mitochondrial function through estrogen-related receptor-gamma activation. *Mol Hum Reprod* **21**, 206-216, doi:10.1093/molehr/gau102 (2015).

26   Coutifaris, C. *et al.* E-cadherin expression during the differentiation of human trophoblasts. *Development* **113**, 767-777 (1991).

27   Gerbaud, P. & Pidoux, G. Review: An overview of molecular events occurring in human trophoblast fusion. *Placenta* **36 Suppl 1**, S35-42, doi:10.1016/j.placenta.2014.12.015 (2015).

28   Ma, Z. *et al.* Biomimetic micropatterned adhesive surfaces to mechanobiologically regulate placental trophoblast fusion. *ACS Appl Mater Interfaces*, doi:10.1021/acsami.9b19906 (2019).

29   Miura, S., Sato, K., Kato-Negishi, M., Teshima, T. & Takeuchi, S. Fluid shear triggers microvilli formation via mechanosensitive activation of TRPV6. *Nat Commun* **6**, 8871, doi:10.1038/ncomms9871 (2015).

30   McConkey, C. A. *et al.* A three-dimensional culture system recapitulates placental syncytiotrophoblast development and microbial resistance. *Sci Adv* **2**, e1501462, doi:10.1126/sciadv.1501462 (2016).

31   Msheik, H. *et al.* Transcriptomic Profiling of Trophoblast Fusion Using BeWo and JEG-3 Cell Lines. *Molecular human reproduction*, gaz061, doi:10.1093/molehr/gaz061 (2019).

32   Zheng, R. *et al.* Deep RNA sequencing analysis of syncytialization-related genes during BeWo cell fusion. *Reproduction*, doi:10.1530/REP-16-0343 (2016).

33   Shankar, K. *et al.* Transcriptomic and epigenomic landscapes during cell fusion in BeWo trophoblast cells. *Placenta* **36**, 1342-1351, doi:10.1016/j.placenta.2015.10.010 (2015).

34   Nampoothiri, L. P., Neelima, P. S. & Rao, A. J. Proteomic profiling of forskolin-induced differentiated BeWo cells: an in-vitro model of cytotrophoblast differentiation. *Reprod Biomed Online* **14**, 477-487 (2007).

35   Al-Nasiry, S., Spitz, B., Hanssens, M., Luyten, C. & Pijnenborg, R. Differential effects of inducers of syncytialization and apoptosis on BeWo and JEG-3 choriocarcinoma cells. *Hum Reprod* **21**, 193-201, doi:10.1093/humrep/dei272 (2006).

36   Farhadi, A., Ho, G. H., Sawyer, D. P., Bourdeau, R. W. & Shapiro, M. G. Ultrasound imaging of gene expression in mammalian cells. *Science* **365**, 1469-1475, doi:10.1126/science.aax4804 (2019).

37   Friesen-Waldner, L. J. *et al.* Hyperpolarized [1-(13) C]pyruvate MRI for noninvasive examination of placental metabolism and nutrient transport: A feasibility study in pregnant guinea pigs. *J Magn Reson Imaging* **43**, 750-755, doi:10.1002/jmri.25009 (2016).

38   Blundell, C. *et al.* Placental Drug Transport-on-a-Chip: A Microengineered In Vitro Model of Transporter-Mediated Drug Efflux in the Human Placental Barrier. *Adv Healthc Mater* **7**, doi:10.1002/adhm.201700786 (2018).

39   Blundell, C. *et al.* A microphysiological model of the human placental barrier. *Lab Chip*, doi:10.1039/c6lc00259e (2016).

40   Lee, J. S. *et al.* Placenta-on-a-chip: a novel platform to study the biology of the human placenta. *The Journal of Maternal-Fetal & Neonatal Medicine*, 1-9, doi:10.3109/14767058.2015.1038518 (2015).

41   Nandi, P., Lim, H., Torres-Garcia, E. J. & Lala, P. K. Human trophoblast stem cell self-renewal and differentiation: Role of decorin. *Scientific reports* **8**, 8977, doi:10.1038/s41598-018-27119-4 (2018).

42   Haider, S. *et al.* Self-Renewing Trophoblast Organoids Recapitulate the Developmental Program of the Early Human Placenta. *Stem Cell Reports* **11**, 537-551, doi:10.1016/j.stemcr.2018.07.004 (2018).

43   Turco, M. Y. *et al.* Trophoblast organoids as a model for maternal-fetal interactions during human placentation. *Nature* **564**, 263-267, doi:10.1038/s41586-018-0753-3 (2018).

44   Takebe, T., Zhang, B. & Radisic, M. Synergistic Engineering: Organoids Meet Organs-on-a-Chip. *Cell Stem Cell* **21**, 297-300, doi:10.1016/j.stem.2017.08.016 (2017).

45   Hirschhaeuser, F. *et al.* Multicellular tumor spheroids: an underestimated tool is catching up again. *J Biotechnol* **148**, 3-15, doi:10.1016/j.jbiotec.2010.01.012 (2010).

46   Liu, J., Mosavati, B., Oleinikov, A. V. & Du, E. Biosensors for Detection of Human Placental Pathologies: A Review of Emerging Technologies and Current Trends. *Transl Res* **213**, 23-49, doi:10.1016/j.trsl.2019.05.002 (2019).

47   Zhang, B., Korolj, A., Lai, B. F. L. & Radisic, M. Advances in organ-on-a-chip engineering. *Nature Reviews Materials* **3**, 257-278 (2018).

48   Skardal, A., Shupe, T. & Atala, A. Organoid-on-a-chip and body-on-a-chip systems for drug screening and disease modeling. *Drug Discov Today*, doi:10.1016/j.drudis.2016.07.003 (2016).

49   Huppertz, B. & Gauster, M. in *Cell Fusions*   Ch. Chapter 9, 203-217 (2011).

50   Yin, F. *et al.* A 3D human placenta-on-a-chip model to probe nanoparticle exposure at the placental barrier. *Toxicology in vitro : an international journal published in association with BIBRA* **54**, 105-113, doi:10.1016/j.tiv.2018.08.014 (2019).

51   Pemathilaka, R. L., Caplin, J. D., Aykar, S. S., Montazami, R. & Hashemi, N. N. Placenta-on-a-Chip: In Vitro Study of Caffeine Transport across Placental Barrier Using Liquid Chromatography Mass Spectrometry. *Global Challenges* **3**, doi:10.1002/gch2.201800112 (2019).

52   Pemathilaka, R. L., Reynolds, D. E. & Hashemi, N. N. Drug transport across the human placenta: review of placenta-on-a-chip and previous approaches. *Interface Focus* **9**, 20190031, doi:10.1098/rsfs.2019.0031 (2019).

53   Arumugasaamy, N. *et al.* Biomimetic Placenta-Fetus Model Demonstrating Maternal-Fetal Transmission and Fetal Neural Toxicity of Zika Virus. *Ann Biomed Eng*, doi:10.1007/s10439-018-2090-y (2018).

54   Lee, H. & Kang, K. T. Advanced tube formation assay using human endothelial colony forming cells for in vitro evaluation of angiogenesis. *Korean J Physiol Pharmacol* **22**, 705-712, doi:10.4196/kjpp.2018.22.6.705 (2018).

55   Andrique, L. *et al.* A model of guided cell self-organization for rapid and spontaneous formation of functional vessels. *Sci Adv* **5**, eaau6562, doi:10.1126/sciadv.aau6562 (2019).

56   Attalla, R., Ling, C. & Selvaganapathy, P. Fabrication and characterization of gels with integrated channels using 3D printing with microfluidic nozzle for tissue engineering applications. *Biomedical microdevices* **18**, 17, doi:10.1007/s10544-016-0042-6 (2016).

57   Kuo, C.-Y. *et al.* Development of a 3D Printed, Bioengineered Placenta Model to Evaluate the Role of Trophoblast Migration in Preeclampsia. *ACS Biomaterials Science & Engineering*, doi:10.1021/acsbiomaterials.6b00031 (2016).

58   Kuo, C. Y. *et al.* Trophoblast-endothelium signaling involves angiogenesis and apoptosis in a dynamic bioprinted placenta model. *Biotechnol Bioeng* **116**, 181-192, doi:10.1002/bit.26850 (2019).

59   Moser, G., Windsperger, K., Pollheimer, J., de Sousa Lopes, S. C. & Huppertz, B. Human trophoblast invasion: new and unexpected routes and functions. *Histochem Cell Biol* **150**, 361-370, doi:10.1007/s00418-018-1699-0 (2018).

60   Attalla, R., Puersten, E., Jain, N. & Selvaganapathy, P. R. 3D bioprinting of heterogeneous bi- and tri-layered hollow channels within gel scaffolds using scalable multi-axial microfluidic extrusion nozzle. *Biofabrication* **11**, 015012, doi:10.1088/1758-5090/aaf7c7 (2018).

61   Wallace, A. E., Fraser, R. & Cartwright, J. E. Extravillous trophoblast and decidual natural killer cells: a remodelling partnership. *Hum Reprod Update* **18**, 458-471, doi:10.1093/humupd/dms015 (2012).

62   Lavazza, A. & Massimini, M. Cerebral organoids: ethical issues and consciousness assessment. *J Med Ethics* **44**, 606-610, doi:10.1136/medethics-2017-104555 (2018).

63   Chen, H. I. *et al.* Transplantation of Human Brain Organoids: Revisiting the Science and Ethics of Brain Chimeras. *Cell Stem Cell* **25**, 462-472, doi:10.1016/j.stem.2019.09.002 (2019).

64   Mansour, A. A. *et al.* An in vivo model of functional and vascularized human brain organoids. *Nat Biotechnol* **36**, 432-441, doi:10.1038/nbt.4127 (2018).

65   Partridge, E. A. *et al.* An extra-uterine system to physiologically support the extreme premature lamb. *Nat Commun* **8**, 15112, doi:10.1038/ncomms15112 (2017).

66   Becker, R. *An artificial womb successfully grew baby sheep — and humans could be next*, <https://www.theverge.com/2017/4/25/15421734/artificial-womb-fetus-biobag-uterus-lamb-sheep-birth-premie-preterm-infant> (2017).

67   Breyer, M. D., Look, A. T. & Cifra, A. From bench to patient: model systems in drug discovery. *Dis Model Mech* **8**, 1171-1174, doi:10.1242/dmm.023036 (2015).

68   Barker, D. J. & Thornburg, K. L. Placental programming of chronic diseases, cancer and lifespan: a review. *Placenta* **34**, 841-845, doi:10.1016/j.placenta.2013.07.063 (2013).

69   Burton, G. J. & Fowden, A. L. The placenta: a multifaceted, transient organ. *Philosophical transactions of the Royal Society of London. Series B, Biological sciences* **370**, 20140066, doi:10.1098/rstb.2014.0066 (2015).
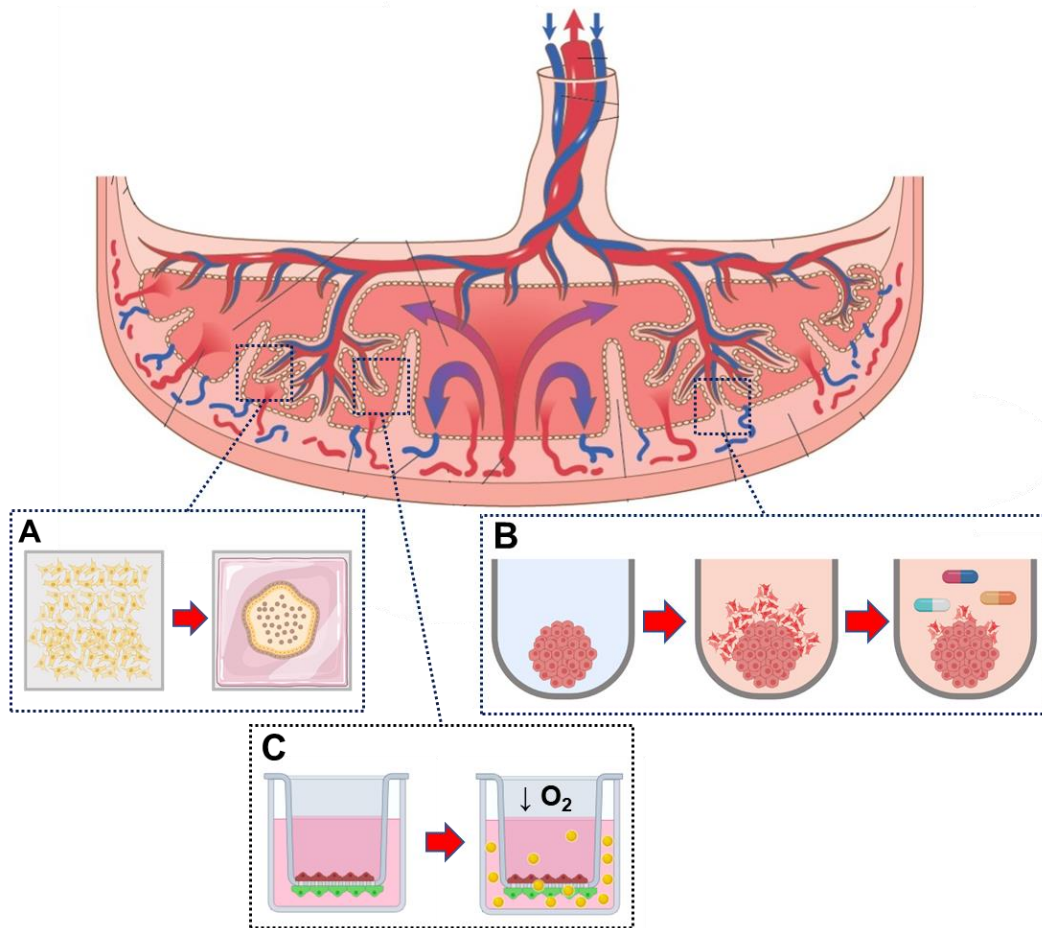
Figures and Figure Legends

Figure 1. Summary of three microphysiological models of the human placenta. (**A**) Extracellular matrix-driven self-assembly of placental trophoblast spheroids to investigate biophysical regulation of cell behaviour and function. (**B**) Invasive, extravillous trophoblast spheroids that could be used for drug and toxin screening. (**C**) Multi-layered placental barrier model to investigate transport and function under physiologically-low oxygen levels.
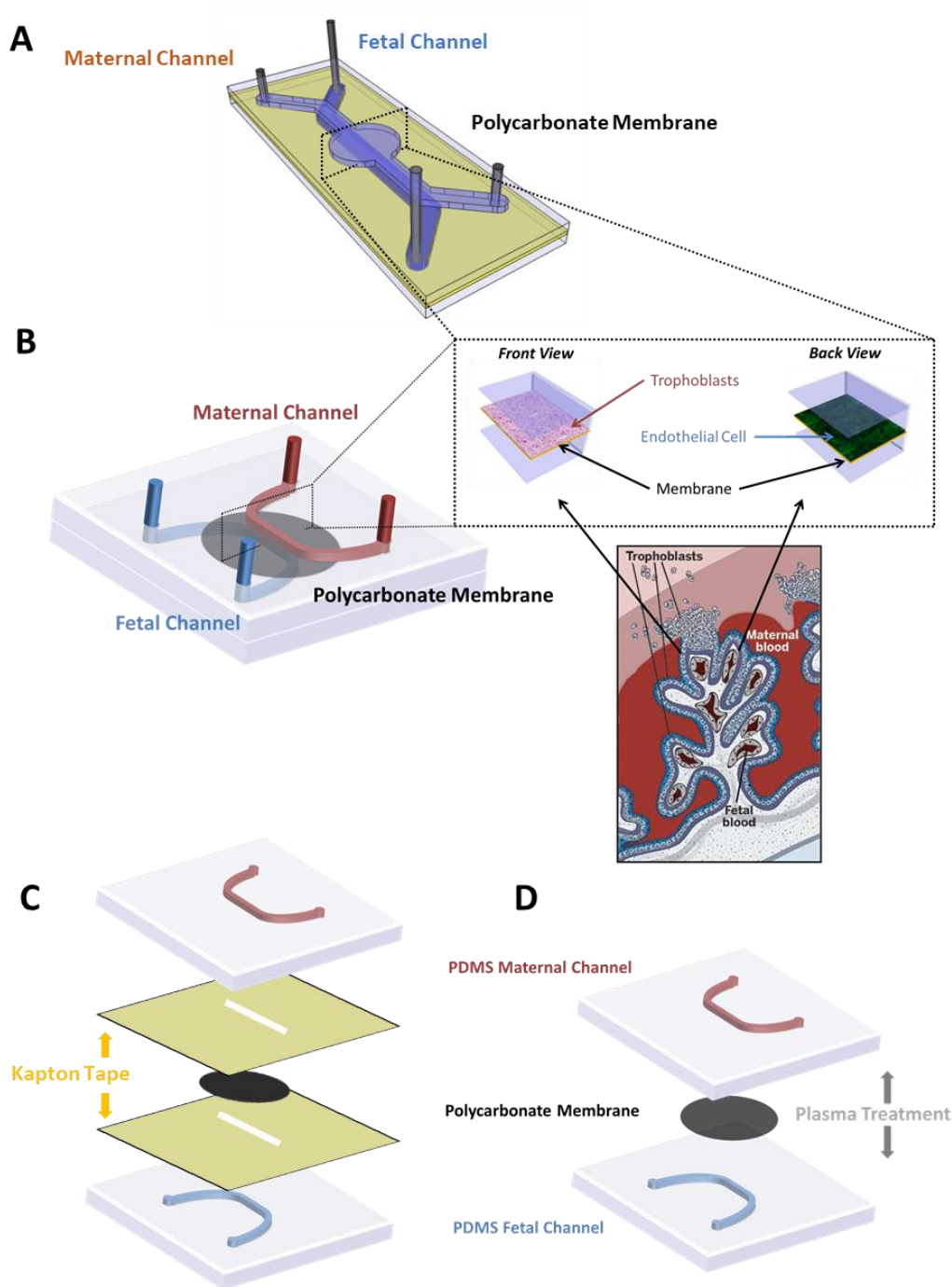
Figure 2. Computer-Aided Design (CAD) images of **(A)** a placenta-on-a-chip made with a circular maternal channel and straight fetal channel and **(B)** a placenta-on-a-chip made with straight maternal and fetal channels. CAD images demonstrating the bonding of the PDMS slabs with the polycarbonate membrane using **(C)** Kapton tape adhesive and **(D)** plasma-activation.
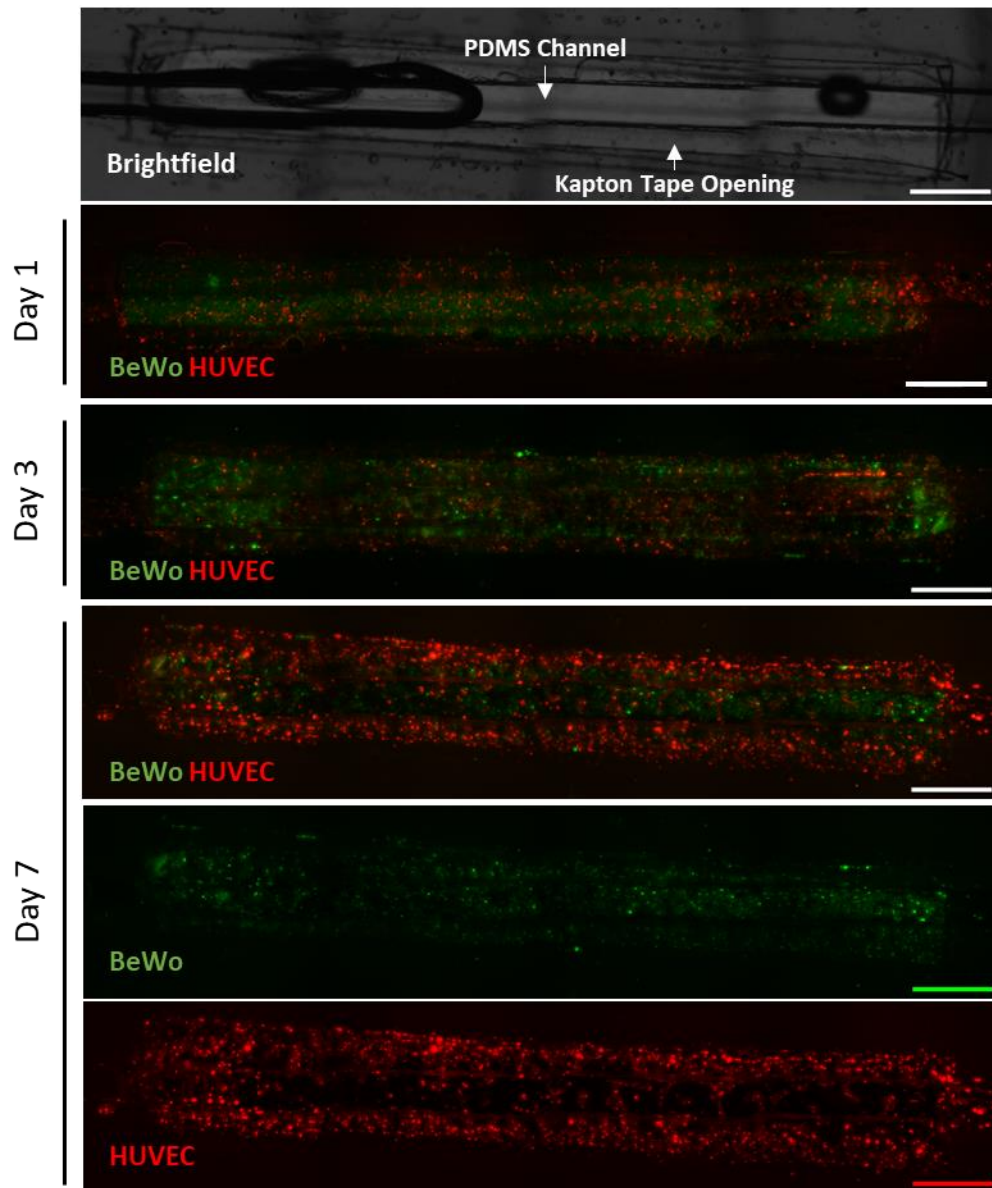
Figure 3. Brightfield and fluorescent images of BeWo and HUVEC cells inside Kapton-tape bonded placenta-on-a-chip device cultured at 100 µL/hr flow rate for 1, 3, and 7 days. Green fluorescence indicates BeWo cells and red fluorescence indicates HUVEC cells. Image captured at 4x magnification using Large Image stitching on NIS Elements software (Nikon). Scale bar indicates 200 µm. n ≥ 3.
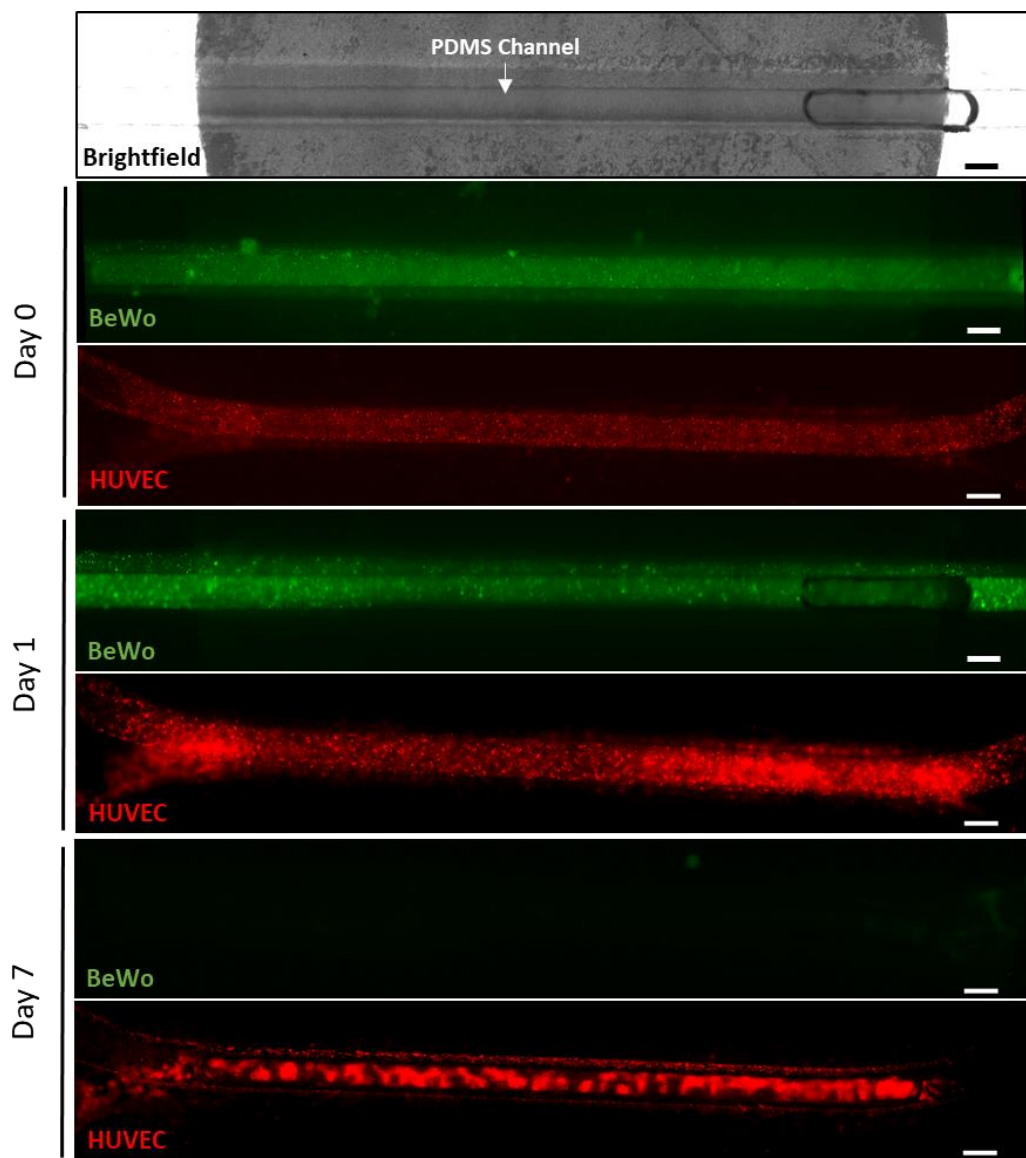
Figure 4. Brightfield and fluorescent images of BeWo and HUVEC cells inside plasma-activation bonded placenta-on-a-chip device cultured at 100 µL/hr flow rate for 0, 1, and 7 days. Green fluorescence indicates BeWo cells and red fluorescence indicates HUVEC cells. Image captured at 4x magnification using Large Image stitching on NIS Elements software (Nikon). Scale bar indicates 100 µm. n ≥ 3.
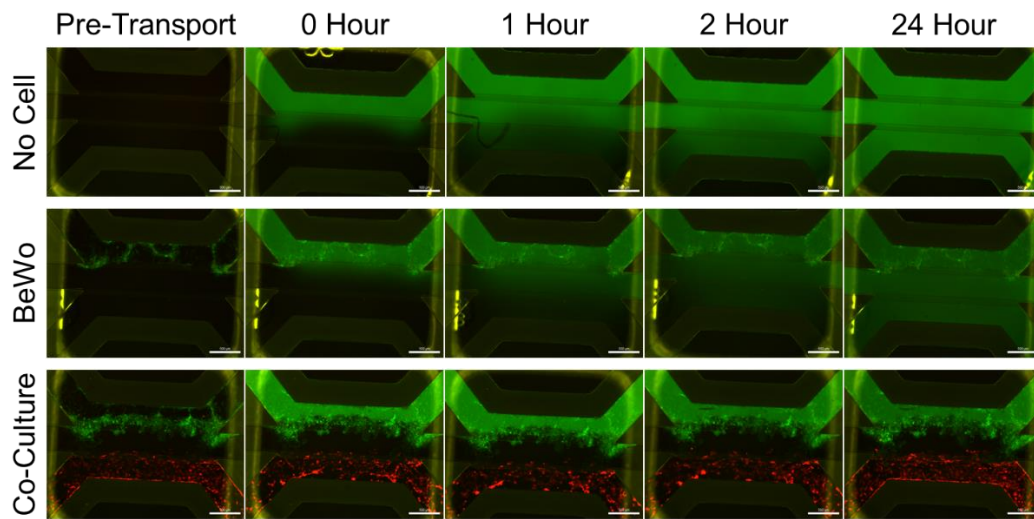
Figure 5. Barrier permeability experiment using Mimetas OrganoPlate 3-lane.
70,000 Da fluorescein-dextran molecules (10 μM) were pipetted into the top, maternal channel and allowed to permeate across to the bottom, fetal channel over 24 hours. There were either no cells present in the channel, BeWo cells only in the maternal channel, or a co-culture of BeWo cells and HUVECs. Green colour in channels represents fluorescein-dextran molecules. Brighter green colours present in pre-transport represents BeWo cells. Red colour represents HUVECs. Scale bar represents 500 μm.

APPENDIX 1: COPYRIGHT LICENSES

Copyright Permission Request - PLoS One

Dear Dr. Wong,
Thank you for your message. PLOS ONE publishes all of the content in the articles under an open access license called "CC-BY." This license allows you to download, reuse, reprint, modify, distribute, and/or copy articles or images in PLOS journals, so long as the original creators are credited (e.g., including the article's citation and/or the image credit). Additional permissions are not required. You can read about our open access license
here: http://journals.plos.org/plosone/s/licenses-and-copyright
There are many ways to access our content, including HTML, XML, and PDF versions of each article. Higher resolution versions of figures can be downloaded directly from the article.
Thank you for your interest in PLOS ONE and for your continued support of the Open Access model. Please do not hesitate to be in touch with any additional questions.

Kind regards,
Allie
PLOS | OPEN FOR DISCOVERY
Allie Chen | Publications Assistant, PLOS ONE
1160 Battery Street, Suite 225, San Francisco, CA 94111
achen@plos.org

Case Number: 06448945
ref:_00DU0Ifis._5004Pzqvuz:ref

Licenses and Copyright

Copyright Permission Request – Scientific Reports

Dear Michael,

Thank you for your recent Springer Nature permissions request. This work is licensed under the Creative Commons Attribution 4.0 International License, which permits unrestricted use, distribution, modification, and reproduction in any medium, provided you:

1) give appropriate acknowledgment to the original author(s) including the publication source,
2) provide a link to the Creative Commons license/include a notice of the CC license in legend and reference, and indicate if changes were made.

You are not required to obtain permission to reuse this article, but you must follow the above two requirements.

Images or other third party material included in the article are encompassed under the Creative Commons license, unless indicated otherwise in the credit line. If the material is not included under the Creative Commons license, users will need to obtain permission from the license holder to reproduce the material.

To view a copy of the Creative Commons license, please visit http://creativecommons.org/licenses/by/4.0/

Please let me know if you have any questions.

Best wishes,
Oda

Oda Siqveland
Rights Executive

SpringerNature
The Campus, 4 Crinan Street, London N1 9XW,
United Kingdom
T +44 (0) 207 014 6851

http://www.nature.com
http://www.springer.com
http://www.palgrave.com

APPENDIX 2: PLACENTA-ON-A-CHIP METHODS

This appendix chapter is intended to supplement the Discussion chapter with any relevant, unpublished primary work that I completed during my doctoral thesis. Only information relevant to the discussion and overall theme of this doctoral thesis has been included here.

Device design and fabrication

Polydimethylsiloxane (PDMS) (Sylguard 180 elastomer kit, Dow Corning Inc.) was mixed with a curing agent in a weight ratio of 10:1 and degassed for 20 min to remove air bubbles. The mixture was poured into 3D-printed molds of the maternal and fetal channels at a thickness of 2.5mm each and cured for 2 hours at 50 degrees. The upper "maternal" channel was designed for culturing placental cells and a lower "fetal" channel for vascular endothelial cells. There were two major channel design prototypes tested: (1) circular maternal channel and a straight, narrow fetal channel, which better represented the spacious, maternal intervillous space and narrow fetal vasculature, respectively, and (2) straight maternal and fetal channels, which offered greater simplicity. The channel dimensions were 0.5mm, 0.5mm, and 35mm for the width, height, and length, respectively. The molds imprinted the specific microfluidic channel designs into the PDMS.

Device bonding

The two PDMS slabs were removed from the molds and bonded to a semi-permeable polycarbonate membrane containing 0.4 μm pores (Sterlitech). There were two major methods that we tested for bonding: (1) Kapton tape adhesive and (2) Plasma-activated bonding using a BD-20AC Laboratory Corona Treater (Electro-Technic Products). Kapton tape is a highly stable, polyimide-based, double-sided adhesive that may be used to bond many types of materials. Plasma-activated bonding involves bombarding the surface of interest with oxygen ions, which "activates" the surface. Surfaces may then be pressed together, forming a covalent bond. For both methods, the PDMS layers were manually aligned with the polyester membrane and pressed together to bond. The device was sterilized via UV exposure for 30 minutes prior to use.

Microfluidic cell culture

Fibronectin (0.1 mg/mL) was infused into device channels and incubated at 37°C for >4 hours to promote cell adherence (Please see Committee Report 2 for optimization experiments). BeWo cells were stained with Cytopainter green fluorescence staining reagent (Abcam) then seeded into the maternal channel and red fluorescent protein (RFP)-HUVEC cells were seeded into the fetal channel, both at $1x10^6$ cells/mL using a micropipette. Devices were then incubated at 37°C in a humidified atmosphere of 5% CO2/95% air for ≥12 hours to allow cells to adhere to the surface of the membrane. Devices were then connected to the entire placenta-

on-a-chip set-up (please see methods below) and cultured at a flow rate of 100 µL/hr

for up to 7 days.

Placenta-on-a-chip set-up

The set-up for the placenta-on-a-chip devices included: NE-1600 syringe

pumps (New Era Pump Systems Inc.), one 20mL syringe per device to provide

media to cells, silicone tubing to connect syringes with device and device with

output tubes, Luer locks to connect tubing, and one 50mL Falcon tube to collect

output media per device channel. Tin foil was used to cover the top of output tubes

to prevent evaporation of output media. The current setup can support up to three

devices simultaneously and may be further scaled up through the addition of pumps

or splitters. Entire set-up is housed inside a Hypoxic Glove Box (Coy Laboratory

Products Inc.) set at 37°C in a humidified atmosphere of 5% CO_2/95% air.

Live cell imaging

Brightfield and fluorescent images were captured using an Eclipse Ti-E

Inverted Microscope (Nikon) under 4x or 10x objective magnification. Brightfield

was used to capture images of the channel structure. FITC was used to capture

images of BeWo cells stained with Cytopainter green fluorescence staining reagent.

TRITC was used to capture images of RFP-HUVEC cells.